

Electron diffraction from carbon nanotubes

Lu-Chang Qin

W M Keck Laboratory for Atomic Imaging and Manipulation, Department of Physics and Astronomy and Curriculum in Applied and Materials Sciences, University of North Carolina at Chapel Hill, Chapel Hill, NC 27599-3255, USA

E-mail: lcqin@unc.edu

Received 17 July 2006

Published 20 September 2006

Online at stacks.iop.org/RoPP/69/2761

Abstract

The properties of a carbon nanotube are dependent on its atomic structure. The atomic structure of a carbon nanotube can be defined by specifying its chiral indices, (u, v) , that specify its perimeter vector (chiral vector), with which the diameter and helicity are also determined. The fine electron beam available in a modern transmission electron microscope (TEM) offers a unique probe to reveal the atomic structure of individual nanotubes.

This review covers two aspects related to the use of the electron probe in the TEM for the study of carbon nanotubes: (a) to understand the electron diffraction phenomena for interpretation of the electron diffraction patterns of carbon nanotubes and (b) to obtain the chiral indices, (u, v) , of the carbon nanotubes from the electron diffraction patterns.

For a nanotube of a given structure, the electron scattering amplitude from the carbon nanotube is first described analytically in closed form using the helical diffraction theory. From a known structure as given by the chiral indices (u, v) , its electron diffraction pattern can be calculated and understood.

The reverse problem, i.e. assignment of the chiral indices from an electron diffraction pattern of a carbon nanotube, is approached from the relationship between the electron scattering intensity distribution and the chiral indices (u, v) . We show that electron diffraction patterns can provide an accurate and unambiguous assignment of the chiral indices of carbon nanotubes. The chiral indices (u, v) can be read indiscriminately with a high accuracy from the intensity distribution on the principal layer lines in an electron diffraction pattern.

The symmetry properties of electron diffraction from carbon nanotubes and the electron diffraction from deformed carbon nanotubes are also discussed in detail. It is shown that 2mm symmetry is always preserved for single-walled carbon nanotubes, but it can break down for multiwalled carbon nanotubes under some special circumstances.

Finally, determination of the handedness of carbon nanotubes using electron diffraction is reviewed and discussed with both theoretical analysis and experimental examples.

(Some figures in this article are in colour only in the electronic version)

This article was invited by Professor S Washburn.

Contents

	Page
1. Introduction	2763
2. Structure description of carbon nanotubes	2764
3. Electron diffraction from single-walled carbon nanotubes	2768
3.1. Atomic scattering amplitude	2768
3.2. Electron diffraction from a continuous helix	2768
3.3. Electron diffraction from a nanotube	2770
3.4. Selection rule	2771
3.5. Structure factor of a carbon nanotube	2772
3.6. Cylindrical correction	2775
3.7. Calculation of electron diffraction patterns	2777
3.8. Electron diffraction from multiwalled carbon nanotubes	2778
4. Determination of chiral indices of carbon nanotubes	2779
4.1. Principal layer lines	2779
4.2. Direct method	2780
4.3. Ratio of indices v/u	2783
4.4. Examples: single-walled carbon nanotubes	2784
4.5. Bundles of single-walled carbon nanotubes	2789
4.6. Multiwalled carbon nanotubes	2791
5. Symmetry of electron diffraction from carbon nanotubes	2793
5.1. Single-walled carbon nanotubes	2794
5.2. Multiwalled carbon nanotubes	2796
5.3. Rotational extinctions	2799
6. Deformed carbon nanotubes	2802
6.1. Elliptical nanotubes	2803
6.2. Twisted nanotubes	2807
6.3. Carbon nanotube ropes	2809
7. Handedness of carbon nanotubes	2809
7.1. Single-walled carbon nanotubes	2809
7.2. Multiwalled carbon nanotubes	2810
Appendix	2812
Acknowledgments	2815
References	2816

1. Introduction

Diamond and graphite have long been known as the only allotropes of crystalline carbon and their atomic structures were determined soon after the x-ray diffraction method was developed [1–3]. Carbon nanotubes were first discovered in 1991 in the cathodic deposits when two graphite electrodes were dc arc-discharged [4] in an apparatus developed to produce fine particles [5] and fullerenes [6, 7]. The ultimate form of carbon nanotubes is single-walled carbon nanotubes [8, 9], which can be constructed by rolling up a rectangular cut of graphene about a chosen axis to form a seamless cylinder of diameter on the nanometre scale.

In addition to the arc-discharge technique to produce carbon nanotubes, both multiwalled and single-walled carbon nanotubes [10–13], other production techniques have been developed and refined to produce carbon nanotubes, including laser evaporation [14–16], pyrolytic chemical vapour deposition (CVD) involving various catalysts and hydrothermal and solvothermal methods [17–37] and plasma-enhanced CVD [38–40]. At present, these three methods (arc-discharge, CVD and laser evaporation) are the major production techniques to make large quantities of carbon nanotubes, both single-walled and multiwalled.

The helical structure of carbon nanotubes was recognized when the first carbon nanotubes were observed in a transmission electron microscope (TEM) using electron diffraction [4]. The diameter and helicity define the atomic structure of a carbon nanotube, which in turn determines the properties of the nanotube. For example, a carbon nanotube can be either metallic or semiconducting, an extraordinary property of carbon nanotubes that was soon recognized [41–46] and has excited a great many envisaged proposals on the potential nanoelectronics and photonics applications based on this tuneable electronic structure [47–53].

Apart from the unique one-dimensional structure of carbon nanotubes, their extraordinary properties are the major reasons for the explosion in research activity that has been seen over the past decade and a half since carbon nanotubes were discovered. Based on the strongest carbon–carbon covalent bond, carbon nanotubes have shown the highest Young's modulus approaching the theoretical value of graphite, i.e. about 2 TPa [54–63].

There have also been noticeable practical applications of carbon nanotubes. Due to their small diameter and large aspect ratio, carbon nanotubes have been demonstrated to be excellent electric field-induced emitters of electrons [64–70]. When thin films are made, a large emission current has been obtained, and devices for generating x-rays have been developed [69–72]. Carbon nanotube cathodes have also been fabricated to produce flat panel displays [73]. When a single carbon nanotube is used, it can serve as a point electron source that offers higher brightness and lower energy spread. These qualities make carbon nanotubes promising point emitters for electron microscope filaments [74–79]. In addition, carbon nanotubes have also been explored as high-aspect-ratio atomic force microscope tips [80–83].

The atomic structure of carbon nanotubes has been at the centre stage of research ever since carbon nanotubes were discovered. Transmission electron microscopy (TEM) has been the most powerful and most popular technique for characterizing the morphology and structure of carbon nanotubes. In addition to the TEM method, other analytical techniques, such as Raman spectroscopy [84, 85], optical absorption spectroscopy [86, 87] and scanning tunnelling microscopy [88–92], have also been used extensively in an attempt to elucidate the atomic structure of carbon nanotubes. However, due to various limitations, there are still formidable difficulties in determining the atomic structure of carbon nanotubes accurately with these techniques.

Electron diffraction was the first technique employed to identify the helical structure of carbon nanotubes and it has continued to play an important role in the structural studies of carbon nanotubes. Based on the helical theory developed for the study of α -helix and

the helical DNA molecules [93–100], the kinematical diffraction theory for the scattering of electrons or x-rays from carbon nanotubes was formulated by Qin in 1994 [101] and subsequently by Lucas *et al* in 1996 [102, 103]. Electron diffraction from carbon nanotubes was also discussed using mostly geometric illustrations [104–108] that has been well covered in the review paper by Amelinckx *et al* [109]. On the other hand, electron diffraction has also been explored for the possibility of solving the atomic structure of carbon nanotubes, in particular, to obtain the helicity of carbon nanotubes [110–142]. Two approaches have been developed, one uses a correction factor to obtain the chiral angle from the electron diffraction pattern [113] and the other uses the ratio of the layer lines measured in the electron diffraction patterns [120]. The atomic structure of a double-walled carbon nanotube was also obtained by electron crystallographic method using phase retrieval [121]. A one-step direct method has been developed recently [122] and has been applied to determine the atomic structure of a large number of carbon nanotubes, both single-walled and multiwalled [123, 124]. Electron diffraction is by far the most powerful technique to study the atomic structure of carbon nanotubes with high accuracy as can be seen in the literature [125–142].

In this review, we will first define the structural parameters of carbon nanotubes (section 2). In section 3, the kinematical diffraction theory is described in detail using analytic expressions in terms of their structural parameters, i.e. the chiral indices (u, v) for both single-walled and multiwalled carbon nanotubes. Electron scattering intensities are expressed analytically using these structural parameters and numerical calculations are given together with illustrated experimental data. To answer the crucial question—determination of the atomic structure of carbon nanotubes by electron diffraction, section 4 details a one-step systematic method that allows the assignment of the chiral indices of carbon nanotubes from a single electron diffraction pattern with high precision. In section 5, the symmetry properties of electron diffraction from carbon nanotubes, both single-walled and multiwalled, are discussed. In section 6, the electron diffraction from deformed carbon nanotubes is considered, including elliptical nanotubes, twisted nanotubes and carbon nanotube ropes. The determination of the handedness of carbon nanotubes using electron diffraction is reviewed and discussed in section 7.

2. Structure description of carbon nanotubes

The solid state physics convention is chosen in this paper to describe the graphene lattice structure, where the basis vectors of the graphene net, \vec{a}_1 and \vec{a}_2 ($a_1 = a_2 = a_0 = 0.246$ nm), are separated with an inter-angle of 60° , as schematically shown in figure 1(a). The planar net is also referred to as the radial projection of the nanotube. With the crystallographic basis vectors defined in the real space, the basis vectors, \vec{a}_1^* and \vec{a}_2^* , in the reciprocal space are

$$\begin{aligned}\vec{a}_1^* &= \frac{2}{3a_0^2}(2\vec{a}_1 - \vec{a}_2), \\ \vec{a}_2^* &= \frac{2}{3a_0^2}(-\vec{a}_1 + 2\vec{a}_2).\end{aligned}\tag{1}$$

On the graphene lattice, a single-walled carbon nanotube can be conveniently described by a lattice vector (u, v) that specifies its perimeter, as shown in figure 1(a) for the lattice vector (7,1) and these two integer indices (u, v) are referred to as the chiral indices of the nanotube. For a carbon nanotube of given chiral indices (u, v), its perimeter vector is

$$\vec{A} = (u, v) = u \vec{a}_1 + v \vec{a}_2,\tag{2}$$

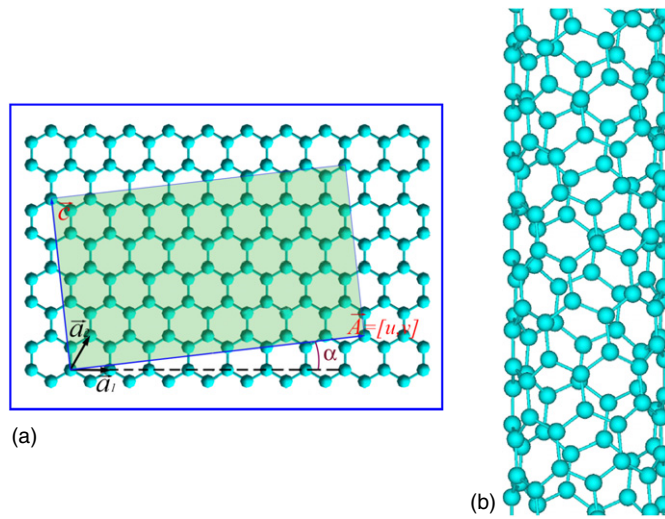


Figure 1. (a) Schematic structure of graphene with basis vectors \vec{a}_1 and \vec{a}_2 . The shadowed rectangle is the radial projection of carbon nanotube (7,1) with perimeter \vec{A} and helical angle α . (b) Single-walled carbon nanotube (7,1) is formed from the cut by rolling it up about axis \vec{A} perpendicular to the perimeter vector \vec{A} .

with magnitude $A = a_0(u^2 + v^2 + uv)^{1/2}$, and the diameter of the nanotube is $d = A/\pi$. Once the chiral indices (u, v) are defined, the tubule axis, (u_c, v_c) , perpendicular to the chiral vector \vec{A} , can be calculated by applying the orthogonality relationship between the tubule perimeter and the tubule axis

$$(u, v) \cdot (u_c, v_c) = uu_c + vv_c + \frac{uv_c + uv_c}{2} = 0, \quad (3)$$

which yields

$$\frac{u_c}{v_c} = -\frac{u + 2v}{2u + v}. \quad (4)$$

The indices of the tubule axis (u_c, v_c) should be chosen as the pair which has no common factors other than 1. Denoting M as the greatest common integer divisor of $(2u + v)$ and $(u + 2v)$, the axial lattice vector (u_c, v_c) can be written as

$$\begin{aligned} u_c &= -\frac{u + 2v}{M}, \\ v_c &= \frac{2u + v}{M}, \end{aligned} \quad (5)$$

and the periodicity c of carbon nanotube (u, v) can be expressed as [143]

$$\begin{aligned} c &= a_0 \sqrt{u_c^2 + v_c^2 + u_c v_c} \\ &= \frac{\sqrt{3}a_0}{M} \sqrt{u^2 + v^2 + uv} = \frac{\sqrt{3}A}{M}. \end{aligned} \quad (6)$$

When a rectangle with sides A and c is cut out of the graphene and is then rolled up about an axis perpendicular to the perimeter A , a cylindrical nanotube (7,1) is formed as depicted in figure 1(b). The helical angle α , defined as the angle between the perimeter vector $\vec{A} = (u, v)$

and the basis vector \vec{a}_1 , illustrated in figure 1(a), of the nanotube (u, v) is

$$\begin{aligned}\alpha &= \cos^{-1} \left(\frac{2u + v}{2(u^2 + v^2 + uv)^{1/2}} \right) \\ &= \sin^{-1} \left(\frac{\sqrt{3}v}{2\sqrt{u^2 + v^2 + uv}} \right) \\ &= \tan^{-1} \left(\frac{\sqrt{3}v}{2u + v} \right).\end{aligned}\quad (7)$$

The atomic positions can be expressed in two convenient ways. One is to use the Cartesian coordinates (x_j, z_j) in the radial projection, where the nanotube is projected onto a rectangle with sides A and c as described above. An alternative is to express the atomic positions in cylindrical coordinates (ϕ_j, z_j) and the atomic structure of a single-walled carbon nanotube can be described by pairs of parallel atomic helices. However, it should be noted that there are three equivalent helices in a carbon nanotube. They are parallel to the crystallographic directions \vec{a}_1, \vec{a}_2 and $\vec{a}_3 = \vec{a}_2 - \vec{a}_1$, respectively. Each helix consists of a pair of atomic helices, displaced by a respective vector. In a unit cell, there are v helix pairs parallel to \vec{a}_1 or u helix pairs parallel to \vec{a}_2 or $u + v$ helix pairs parallel to $\vec{a}_3 = \vec{a}_2 - \vec{a}_1$.

With respect to a chosen carbon atom located at the origin $\phi_0^{(0)} = 0$ and $z_0^{(0)} = 0$, the atomic positions on the primary helix parallel to \vec{a}_1 are

$$\begin{cases} \phi_j^{(1,0)} = -2\pi j a_0 \cos(\alpha)/A, \\ z_j^{(1,0)} = j a_0 \sin(\alpha), \end{cases} \quad j = 0, 1, 2, \dots, u + v \quad (8)$$

and the secondary helix is

$$\begin{cases} \phi_j^{(1,1)} = \phi_j^{(1,0)} + \Delta\phi_0^{(1)}, \\ z_j^{(1,1)} = z_j^{(1,0)} + \Delta z_0^{(1)}, \end{cases} \quad j = 0, 1, 2, \dots, u + v, \quad (9)$$

where

$$\begin{aligned}\Delta\phi_0^{(1)} &= \frac{2\pi a_0}{\sqrt{3}A} \cos(30^\circ + \alpha), \\ \Delta z_0^{(1)} &= -\frac{a_0}{\sqrt{3}} \sin(30^\circ + \alpha)\end{aligned}\quad (10)$$

The atomic positions on the primary helix (left-handed) parallel to \vec{a}_2 are

$$\begin{cases} \phi_j^{(2,0)} = 2\pi j a_0 \cos(60^\circ - \alpha)/A, \\ z_j^{(2,0)} = -j a_0 \sin(60^\circ - \alpha), \end{cases} \quad j = 0, 1, 2, \dots, 2u - v \quad (11)$$

and the secondary helix is

$$\begin{cases} \phi_j^{(2,1)} = \phi_j^{(2,0)} + \frac{2\pi a_0}{\sqrt{3}A} \sin(\alpha), \\ z_j^{(2,1)} = z_j^{(2,0)} - \frac{a_0}{\sqrt{3}} \cos(\alpha), \end{cases} \quad j = 0, 1, 2, \dots, 2u - v. \quad (12)$$

The atomic positions on the primary helix parallel to $\vec{a}_3 = \vec{a}_2 - \vec{a}_1$ are

$$\begin{cases} \phi_j^{(3,0)} = -2\pi j a_0 \cos(60^\circ + \alpha)/A, \\ z_j^{(3,0)} = j a_0 \sin(60^\circ + \alpha)/A, \end{cases} \quad j = 0, 1, 2, \dots, 2u + v \quad (13)$$

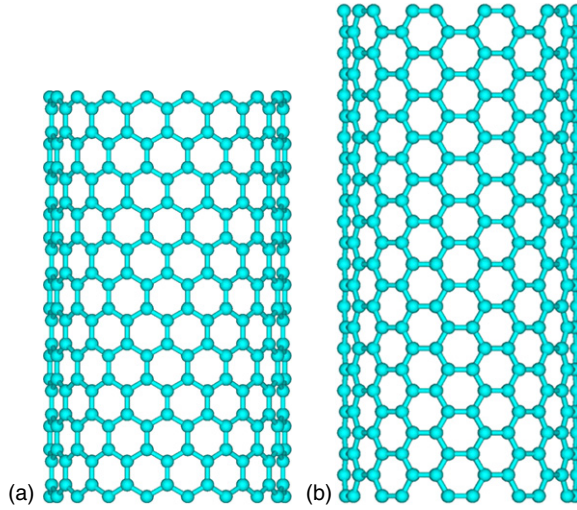


Figure 2. (a) Carbon nanotube (18,0) (diameter 1.409 nm and helicity 0°) of zigzag structure; (b) nanotube (10,10) (diameter 1.36 nm and helicity 30°) of armchair structure.

and the secondary helix is

$$\begin{cases} \phi_j^{(3,1)} = \phi_j^{(3,0)} + \frac{2\pi j a_0}{\sqrt{3}A} \sin(\alpha), \\ z_j^{(3,1)} = z_j^{(3,0)} + \frac{a_0}{\sqrt{3}} \cos(\alpha), \end{cases} \quad j = 0, 1, 2, \dots, 2u + v. \quad (14)$$

Since the graphene lattice has hexagonal rotational symmetry, the non-degenerate range for the helical angle is 60° , which can be confined to the range of $[0^\circ, 60^\circ]$. The values in $[30^\circ, 60^\circ]$ can be assigned to the left-handed tubules, while the values $[0^\circ, 30^\circ]$ are for the right-handed tubules. Among the three helices, two of them have the same handedness and the third has opposite handedness. Therefore, though the structure of carbon nanotubes is enantiomorphic, the choice of absolute handedness is arbitrary.

When the handedness of a tubule is ignored, the helical angle can be limited to $[0^\circ, 30^\circ]$. Within this range, the chiral indices can be limited to the following values:

$$\begin{aligned} u &> 0, \\ u &\geq v \geq 0. \end{aligned} \quad (15)$$

The rotational symmetry of a nanotube can be recognized by examining its chiral indices. For a tubule of indices (u, v) , it should have m -fold rotational symmetry where m is the greatest common divisor of u and v . When $v = 0$, the nanotube possesses u -fold rotational symmetry, and it does not have a two-fold rotational symmetry when u is an odd number. On the other hand, when a two-fold axis is present, the nanotube is also centrosymmetric.

There are two special cases that deserve special attention, which have non-helical structures. One is the so-called zigzag structure, which has chiral indices of the form $(u, 0)$ having helical angle 0° as shown in figure 2(a); the other is the armchair structure, which has chiral indices of (u, u) having helical angle 30° , which is shown in figure 2(b). In the zigzag structure, where $(u, v) = (u, 0)$, its tubule axis is $(u_c, v_c) = (-1, 2)$. In the armchair structure, where $(u, v) = (u, u)$, its tubule axis is $(u_c, v_c) = (-1, 1)$.

It should be noted that, though the choice of origin is arbitrary, the relative orientation between the real space lattice and the corresponding reciprocal space lattice is fixed. It is often found in the literature that the crystallographic convention is used where the two basis vectors, \vec{a}'_1, \vec{a}'_2 , are separated with an inter-angle of 120° . Though the physical results should be independent of the choice of basis vectors, the chiral indices usually appear to be different. The two sets of basis vectors are related by the following equations

$$\begin{cases} \vec{a}'_1 = \vec{a}_1, \\ \vec{a}'_2 = -\vec{a}_1 + \vec{a}_2, \end{cases} \quad (16)$$

and

$$\begin{cases} \vec{a}_1 = \vec{a}'_1, \\ \vec{a}_2 = \vec{a}'_1 + \vec{a}'_2. \end{cases} \quad (17)$$

The relationships between the chiral indices, (u, v) and (u', v') , which determine the perimeter vector of the nanotube, $\vec{A} = u\vec{a}_1 + v\vec{a}_2 = u'\vec{a}'_1 + v'\vec{a}'_2$, on the radial projection net are

$$\begin{cases} u = u' - v', \\ v = v', \end{cases} \quad (18)$$

and

$$\begin{cases} u' = u + v, \\ v' = v. \end{cases} \quad (19)$$

3. Electron diffraction from single-walled carbon nanotubes

3.1. Atomic scattering amplitude

When fast electrons are incident on an atom, the atomic scattering amplitude for electrons is well described by the first Born approximation [144–146]

$$f(\vec{q}) = \frac{2\pi m e}{h^2} \int v(\vec{r}) \exp(2\pi i \vec{q} \cdot \vec{r}) d\vec{r}, \quad (20)$$

where $v(\vec{r})$ is the coulombic potential of the scattering atom, $-e$ is the electric charge of electron, m is the relativistic mass of electron, h is the Planck constant and \vec{q} is the scattering vector with magnitude q defined as

$$q = \frac{2 \sin(\Theta/2)}{\lambda}, \quad (21)$$

in which Θ is the total scattering angle and λ is the wave length of the incident electron wave. The numerical calculation of the atomic scattering amplitudes has been well developed with tabulated numerical values available [147–149].

It is also worth mentioning that equation (20) is the Fourier transform of the scattering potential of the atom.

3.2. Electron diffraction from a continuous helix

The electron scattering amplitude can be expressed by the structure factor

$$F(\vec{q}) = \int V(\vec{r}) \exp(2\pi i \vec{q} \cdot \vec{r}) d\vec{r}, \quad (22)$$

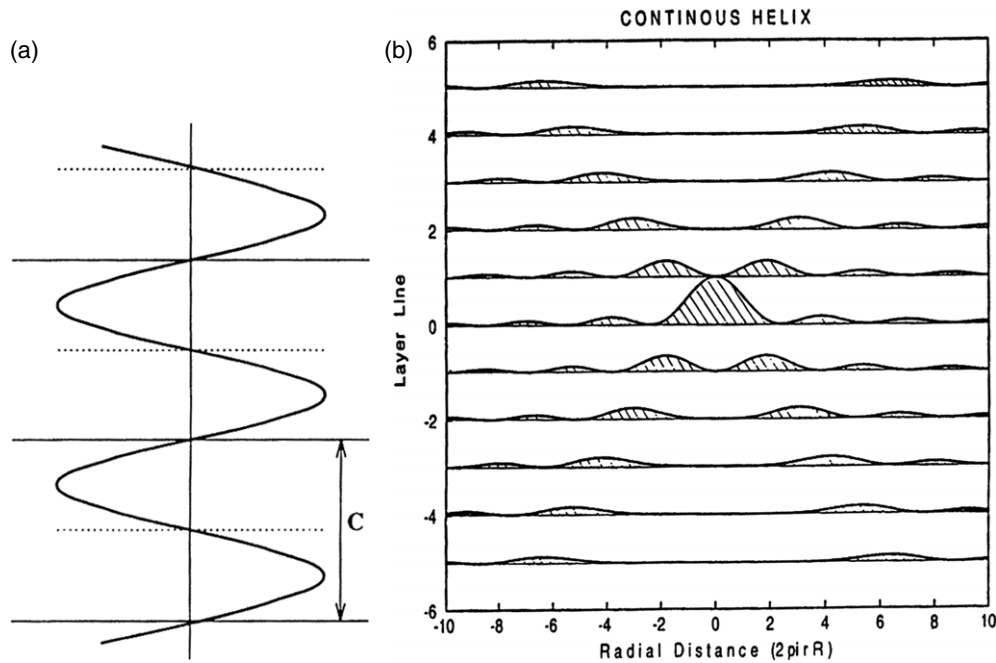


Figure 3. (a) Schematic of a continuous helix of pitch length C . (b) Corresponding electron diffraction pattern of the continuous helix. It consists of a set of layer lines separated by $1/C$ and the intensity on layer line l is proportional to $|J_l(X)|^2$.

where $V(\vec{r}) = ((2\pi me)/h^2)U(\vec{r})$ is the modified scattering potential with $U(\vec{r})$ being the coulombic potential of the scattering object, and the physically measurable diffraction intensity distribution $I(\vec{q})$ in the reciprocal space is

$$I(\vec{q}) = |F(\vec{q})|^2. \tag{23}$$

For the general case of kinematical diffraction, where Friedel’s law holds, the diffraction intensity distribution is always centro-symmetric regardless of the symmetry of the scattering potential, i.e.

$$I(-\vec{q}) = I(\vec{q}). \tag{24}$$

For a cylindrical object such as a nanotube, it is more convenient to express the scattering amplitude in polar coordinates (R, Φ, l) (cf appendix)

$$F(R, \Phi, l) = \frac{1}{c} \sum_{n=1}^{\infty} \exp \left[in \left(\Phi + \frac{\pi}{2} \right) \right] \times \int_0^c \int_0^{2\pi} \int_0^{\infty} V(r, \phi, z) J_n(2\pi r R) \exp \left[i \left(-n\phi + \frac{2\pi lz}{c} \right) r \right] r dr d\phi dz, \tag{25}$$

where J_n is the Bessel function of order n and c is the periodicity of the tubular object along its unique axis (z -direction).

As an example to illustrate the scattering of helical structures, figure 3(a) shows a continuous right-handed helix, where the scattering potential is expressed by

$$V(r, \phi, z) = V_0 \delta(r - r_0) \delta \left(\frac{2\pi z}{C} - \phi \right), \tag{26}$$

in which r_0 is the radius of the helix and C the pitch length. Using this potential, the scattering amplitude (25) becomes

$$F(R, \Phi, l) = r_0 V_0 J_l(2\pi r_0 R) \exp \left[i \left(\Phi + \frac{\pi}{2} \right) l \right], \quad (27)$$

and the corresponding scattering intensity distribution is

$$I(R, \Phi, l) = |F(R, \Phi, l)|^2 = r_0^2 V_0^2 [J_l(2\pi r_0 R)]^2, \quad (28)$$

which is plotted in figure 3(b).

There are two distinctive characteristics in the diffraction pattern of a helix that deserve special mention. One is that the intensity falls only on discrete lines (layer lines) indexed by integer l ; the other is that the intensity on a layer line l is proportional to the square of Bessel function of order l .

When there are two helices related by a twofold rotation axis, i.e.

$$V(r, \phi, z) = V_0 \delta(r - r_0) \left[\delta \left(\frac{2\pi z}{C} - \phi \right) + \delta \left(\frac{2\pi z}{C} - \phi + \pi \right) \right], \quad (29)$$

the scattering amplitude then becomes

$$\begin{aligned} F(R, \Phi, l) &= r_0 V_0 J_l(2\pi r_0 R) \left\{ \exp \left[i \left(\Phi + \frac{\pi}{2} \right) l \right] + \exp \left[i \left(\Phi - \frac{\pi}{2} \right) l \right] \right\} \\ &= r_0 V_0 J_l(2\pi r_0 R) [1 + \exp(-i\pi l)] \exp \left[i \left(\Phi + \frac{\pi}{2} \right) l \right]. \end{aligned} \quad (30)$$

The intensity distribution is

$$I(R, \Phi, l) = |F(R, \Phi, l)|^2 = \begin{cases} 4r_0^2 V_0^2 [J_l(2\pi r_0 R)]^2, & l = \text{even}, \\ 0, & l = \text{odd}. \end{cases} \quad (31)$$

The layer lines of odd index l are in extinction.

When there is an N -fold rotation axis, the layer lines will be in extinction except those of layer line index equal to multiples of N .

3.3. Electron diffraction from a nanotube

In a single-walled carbon nanotube of radius r_0 , where the carbon atoms are located at discrete positions on a helix of radius r_0 , as schematically shown in figure 4(a), the corresponding structure factor takes the following form (cf appendix)

$$F(R, \Phi, l) = \sum_n \exp \left[i n \left(\Phi + \frac{\pi}{2} \right) \right] J_n(2\pi r_0 R) \sum_j f_j \exp \left[i \left(-n\phi_j + \frac{2\pi l z_j}{c} \right) \right], \quad (32)$$

where the summation for j is done over all atoms in an asymmetric cell and n over all integers as allowed by the selection rule discussed in section 3.4. This is a generic formula that is valid for all forms of nanotubes.

The structure factor (32) can also be rewritten as

$$F(R, \Phi, l) = \sum_n B_n(R, \Phi) T_{nl}, \quad (33)$$

where

$$B_n(R, \Phi) = \exp \left[i n \left(\Phi + \frac{\pi}{2} \right) \right] J_n(2\pi r_0 R) \quad (34)$$

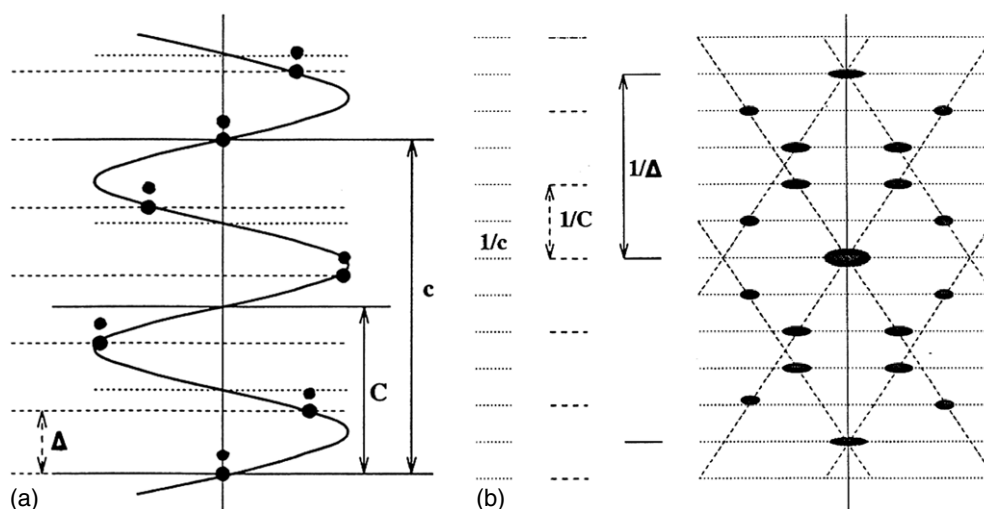


Figure 4. (a) Schematic of a discontinuous helix where discrete groups of scatterers (atoms) are located on a helix of pitch length C . c and Δ are the periodicity of the structure and the separation between the neighbouring molecular groups in the axial direction, respectively. (b) Corresponding Fraunhofer diffraction pattern.

and

$$T_{nl} = \sum_j f_j \exp \left[2\pi i \left(\frac{nx_j}{A} + \frac{lz_j}{c} \right) \right], \quad (35)$$

where A is the perimeter of the nanotube and (x_j, z_j) are the atomic coordinates in radial projection in the horizontal and axial directions, respectively. Herewith the diffraction effects from a cylindrical nanotube are more clearly seen by looking at the physical meaning of the two parts in equation (33): (a) the structure factor in radial projection described by T_{nl} and (b) the modifying function $B_n(R, \Phi)$ taking into account the effects of cylindrical curvature. For the case of single-walled carbon nanotubes, T_{nl} gives rise to the regular hexagonal diffraction pattern from a graphene. As shown by equation (33), the modifying Bessel function alters the diffraction intensity peak positions in the diffraction pattern, and the shifts are determined by the order of the operating Bessel functions.

3.4. Selection rule

When there is a discrete distribution of scatterers located on a helix, the discrete scattering potential can be regarded as the product of the continuous helix and a set of equally spaced planes of spacing Δ , as illustrated in figure 4(a). The Fraunhofer diffraction can then be calculated by the convolution of the structure factor of the continuous helix and that of the equally spaced planes. Since the latter is just a row of points located along the tubule axis with equal spacing $1/\Delta$, the compounded result is a set of diffraction patterns of the single continuous helix with origins at each of the points along the tubule axis, as schematically depicted in figure 4(b). If we designate c as the new structural periodicity along the tubule axis of a single helix, C as the pitch length of the continuous helix ($c \geq C$), then the allowed reflection on layer line l should satisfy

$$\frac{l}{c} = \frac{n}{C} + \frac{m}{\Delta}, \quad (36)$$

where m is an integer. For a given layer line l , the allowed orders of Bessel functions $J_n(2\pi r_o R)$ are determined by combinations of n and all possible integers m that satisfy equation (36). The selection rule (36) can also be expressed equivalently as

$$l = nt + mp, \quad (37)$$

where $t = c/C$ gives the number of turns per unit periodicity and $p = c/\Delta$ gives the number of scattering units per complete periodicity of the helix.

On the other hand, from the geometry in radial projection, we have

$$C = A \tan(\alpha) = a_0 \frac{v\sqrt{3(u^2 + v^2 + uv)}}{2u + v}, \quad (38)$$

$$\Delta = a_0 \sin(\alpha) = a_0 \frac{3v}{2\sqrt{3(u^2 + v^2 + uv)}},$$

in terms of the chiral indices (u, v) , the parameters t and p are

$$t = \frac{c}{C} = \frac{2u + v}{Mv}, \quad (39)$$

where M is the greatest common divisor of $(2u + v)$ and $(u + 2v)$, and

$$p = \frac{c}{\Delta} = \frac{2(u^2 + v^2 + uv)}{Mv}. \quad (40)$$

The selection rule for nanotube (u, v) can therefore also be expressed as

$$l = n \frac{2u + v}{Mv} + m \frac{2(u^2 + v^2 + uv)}{Mv}. \quad (41)$$

When the nanotube has rotational symmetry, the same selection rule applies if c is defined as the periodicity related to a specific helix. The additional rotational symmetry will lead to extinction in layer lines. For a nanotube of N -fold rotational symmetry, only $l = kN$ are allowed layer lines. Equivalently, this can be translated into additional constraints on the selection rule. If we use the structural periodicity, then the new periodicity will be shortened by N times to become c/N , and the selection rule (equation (36)) $l = nt + mp$ will limit the values of n and m to be multiples of N , while l takes all possible integers.

3.5. Structure factor of a carbon nanotube

To calculate the scattering amplitude for a single-walled carbon nanotube (u, v) , it is more convenient to express its atomic structure by the v pairs of atomic helices positioned at $(x_j^{(1,0)}, z_j^{(1,0)})$ and $(x_j^{(1,1)}, z_j^{(1,1)})$ where

$$\begin{cases} x_j^{(1,0)} = -ja_0 \cos(30^\circ - \alpha), \\ z_j^{(1,0)} = ja_0 \sin(30^\circ - \alpha), \end{cases} \quad j = 0, 1, 2, \dots, v-1 \quad (42)$$

and

$$\begin{cases} x_j^{(1,1)} = x_j^{(1,0)} + \frac{a_0}{\sqrt{3}} \cos(30^\circ + \alpha), \\ z_j^{(1,1)} = z_j^{(1,0)} - \frac{a_0}{\sqrt{3}} \sin(30^\circ + \alpha), \end{cases} \quad j = 0, 1, 2, \dots, v-1. \quad (43)$$

The scattering amplitude from the v pairs of helices is therefore

$$T_{nl} = \sum_k^{\text{atoms}} f \exp \left[2\pi i \left(\frac{nx_k}{A} + \frac{lz_k}{c} \right) \right] = f \sum_{j=0}^{v-1} \left\{ \exp \left[2\pi i \left(\frac{nx_j^{(1,0)}}{A} + \frac{lz_j^{(1,0)}}{c} \right) \right] \right\} \\ \times \left\{ 1 + \exp \left[\frac{2\pi ia_0}{\sqrt{3}} \left(\frac{n \cos(30^\circ + \alpha)}{A} - \frac{l \sin(30^\circ + \alpha)}{c} \right) \right] \right\}. \quad (44)$$

Inserting

$$\begin{cases} \cos(30^\circ - \alpha) = \frac{\sqrt{3}(u+v)}{2\sqrt{u^2+v^2+uv}}, \\ \sin(30^\circ - \alpha) = \frac{u-v}{2\sqrt{u^2+v^2+uv}}, \end{cases} \quad (45a)$$

$$\begin{cases} \cos(30^\circ + \alpha) = \frac{\sqrt{3}u}{2\sqrt{u^2+v^2+uv}}, \\ \sin(30^\circ + \alpha) = \frac{2u+v}{2\sqrt{u^2+v^2+uv}}, \end{cases} \quad (45b)$$

and the selection rule

$$\frac{l}{c} = \frac{n}{C} + \frac{m}{\Delta} = \frac{1}{a_0} \left(\frac{n}{\sqrt{u^2+v^2+uv}} \frac{2u+v}{\sqrt{3}v} + m \frac{2\sqrt{u^2+v^2+uv}}{\sqrt{3}v} \right) \quad (46)$$

into equation (44), we then have

$$\begin{aligned} T_{nl} &= f \sum_{j=0}^{v-1} \left\{ \exp \left[2\pi i \left(\frac{nx_j^{(1,0)}}{A} + \frac{lz_j^{(1,0)}}{c} \right) \right] \right\} \left\{ 1 + \exp \left[2\pi i \left(-\frac{n+(u+2v)m}{3v} \right) \right] \right\} \\ &= f \sum_{j=0}^{v-1} \exp \left[2\pi i j \frac{n+(u+v)m}{v} \right] \left\{ 1 + \exp \left[2\pi i \left(-\frac{n+(u+2v)m}{3v} \right) \right] \right\} \\ &= f \frac{1 - \exp\{2\pi i[n+(u+v)m]\}}{1 - \exp[2\pi i[n+(u+v)m]/v]} \left\{ 1 + \exp \left[2\pi i \left(-\frac{n+(u+2v)m}{3v} \right) \right] \right\} \\ &= \begin{cases} vf \left\{ 1 + \exp \left[2\pi i \left(-\frac{n+(u+2v)m}{3v} \right) \right] \right\}, & \text{when } [n+(u+v)m]/v = N \text{ (integer),} \\ 0, & \text{otherwise.} \end{cases} \end{aligned} \quad (47)$$

The structure factor can then be expressed as

$$F_{uv}(R, \Phi, l) = \sum_{n,m} f \chi_{uv}(n, m) \gamma_{uv}(n, m) J_n(\pi d R) \exp \left[i n \left(\Phi + \frac{\pi}{2} \right) \right], \quad (48)$$

where

$$\chi_{uv}(n, m) = 1 + \exp \left[2\pi i \left(-\frac{n+(u+2v)m}{3v} \right) \right] \quad (49)$$

and

$$\gamma_{uv}(n, m) = \begin{cases} v, & \text{when } [n+(u+v)m]/v = N \text{ (integer),} \\ 0, & \text{otherwise,} \end{cases} \quad (50)$$

in which n , m , and l are all integers that are governed by the selection rule for carbon nanotube (u, v) stipulated by equation (36):

$$l = \frac{(2u+v)n + 2(u^2+v^2+uv)m}{Mv}, \quad (51)$$

with M being the maximum common divisor of integers $(u + 2v)$ and $(2u + v)$. Equations (50) and (51) put additional constraints on the values of n , the order of Bessel functions contributing to the layer line l .

Visually, it is the helices which have the smallest angle with respect to the tubule axis that appear as the ‘helices’. For this reason, we can also choose the helices parallel to \vec{a}_2 in the calculation of the structure factor. Inserting the atomic positions for a carbon nanotube (u, v) , the scattering amplitude (33) becomes

$$F_{uv}(R, \Phi, l) = \sum_{n,m} f \chi_{uv}(n, m) \gamma_{uv}(n, m) J_n(\pi d R) \exp \left[i n \left(\Phi + \frac{\pi}{2} \right) \right], \quad (52)$$

where

$$\chi_{uv}(n, m) = 1 + \exp \left[-2\pi i \frac{n + (2u + v)m}{3u} \right] \quad (53)$$

and

$$\gamma_{uv}(n, m) = \frac{1 - \exp[2\pi i(n + vm)]}{1 - \exp[2\pi i(n + vm)/u]} = \begin{cases} u, & \text{if } (n + vm)/u = N, \\ 0, & \text{otherwise,} \end{cases} \quad (54)$$

in which n , m , and l are all integers that are governed by the same selection rule for carbon nanotube (u, v) stipulated by equation (36):

$$l = \frac{(u + 2v)n + 2(u^2 + v^2 + uv)m}{Mu}, \quad (55)$$

with M being the maximum common divisor of integers $(u + 2v)$ and $(2u + v)$. Equation (55) is equivalent to equation (51).

When the helices are counted in the direction of $\vec{a}_3 = \vec{a}_2 - \vec{a}_1$, then

$$F_{uv}(R, \Phi, l) = \sum_{n,m} f \chi_{uv}(n, m) \gamma_{uv}(n, m) J_n(\pi d R) \exp \left[i n \left(\Phi + \frac{\pi}{2} \right) \right], \quad (56)$$

where

$$\chi_{uv}(n, m) = 1 + \exp \left[2\pi i \frac{n - (u + 2v)m}{3(u + v)} \right] \quad (57)$$

and

$$\gamma_{uv}(n, m) = \frac{1 - \exp[2\pi i(n - vm)]}{1 - \exp[2\pi i(n - vm)/(u + v)]} = \begin{cases} u + v, & \text{if } (n - vm)/(u + v) = N, \\ 0, & \text{otherwise} \end{cases} \quad (58)$$

and the selection rule for the same carbon nanotube (u, v) appears as

$$l = \frac{(u - v)n + 2(u^2 + v^2 + uv)m}{M(u + v)}, \quad (59)$$

which is equivalent to equations (51) and (55).

The above equations are also valid for x-rays, when $V(\vec{r})$ and f are replaced by the electron charge density function $\rho(\vec{r})$ and the atomic scattering amplitude for x-rays, $f^{(x)}$, respectively.

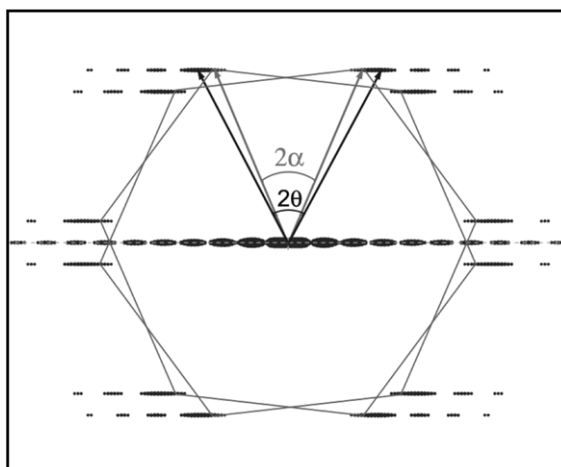


Figure 5. Geometric relationship between the apparent twist angle, θ , measured on an electron diffraction pattern of a carbon nanotube and its true helical angle, α , which usually appears smaller than θ . The cylindrical curvature causes an enlargement of the twist angle, θ .

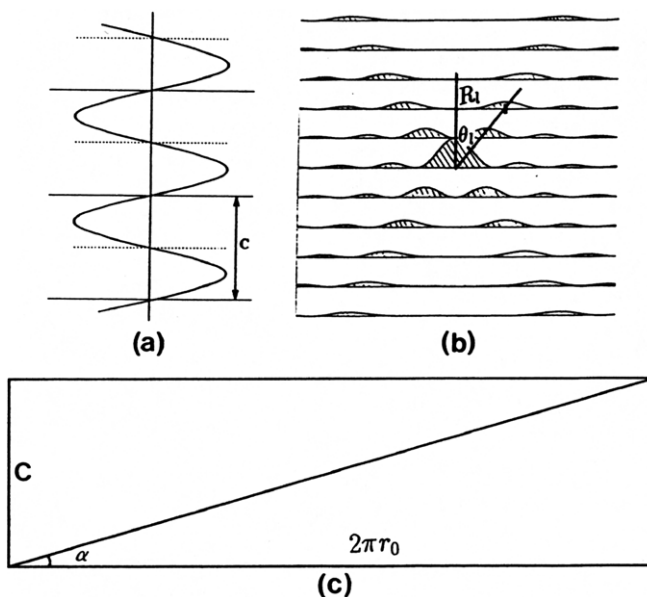


Figure 6. Relationship between the radial projection of a helix and its helical angle for calculating the cylindrical correction factor. (a) A continuous helix of radius r_0 and pitch length C . (b) Corresponding electron diffraction pattern of the helix. θ_l refers to the semi-angle between the first scattering maximum and the axial direction measured on layer line l . (c) Radial projection of the helix.

3.6. Cylindrical correction

As can be seen from equation (33), the geometry of the electron diffraction pattern from a cylindrical nanotube will be different from that of the planar radial projection due to the presence of Bessel functions. Due to the cylindrical curvature and the small diameter of the nanotubes, the graphene reflections are elongated perpendicular to the axial direction to

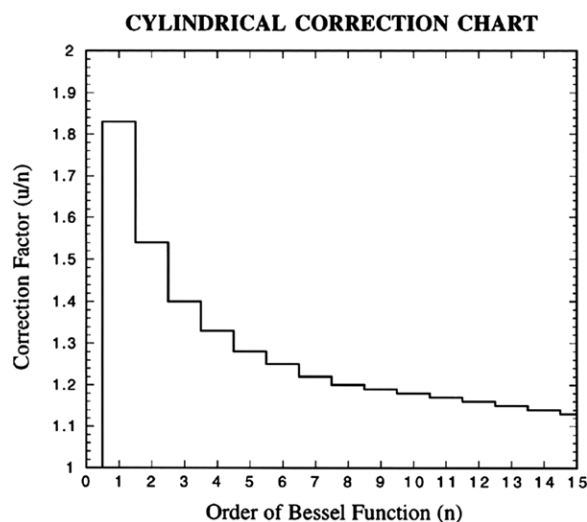


Figure 7. Chart of cylindrical correction factors for various orders of reflections. The correction factor can be as large as 80% for $n = 1$ [113].

become streaks. When measurement is made, as schematically illustrated in figure 5, the twist angle, θ , between the graphene (010) reflections is much larger than the true helical angle, α , of the nanotube. In order to understand the effects on the geometry of electron diffraction patterns from a cylindrical nanotube, for the sake of simplicity but without loss of generality, it is assumed here that there is only one continuous helix as the scattering object as shown in figure 6(a). For this case, as described in section 3.2, the scattering intensities on layer line n are proportional to $|J_n(2\pi r_0 R)|^2$ which is schematically displayed in figure 6(b). In the radial projection, schematically shown in figure 6(c), the helix is the diagonal of a rectangle with width A and height C . The relationship between the apparent twist angle θ measured on the experimental diffraction pattern as shown in figure 6(b) and the true helical angle α can be derived [110]:

$$\tan(\theta) = \frac{R_n}{n/C}. \quad (60)$$

Noticing (cf figure 6(c))

$$\begin{aligned} \frac{R_n}{n/c} &= 2\pi r_0 R_n \frac{C}{2\pi r_0 n} \\ &= \frac{u_n}{n} \tan(\alpha), \end{aligned} \quad (61)$$

we can therefore obtain the relationship between the experimental parameter θ and the true helicity α

$$\tan(\theta) = \frac{u_n}{n} \tan(\alpha), \quad (62)$$

where u_n is the value of u at which the Bessel function $J_n(u)$ assumes its first maximum for $n \neq 0$. The correction factor u_n/n is plotted for various low values of n in figure 7. For instance, the shift for $n = 1$ is about 80%, and for $n = 2$ the shift is about 50%. The large magnitude of the correction factor illustrates that the cylindrical correction cannot be ignored when accurate helicity is sought.

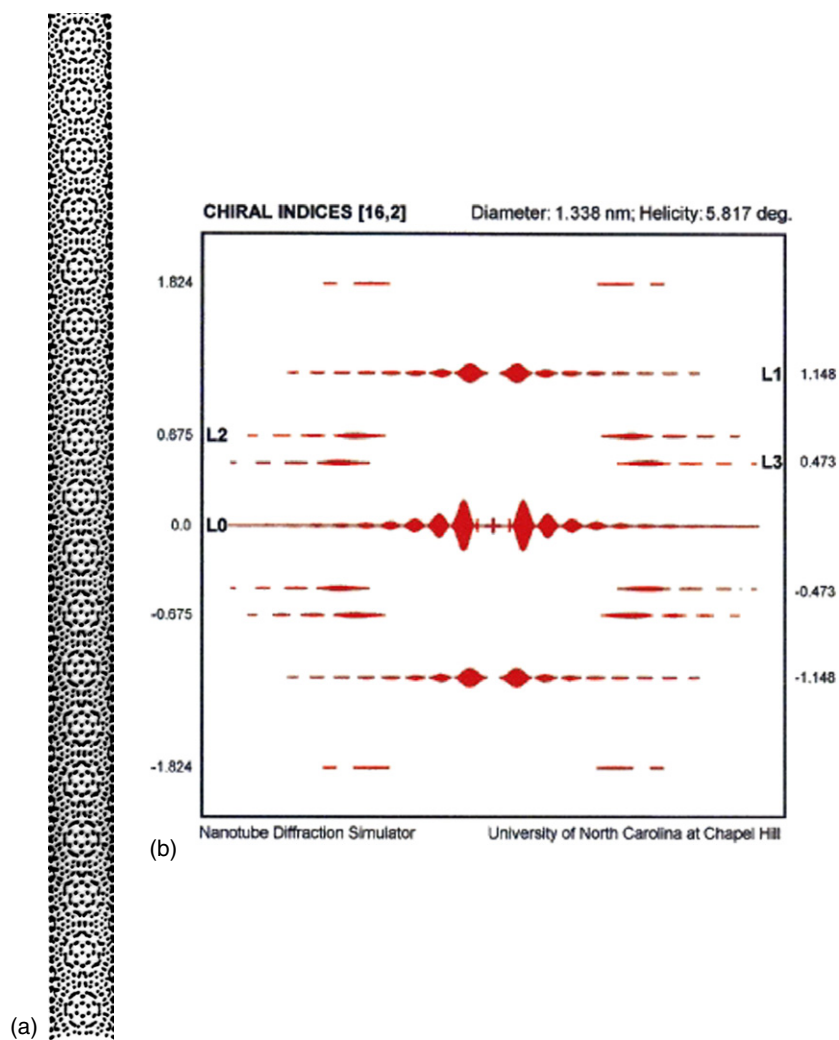


Figure 8. (a) Schematic structure of carbon nanotube (16,2) and (b) its electron diffraction pattern calculated using the kinematical formulae.

3.7. Calculation of electron diffraction patterns

The electron diffraction patterns can be calculated numerically using the analytic equations and the selection rule described in section 3.5. For example, the carbon nanotube of chiral indices (16,2), shown in figure 8(a), has a twofold axis and its axial periodicity is $(-20, 34)$ (along a single helix line). The other structural parameters can also be calculated:

$$\begin{aligned}
 A &= 4.19 \text{ nm}, & d &= 1.33 \text{ nm}, & c &= 7.25 \text{ nm}, \\
 C &= 0.426 \text{ nm}, & \alpha &= 5.8^\circ, & t &= 17, \\
 p &= 292, & \Delta &= 0.0248 \text{ nm}.
 \end{aligned}$$

Applying the selection rule (36) we obtain

$$\begin{aligned}
 \ell = 0, & & n = 0, & & m = 0, \\
 \ell = 2, & & n = 86, & & m = -5, \\
 \ell = 4, & & n = -120, & & m = 7, \\
 \ell = 6, & & n = -34, & & m = 2, \\
 \ell = 8, & & n = 52, & & m = -3, \\
 \ell = 10, & & n = 138, & & m = -8, \\
 \ell = 12, & & n = 68, & & m = -4, \\
 & \dots & & & \\
 \ell = 34, & & n = 2, & & m = 0, \\
 \ell = 68, & & n = 4, & & m = 0, \\
 \ell = 102, & & n = 6, & & m = 0, \\
 & \dots & & &
 \end{aligned}$$

The calculated electron diffraction pattern is shown in figure 8(b).

Though a rigorous calculation should include all the terms allowed by the selection rule in the summation given by equation (33), usually only one term dominates the scattering amplitude on each layer line as shown in section 4. This will greatly simplify the numerical simulations as well as the interpretation of the electron diffraction patterns of carbon nanotubes.

3.8. Electron diffraction from multiwalled carbon nanotubes

An ideal multiwalled carbon nanotube consists of multiple concentric shells with inter-tubular distances similar to the inter-planar spacings of graphite (~ 0.335 nm). The structure factor for a multiwalled carbon nanotube of N shells can be expressed as the coherent sum of the scattering amplitudes from all individual shells in the multiwalled carbon nanotube [150]:

$$\begin{aligned}
 F(R, \Phi, Z) = & \sum_{j=1}^N f \delta \left(Z - \frac{l_j}{c_j} \right) \sum_{n,m} \chi_j(n, m) \gamma_j(n, m) J_n(\pi d_j R) \\
 & \times \exp \left[i n \left(\Phi + \frac{\pi}{2} \right) \right] \exp(i\varphi_j), \quad (63)
 \end{aligned}$$

where j denotes the j th nanotube (u_j, v_j) of axial periodicity c_j and diameter d_j , φ_j denotes the phase shift for the j th shell relative to the reference shell in real space and

$$\chi_j(n, m) = 1 + \exp \left\{ -2\pi i \frac{n + (u_j + 2v_j)m}{3v_j} \right\}, \quad (64)$$

$$\gamma_j(n, m) = \frac{1 - \exp[-2\pi i(n + (u_j + v_j)m)]}{1 - \exp \left[-2\pi i \frac{(u_j + v_j)m}{v_j} \right]} = \begin{cases} v_j, & \text{if } \frac{n + (u_j + v_j)m}{v_j} = \text{integer}, \\ 0, & \text{otherwise} \end{cases} \quad (65)$$

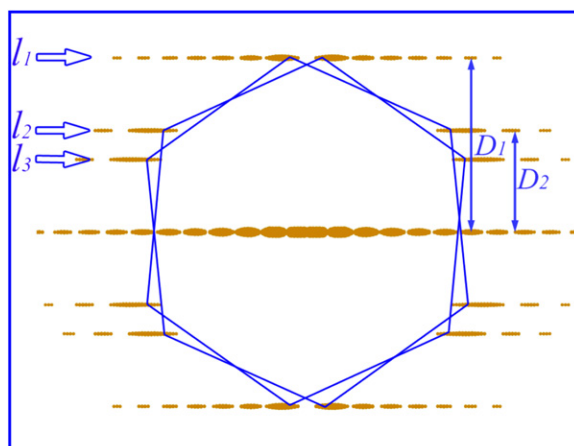


Figure 9. Relationship between the principal graphene reflections (positioned at the six apices of the regular hexagons) and the principal layer line reflections l_1 , l_2 and l_3 of a carbon nanotube. D_1 and D_2 are the respective layer line spacings.

in which n , m and l_j are all integers governed by the selection rule for the j th shell of the nanotube:

$$l_j = \frac{(2u_j + v_j)n + 2(u_j^2 + v_j^2 + u_j v_j)m}{M_j v_j}, \quad (66)$$

with M_j being the maximum common divisor of $(u_j + 2v_j)$ and $(2u_j + v_j)$.

The electron diffraction intensity distribution is $I(R, \Phi, Z) = |F(R, \Phi, Z)|^2$.

As a special case, for electron diffraction from single-walled carbon nanotubes, the summation over j in equation (63) disappears ($N = 1$) and so does the subscript j in equations (64)–(66).

4. Determination of chiral indices of carbon nanotubes

4.1. Principal layer lines

In order to determine the atomic structure of a carbon nanotube, it is necessary to determine the chiral indices (u, v) that in turn determine the diameter and helicity of the nanotube. Traditionally, using transmission electron microscopy, the diameter has been measured directly from high-resolution electron micrographs and the helicity is deduced from the electron diffraction patterns. As discussed in section 3, the electron diffraction pattern of a single-walled carbon nanotube has the primary graphene reflections as the strongest intensity peaks. These reflections form three pairs of layer lines, labelled as l_1 (formed by the graphene (010) reflections), l_2 (formed by the graphene ($\bar{1}00$) reflections) and l_3 (formed by the graphene (110) reflections) with layer line spacings with respect to the equatorial layer line denoted by D_1 , D_2 and D_3 , and they are referred to as the principal layer lines and are schematically illustrated in figure 9. It is experimentally most convenient to use these principal layer lines to characterize the carbon nanotube.

4.2. Direct method

It is important to note that on each layer line, though the scattering amplitude is described by a summation of all Bessel functions that are allowed by the selection rule, there is usually only one order of Bessel function that dominates the intensity distribution on this particular layer line. All the others contribute negligibly to the layer line intensity. We can deduce the above conclusion from the selection rule. Under the constraints governed by the selection rule, all the possible values of n for one chosen layer line l can be expressed as follows [151]:

$$n = n_0 + \frac{2P(u^2 + v^2 + uv)}{M}, \quad (67)$$

where P are positive integers that make n also an integer and n_0 defines the smallest non-negative integer for the chosen layer line l . Because $(u^2 + v^2 + uv)/M$ is always an integer [152], $2P(u^2 + v^2 + uv)/M$ is usually a very large number. Since the magnitude of Bessel functions decreases significantly with the increase of their orders, the diffraction intensity on a particular layer line is essentially dominated by a single Bessel function of the lowest order n_0 . For example, for single-walled carbon nanotube (14,9) (diameter $d = 1.572$ nm and helicity $\alpha = 22.84^\circ$, respectively) for the principal layer line l_1 ($l = 37$), $n_0 = 9$ and the next contributing Bessel function is $n = 797$. The magnitude of the first peak for $|J_9(x)|^2$ is more than 20 times of that for $|J_{797}(x)|^2$. Furthermore, the first peak position on the specified layer line for $J_{797}(x)$ is 75 times larger than that for $J_9(x)$. Therefore, the diffraction intensity distribution on the layer line $l = 37$ for single-walled carbon nanotube (14,9) is only modulated by $|J_9(x)|^2$ within the range of collection where significant experimental data are present in the reciprocal space.

The order of the single operating Bessel function for a given carbon nanotube (u, v) can be obtained by considering the crystallographic indices of the graphene reflections using the extended cell of the nanotube in radial projection which is related to the index n . In the Fraunhofer diffraction pattern of the graphene lattice, the allowed Bragg reflections are described by

$$\vec{g} = h\vec{a}_1^* + k\vec{a}_2^*. \quad (68)$$

For a given nanotube of chiral indices (u, v), the corresponding nanotube reflections can also be indexed by the crystallographic indices (n, l) related to its radial projection net. Therefore the selection rule should be such that the reflection $\vec{G} = n\vec{A}^* + l\vec{B}^*$ indexed using the radial projection net should fall onto the reciprocal lattice point \vec{g} indexed using the graphene lattice, where \vec{A}^* and \vec{B}^* are the basis vectors of the reciprocal lattice of the radial projection net (rectangle with sides \vec{A} and \vec{B}) of the nanotube:

$$\begin{aligned} \vec{A}^* &= \frac{1}{u^2 + v^2 + uv} (u\vec{a}_1 + v\vec{a}_2), \\ \vec{B}^* &= \frac{1}{u_c^2 + v_c^2 + u_c v_c} (u_c\vec{a}_1 + v_c\vec{a}_2). \end{aligned} \quad (69)$$

The selection rule can then be stated as

$$\vec{G} = \vec{g} \quad (70)$$

or

$$n\vec{A}^* + l\vec{B}^* = h\vec{a}_1^* + k\vec{a}_2^*. \quad (71)$$

Multiplying both sides of equation (71) by \vec{a}_1 , we obtain

$$n\vec{A}^* \cdot \vec{a}_1 + l\vec{B}^* \cdot \vec{a}_1 = h \quad (72)$$

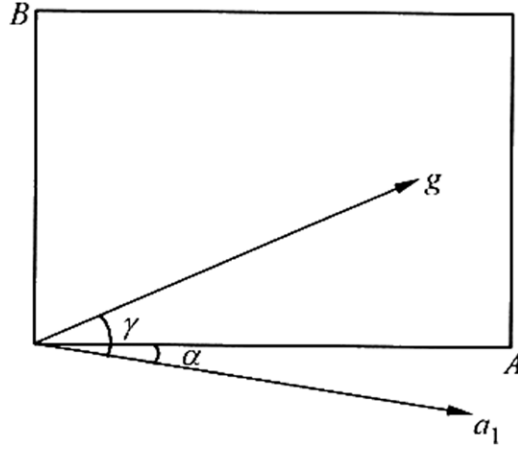


Figure 10. Schematic assisting the deduction of the order of the operating Bessel function on a carbon nanotube of chiral indices (u, v) . \mathbf{a}_1 is the basis vector and \mathbf{g} refers to a particular reflection of interest. \mathbf{A} is the perimeter vector and \mathbf{B} is the axial unit vector of the nanotube. α is the helical angle of the nanotube and γ is the angle between the \mathbf{g} vector and the basis vector \mathbf{a}_1 .

or equivalently

$$\frac{na \cos(\alpha)}{A} - lB^* \sin(\alpha) = h. \quad (73)$$

Noting that (cf figure 10)

$$lB^* = g \sin(\gamma - \alpha), \quad (74)$$

where γ is the angle between the basis vector \vec{a}_1 and the concerned graphene reflection (hk) , then we can obtain the following relationship [113]

$$n = hu + kv. \quad (75)$$

As shown in figure 9, the three principal layer lines l_1 , l_2 and l_3 are formed by graphene reflections (01) , $(\bar{1}0)$ and (110) , respectively. When choosing the reference graphene reflection as (01) , i.e. $h = 0$ and $k = 1$, the order of the dominating Bessel function is

$$n = v, \quad (76)$$

for graphene reflection $(\bar{1}0)$

$$n = -u \quad (77)$$

and for graphene reflection (110)

$$n = u + v. \quad (78)$$

Therefore, the contributing Bessel functions to the three principal layer lines are of orders v , $-u$ and $u + v$, respectively.

The order of the dominant Bessel function on each of the principal layer lines can also be understood by the formation of the electron diffraction pattern from the three principal helices that are parallel to \vec{a}_1 , \vec{a}_2 and $\vec{a}_3 = \vec{a}_2 - \vec{a}_1$, respectively. As discussed in section 3, the numbers of helix pairs are v , u and $u + v$, respectively. From figure 9, one can see that the three principal layer lines correspond to these three helix pairs. Therefore, the first non-extinction reflections due to these three principal helices are expressed by the Bessel functions of order v , u and $u + v$, respectively.

Table 1. Ratio of the second and the first peak positions of Bessel functions.

n	X_2/X_1	n	X_2/X_1	n	X_2/X_1
1	2.892	11	1.373	21	1.239
2	2.197	12	1.350	22	1.232
3	1.907	13	1.332	23	1.226
4	1.751	14	1.315	24	1.218
5	1.639	15	1.301	25	1.211
6	1.565	16	1.287	26	1.206
7	1.507	17	1.275	27	1.201
8	1.465	18	1.266	28	1.196
9	1.428	19	1.256	29	1.192
10	1.398	20	1.247	30	1.188

The same conclusion can also be reached algebraically from the selection rule [122].

Therefore, the reflection intensities of the three principal layer lines, designated as layer line l_1 , l_2 and l_3 as indicated in figure 9, are related to the chiral indices u and v by

$$I_{l_1}(R) \propto |J_v(\pi dR)|^2, \quad (79)$$

$$I_{l_2}(R) \propto |J_u(\pi dR)|^2 \quad (80)$$

and

$$I_{l_3}(R) \propto |J_{u+v}(\pi dR)|^2. \quad (81)$$

The principal layer lines l_1 , l_2 and l_3 are schematically illustrated in figure 9.

The order n of Bessel function $J_n(X)$ can be determined by examining the positions of its peaks, which are unique to each Bessel function. An efficient and convenient means to determine the order n of Bessel function $J_n(X)$ is to examine the ratio X_2/X_1 of the positions of its first two peaks located at X_1 and X_2 , respectively, or any other pair of peaks unique to this Bessel function. Once the orders of the respective Bessel functions are determined, the chiral indices, u and v , are obtained directly. The chiral indices (u, v) can therefore be obtained directly by determining the order of Bessel functions $J_v(X)$ and $J_u(X)$ with $X = \pi dR$ from the scattering intensity distribution on layer lines l_1 and l_2 , whose intensities are proportional to $|J_v(\pi dR)|^2$ and $|J_u(\pi dR)|^2$, respectively. On the experimental diffraction pattern, the positions of the first two peaks, R_1 and R_2 , can be measured and the ratio $R_2/R_1 = X_2/X_1$ is independent of the camera length of the electron microscope at which the electron diffraction pattern is acquired.

This method allows a rapid and accurate assignment of the chiral indices (u, v). From the ratios $R_2/R_1 = X_2/X_1$ measured directly from the electron diffraction pattern, the indices v and u can be obtained from the tabulated values given in table 1. For Bessel functions $J_{18}(X)$ and $J_{19}(X)$, for example, the ratios of $X_2/X_1 = R_2/R_1$ are 1.266 and 1.256, respectively, the difference is large enough to be identified unambiguously. Using our current method, we can obtain the peak positions with a precision of 0.3%, which allows us to assign the chiral indices unambiguously up to index 30 or nanotube diameter up to 4 nm.

For non-helical nanotubes, i.e. zigzag and armchair nanotubes with chiral indices ($u, 0$) and (u, u), respectively, overlap of the principal layer lines occurs. For a zigzag nanotube of indices ($u, 0$), layer lines l_2 and l_3 overlap with each other and its first principal layer line (l_1) has intensity distribution proportional to $|J_0(\pi dR)|^2$ and the second layer line (l_2) has intensity proportional to $|J_u(\pi dR)|^2$. For an armchair nanotube (u, u), the first layer line l_1 and the

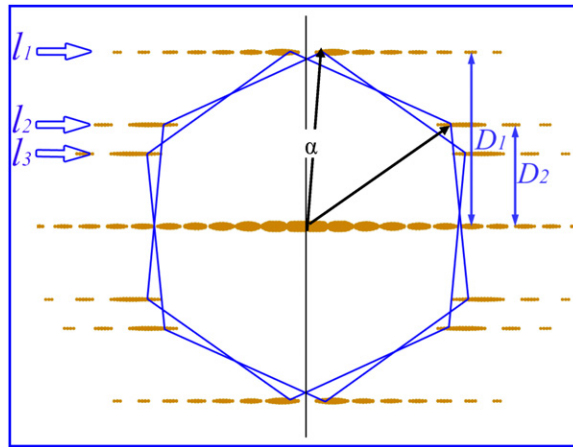


Figure 11. Schematic diffraction pattern of a carbon nanotube of helical angle α —the layer line spacings D_1 , D_2 , etc are not affected by the curvature of the nanotube. Spotty graphene reflections become streaks elongated in the directions perpendicular to the tubule axis.

second line l_2 overlap with intensities proportional to $|J_u(\pi dR)|^2$ and layer line l_3 falls on the equatorial line.

The major sources of error of this direct method are (a) low signal/noise ratio due to the small number of atoms in the scattering carbon nanotube and (b) the identification of the peak positions in the intensity distribution on the principal layer lines. The signal/noise ratio can be enhanced by applying longer exposure in acquiring the experimental electron diffraction pattern.

4.3. Ratio of indices v/u

Since the atomic structure of carbon nanotube (u, v) is periodic in the axial direction, the layer lines are sharp and the respective layer line spacings D_1 , D_2 and D_3 can be measured accurately from the electron diffraction pattern. Although the cylindrical curvature of the nanotube causes severe distortion to the otherwise hexagonal electron diffraction pattern, the layer line spacings will not change due to the cylindrical curvature. The axial distances to the equatorial line of the fundamental reflections that give rise to the principal layers lines can be calculated using the trigonometric relations illustrated in figure 11:

$$\begin{cases} D_1 = a^* \sin(90^\circ - \alpha) = a^* \cos(\alpha), \\ D_2 = a^* \sin(30^\circ + \alpha), \end{cases} \quad (82)$$

then the helical angle α can be deduced from the ratios of the layer line spacings [120]

$$\alpha = \tan^{-1} \left(\frac{2D_2 - D_1}{\sqrt{3}D_1} \right), \quad (83)$$

and the ratio of the chiral indices u and v is given by [124]

$$\frac{v}{u} = \frac{2D_2 - D_1}{2D_1 - D_2}. \quad (84)$$

Equation (84) offers a more convenient method to determine the chiral indices (u, v) for the following reasons.

- (a) The ratio is independent of the camera length at which the electron diffraction pattern is taken.
- (b) The ratio is independent of the relative orientation between the nanotube and the incident electron beam.
- (c) When the signal/noise ratio is low, this ratio can still be conveniently obtained.

The use of equation (84) can result in a very high accuracy. The indeterminacy arising from the uncertainties due to equation (84) leads to only the nanotube of the smallest diameter (u_0, v_0) . Other nanotubes meeting the same equation have chiral indices that are multiples of (u_0, v_0) , i.e. $(u, v) = (mu_0, mv_0)$, where $m = 1, 2, 3, \dots$. Table 2 lists all possible v/u ratios for chiral indices (u, v) up to $(30, 30)$. As can be seen from the possible indices, the largest uncertainty comes from the nanotubes of chiral indices of $(2v, v)$, where the difference in diameter between the neighbouring shells is 0.207 nm. This diameter difference can be discerned from other information such as the real-space electron micrographs.

4.4. Examples: single-walled carbon nanotubes

The methods described in sections 4.2 and 4.3 offer quick and accurate experimental determination of the chiral indices of single-walled carbon nanotubes. In order to minimize radiation damage to the carbon nanotubes, it is advisable to operate the transmission electron microscope at 80 kV. On the JEM-2010F TEM equipped with a field emission gun, the nanobeam electron diffraction patterns were acquired with a parallel beam of 20 nm spot size obtained with the smallest 10 μm condenser aperture and by exciting the first condenser lens to maximum [152]. The nanobeam electron diffraction patterns were recorded either directly with a CCD camera or first on photographic films which were later scanned digitally to obtain a more accurate measurement of the intensity distribution on the concerned layer lines. Figure 12(a) shows a nanobeam electron diffraction pattern of a single-walled carbon nanotube of diameter about 1.4 nm (high-resolution electron microscope image is given as an inset with a 2 nm scale bar). From the intensity profiles on the three principal layer lines (l_1, l_2 and l_3), the ratios $R_2/R_1 = X_2/X_1$ on layer line l_1 and l_2 (figures 12(b) and (c)) were measured to be 2.200 and 1.279, respectively. The orders of Bessel functions, and thus the chiral indices of the nanotube, were determined to be $v = 2$ and $u = 17$ (cf, table 1). Nanotube (17,2) is a metallic nanotube of diameter 1.418 nm and helicity 5.47° . Figure 13 shows the electron diffraction pattern obtained from another nanotube of similar diameter (image shown as inset with scale bar 2 nm). Using the same method, the chiral indices for this single-walled carbon nanotube were determined to be (17,1), which is a semiconducting tubule of diameter 1.374 nm and helicity 2.83° .

When the diameter of the nanotube is large, the ratio of X_2 and X_1 for a Bessel function is closer to that of its neighbours. In this case, layer lines l_3 (formed by the graphene (110) reflections) and/or l_4 (formed by the $(\bar{1}10)$ graphene reflections) whose intensity profiles correspond to $|J_{u+v}(\pi dR)|^2$ and $|J_{u-v}(\pi dR)|^2$, respectively, can be used as supplementary information to narrow down the choices and minimize the possible errors.

Given the experimental limitations, using the ratio of layer line spacings (equation 84) would give rise to results of highest accuracy. The major errors in the measurement of helicity come from the uncertainties in the measurement of the layer line spacings D_1 and D_2 . In our

Table 2. v/u ratios.

v/u	u	v	d (nm)	alpha	v/u	u	v	d (nm)	alpha	v/u	u	v	d (nm)	alpha	v/u	u	v	d (nm)	alpha
0.0000	u	0	—	0.000	0.1538	13	2	1.105	7.053	0.2759	29	8	2.640	11.857	0.4000	5	2	0.489	16.102
0.0333	30	1	2.389	1.626	0.1538	26	4	2.209	7.053	0.2778	18	5	1.641	11.927	0.4000	10	4	0.978	16.102
0.0345	29	1	2.311	1.682	0.1579	19	3	1.618	7.223	0.2800	25	7	2.282	12.008	0.4000	15	6	1.467	16.102
0.0357	28	1	2.233	1.740	0.1600	25	4	2.132	7.311	0.2857	7	2	0.641	12.216	0.4000	20	8	1.956	16.102
0.0370	27	1	2.154	1.804	0.1667	6	1	0.513	7.589	0.2857	14	4	1.282	12.216	0.4000	25	10	2.445	16.102
0.0385	26	1	2.076	1.872	0.1667	12	2	1.027	7.589	0.2857	21	6	1.923	12.216	0.4000	30	12	2.934	16.102
0.0400	25	1	1.998	1.945	0.1667	18	3	1.540	7.589	0.2857	28	8	2.564	12.216	0.4074	27	11	2.652	16.337
0.0417	24	1	1.920	2.024	0.1667	24	4	2.054	7.589	0.2917	24	7	2.205	12.432	0.4091	22	9	2.163	16.390
0.0435	23	1	1.841	2.111	0.1667	30	5	2.567	7.589	0.2941	17	5	1.564	12.520	0.4118	17	7	1.674	16.474
0.0455	22	1	1.763	2.204	0.1724	29	5	2.490	7.827	0.2963	27	8	2.487	12.598	0.4138	29	12	2.859	16.537
0.0476	21	1	1.685	2.307	0.1739	23	4	1.976	7.889	0.3000	10	3	0.923	12.730	0.4167	12	5	1.185	16.627
0.0500	20	1	1.607	2.419	0.1765	17	3	1.463	7.994	0.3000	20	6	1.846	12.730	0.4167	24	10	2.370	16.627
0.0526	19	1	1.528	2.543	0.1786	28	5	2.412	8.080	0.3000	30	9	2.770	12.730	0.4211	19	8	1.881	16.764
0.0556	18	1	1.450	2.680	0.1818	11	2	0.949	8.213	0.3043	23	7	2.129	12.885	0.4231	26	11	2.577	16.826
0.0588	17	1	1.372	2.833	0.1818	22	4	1.899	8.213	0.3077	13	4	1.205	13.004	0.4286	7	3	0.696	16.996
0.0625	16	1	1.294	3.004	0.1852	27	5	2.335	8.350	0.3077	26	8	2.411	13.004	0.4286	14	6	1.392	16.996
0.0667	15	1	1.216	3.198	0.1875	16	3	1.385	8.445	0.3103	29	9	2.693	13.098	0.4286	21	9	2.088	16.996
0.0667	30	2	2.431	3.198	0.1905	21	4	1.821	8.565	0.3125	16	5	1.488	13.174	0.4286	28	12	2.784	16.996
0.0690	29	2	2.353	3.304	0.1923	26	5	2.257	8.639	0.3158	19	6	1.770	13.289	0.4333	30	13	2.991	17.142
0.0714	14	1	1.137	3.418	0.2000	5	1	0.436	8.948	0.3182	22	7	2.052	13.373	0.4348	23	10	2.295	17.187
0.0714	28	2	2.275	3.418	0.2000	10	2	0.872	8.948	0.3200	25	8	2.335	13.436	0.4375	16	7	1.599	17.269
0.0741	27	2	2.197	3.540	0.2000	15	3	1.308	8.948	0.3214	28	9	2.617	13.486	0.4400	25	11	2.502	17.345
0.0769	13	1	1.059	3.670	0.2000	20	4	1.744	8.948	0.3333	3	1	0.282	13.898	0.4444	9	4	0.903	17.480
0.0769	26	2	2.119	3.670	0.2000	25	5	2.180	8.948	0.3333	6	2	0.565	13.898	0.4444	18	8	1.806	17.480
0.0800	25	2	2.040	3.811	0.2000	30	6	2.616	8.948	0.3333	9	3	0.847	13.898	0.4444	27	12	2.709	17.480
0.0833	12	1	0.981	3.963	0.2069	29	6	2.539	9.223	0.3333	12	4	1.129	13.898	0.4483	29	13	2.916	17.596
0.0833	24	2	1.962	3.963	0.2083	24	5	2.103	9.280	0.3333	15	5	1.412	13.898	0.4500	20	9	2.013	17.647
0.0870	23	2	1.884	4.128	0.2105	19	4	1.667	9.367	0.3333	18	6	1.694	13.898	0.4545	11	5	1.110	17.784

Table 2. (Continued.)

v/u	u	v	d (nm)	alpha	v/u	u	v	d (nm)	alpha	v/u	u	v	d (nm)	alpha	v/u	u	v	d (nm)	alpha
0.0909	11	1	0.903	4.307	0.2143	14	3	1.231	9.515	0.3333	21	7	1.976	13.898	0.4545	22	10	2.220	17.784
0.0909	22	2	1.806	4.307	0.2143	28	6	2.461	9.515	0.3333	24	8	2.259	13.898	0.4583	24	11	2.427	17.897
0.0952	21	2	1.728	4.502	0.2174	23	5	2.025	9.637	0.3333	27	9	2.541	13.898	0.4615	13	6	1.317	17.992
0.1000	10	1	0.825	4.715	0.2222	9	2	0.795	9.826	0.3333	30	10	2.823	13.898	0.4615	26	12	2.635	17.992
0.1000	20	2	1.650	4.715	0.2222	18	4	1.589	9.826	0.3448	29	10	2.747	14.290	0.4643	28	13	2.842	18.073
0.1000	30	3	2.475	4.715	0.2222	27	6	2.384	9.826	0.3462	26	9	2.465	14.335	0.4667	15	7	1.524	18.143
0.1034	29	3	2.397	4.869	0.2273	22	5	1.948	10.023	0.3478	23	8	2.183	14.392	0.4667	30	14	3.049	18.143
0.1053	19	2	1.572	4.950	0.2308	13	3	1.153	10.158	0.3500	20	7	1.900	14.465	0.4706	17	8	1.732	18.258
0.1071	28	3	2.319	5.033	0.2308	26	6	2.307	10.158	0.3529	17	6	1.618	14.564	0.4737	19	9	1.939	18.349
0.1111	9	1	0.747	5.209	0.2333	30	7	2.666	10.257	0.3571	14	5	1.336	14.705	0.4762	21	10	2.146	18.422
0.1111	18	2	1.494	5.209	0.2353	17	4	1.512	10.333	0.3571	28	10	2.672	14.705	0.4783	23	11	2.353	18.482
0.1111	27	3	2.241	5.209	0.2381	21	5	1.871	10.440	0.3600	25	9	2.389	14.800	0.4800	25	12	2.560	18.533
0.1154	26	3	2.163	5.397	0.2400	25	6	2.230	10.513	0.3636	11	4	1.053	14.921	0.4815	27	13	2.767	18.576
0.1176	17	2	1.416	5.496	0.2414	29	7	2.589	10.566	0.3636	22	8	2.107	14.921	0.4828	29	14	2.975	18.613
0.1200	25	3	2.085	5.599	0.2500	4	1	0.359	10.893	0.3667	30	11	2.878	15.021	0.5000	2	1	0.207	19.107
0.1250	8	1	0.669	5.818	0.2500	8	2	0.718	10.893	0.3684	19	7	1.825	15.079	0.5000	4	2	0.414	19.107
0.1250	16	2	1.338	5.818	0.2500	12	3	1.077	10.893	0.3704	27	10	2.596	15.143	0.5000	6	3	0.622	19.107
0.1250	24	3	2.007	5.818	0.2500	16	4	1.435	10.893	0.3750	8	3	0.771	15.295	0.5000	8	4	0.829	19.107
0.1304	23	3	1.929	6.053	0.2500	20	5	1.794	10.893	0.3750	16	6	1.542	15.295	0.5000	10	5	1.036	19.107
0.1333	15	2	1.260	6.178	0.2500	24	6	2.153	10.893	0.3750	24	9	2.314	15.295	0.5000	12	6	1.243	19.107
0.1333	30	4	2.520	6.178	0.2500	28	7	2.512	10.893	0.3793	29	11	2.803	15.436	0.5000	14	7	1.450	19.107
0.1364	22	3	1.851	6.309	0.2593	27	7	2.435	11.242	0.3810	21	8	2.031	15.490	0.5000	16	8	1.657	19.107
0.1379	29	4	2.443	6.376	0.2609	23	6	2.076	11.302	0.3846	13	5	1.260	15.608	0.5000	18	9	1.865	19.107
0.1429	7	1	0.591	6.587	0.2632	19	5	1.717	11.387	0.3846	26	10	2.520	15.608	0.5000	20	10	2.072	19.107
0.1429	14	2	1.182	6.587	0.2667	15	4	1.359	11.517	0.3889	18	7	1.749	15.746	0.5000	22	11	2.279	19.107
0.1429	21	3	1.774	6.587	0.2667	30	8	2.717	11.517	0.3913	23	9	2.238	15.824	0.5000	24	12	2.486	19.107
0.1429	28	4	2.365	6.587	0.2692	26	7	2.358	11.612	0.3929	28	11	2.727	15.874	0.5000	26	13	2.693	19.107
0.1481	27	4	2.287	6.812	0.2727	11	3	1.000	11.742	—	—	—	—	—	0.5000	28	14	2.900	19.107

Table 2. (Continued.)

v/u	u	v	d (nm)	alpha	v/u	u	v	d (nm)	alpha	v/u	u	v	d (nm)	alpha	v/u	u	v	d (nm)	alpha
0.1500	20	3	1.696	6.890	0.2727	22	6	1.999	11.742	—	—	—	—	—	0.5000	30	15	3.108	19.107
0.5172	29	15	3.034	19.591	0.6364	11	7	1.231	22.689	0.7500	4	3	0.476	25.285	0.8500	20	17	2.512	27.320
0.5185	27	14	2.827	19.626	0.6364	22	14	2.461	22.689	0.7500	8	6	0.953	25.285	0.8519	27	23	3.394	27.355
0.5200	25	13	2.619	19.667	0.6400	25	16	2.803	22.777	0.7500	12	9	1.429	25.285	0.8571	7	6	0.882	27.457
0.5217	23	12	2.412	19.715	0.6429	14	9	1.572	22.846	0.7500	16	12	1.905	25.285	0.8571	14	12	1.765	27.457
0.5238	21	11	2.205	19.773	0.6429	28	18	3.144	22.846	0.7500	20	15	2.382	25.285	0.8571	21	18	2.647	27.457
0.5263	19	10	1.998	19.842	0.6471	17	11	1.913	22.947	0.7500	24	18	2.858	25.285	0.8571	28	24	3.530	27.457
0.5294	17	9	1.791	19.927	0.6500	20	13	2.255	23.018	0.7500	28	21	3.334	25.285	0.8621	29	25	3.665	27.551
0.5333	15	8	1.584	20.034	0.6522	23	15	2.596	23.070	0.7500	24	18	2.858	25.285	0.8636	22	19	2.783	27.581
0.5333	30	16	3.167	20.034	0.6538	26	17	2.937	23.110	0.7586	29	22	3.469	25.469	0.8667	15	13	1.900	27.638
0.5357	28	15	2.960	20.099	0.6552	29	19	3.278	23.141	0.7600	25	19	2.993	25.498	0.8696	23	20	2.918	27.693
0.5385	13	7	1.376	20.174	0.6667	3	2	0.341	23.413	0.7600	25	19	2.993	25.498	0.8750	8	7	1.018	27.796
0.5385	26	14	2.753	20.174	0.6667	6	4	0.683	23.413	0.7619	21	16	2.517	25.539	0.8750	16	14	2.036	27.796
0.5417	24	13	2.546	20.260	0.6667	9	6	1.024	23.413	0.7647	17	13	2.040	25.598	0.8750	24	21	3.054	27.796
0.5455	11	6	1.169	20.363	0.6667	12	8	1.365	23.413	0.7667	30	23	3.605	25.639	0.8800	25	22	3.189	27.889
0.5455	22	12	2.339	20.363	0.6667	15	10	1.707	23.413	0.7692	13	10	1.564	25.693	0.8824	17	15	2.171	27.933
0.5500	20	11	2.132	20.485	0.6667	18	12	2.048	23.413	0.7692	26	20	3.128	25.693	0.8846	26	23	3.325	27.975
0.5517	29	16	3.094	20.531	0.6667	21	14	2.389	23.413	0.7727	22	17	2.652	25.767	0.8889	9	8	1.153	28.055
0.5556	9	5	0.962	20.633	0.6667	24	16	2.731	23.413	0.7778	9	7	1.088	25.872	0.8889	18	16	2.307	28.055
0.5556	18	10	1.924	20.633	0.6667	27	18	3.072	23.413	0.7778	18	14	2.176	25.872	0.8889	27	24	3.460	28.055
0.5556	27	15	2.887	20.633	0.6667	30	20	3.413	23.413	0.7778	27	21	3.264	25.872	0.8929	28	25	3.596	28.128
0.5600	25	14	2.680	20.751	0.6786	28	19	3.207	23.691	0.7778	27	21	3.264	25.872	0.8947	19	17	2.443	28.163
0.5625	16	9	1.717	20.817	0.6800	25	17	2.865	23.724	0.7826	23	18	2.787	25.972	0.8966	29	26	3.732	28.196
0.5652	23	13	2.472	20.889	0.6818	22	15	2.524	23.766	0.7857	14	11	1.699	26.037	0.9000	10	9	1.289	28.259
0.5667	30	17	3.228	20.927	0.6842	19	13	2.183	23.822	0.7857	28	22	3.399	26.037	0.9000	20	18	2.578	28.259
0.5714	7	4	0.755	21.052	0.6842	19	13	2.183	23.822	0.7857	28	22	3.399	26.037	0.9000	30	27	3.867	28.259
0.5714	14	8	1.510	21.052	0.6875	16	11	1.841	23.897	0.7895	19	15	2.311	26.114	0.9048	21	19	2.714	28.346
0.5714	21	12	2.265	21.052	0.6897	29	20	3.341	23.947	0.7917	24	19	2.923	26.159	0.9091	11	10	1.425	28.425

Table 2. (Continued.)

v/u	u	v	d (nm)	alpha	v/u	u	v	d (nm)	alpha	v/u	u	v	d (nm)	alpha	v/u	u	v	d (nm)	alpha
0.5714	28	16	3.021	21.052	0.6923	13	9	1.500	24.007	0.7931	29	23	3.534	26.189	0.9091	22	20	2.849	28.425
0.5769	26	15	2.814	21.195	0.6923	26	18	3.000	24.007	0.7931	29	23	3.534	26.189	0.9130	23	21	2.985	28.497
0.5789	19	11	2.058	21.247	0.6957	23	16	2.659	24.084	0.8000	5	4	0.612	26.329	0.9167	12	11	1.560	28.562
0.5833	12	7	1.303	21.361	0.7000	10	7	1.159	24.182	0.8000	10	8	1.223	26.329	0.9167	24	22	3.120	28.562
0.5833	24	14	2.606	21.361	0.7000	20	14	2.318	24.182	0.8000	15	12	1.835	26.329	0.9200	25	23	3.256	28.622
0.5862	29	17	3.155	21.435	0.7000	30	21	3.476	24.182	0.8000	20	16	2.446	26.329	0.9231	13	12	1.696	28.677
0.5882	17	10	1.851	21.487	0.7000	20	14	2.318	24.182	0.8000	25	20	3.058	26.329	0.9231	26	24	3.392	28.677
0.5909	22	13	2.399	21.555	0.7037	27	19	3.135	24.266	0.8000	30	24	3.669	26.329	0.9259	27	25	3.527	28.728
0.5926	27	16	2.948	21.598	0.7059	17	12	1.976	24.315	0.8000	30	24	3.669	26.329	0.9286	14	13	1.831	28.775
0.6000	5	3	0.548	21.787	0.7083	24	17	2.794	24.370	0.8077	26	21	3.193	26.485	0.9286	28	26	3.663	28.775
0.6000	10	6	1.096	21.787	0.7143	7	5	0.818	24.504	0.8095	21	17	2.582	26.522	0.9310	29	27	3.798	28.819
0.6000	15	9	1.644	21.787	0.7143	14	10	1.635	24.504	0.8125	16	13	1.970	26.582	0.9333	15	14	1.967	28.859
0.6000	20	12	2.193	21.787	0.7143	21	15	2.453	24.504	0.8148	27	22	3.329	26.628	0.9333	30	28	3.934	28.859
0.6000	25	15	2.741	21.787	0.7143	28	20	3.270	24.504	0.8182	11	9	1.359	26.696	0.9375	16	15	2.103	28.933
0.6000	30	18	3.289	21.787	0.7143	21	15	2.453	24.504	0.8182	22	18	2.717	26.696	0.9412	17	16	2.238	28.998
0.6071	28	17	3.082	21.967	0.7200	25	18	2.929	24.631	0.8214	28	23	3.464	26.760	0.9444	18	17	2.374	29.055
0.6087	23	14	2.534	22.006	0.7222	18	13	2.111	24.680	0.8235	17	14	2.105	26.802	0.9474	19	18	2.509	29.106
0.6111	18	11	1.986	22.066	0.7241	29	21	3.405	24.722	0.8261	23	19	2.852	26.853	0.9500	20	19	2.645	29.152
0.6154	13	8	1.437	22.173	0.7273	11	8	1.294	24.791	0.8276	29	24	3.599	26.882	0.9524	21	20	2.781	29.193
0.6154	26	16	2.875	22.173	0.7273	22	16	2.588	24.791	0.8333	6	5	0.747	26.995	0.9545	22	21	2.916	29.231
0.6190	21	13	2.327	22.264	0.7308	26	19	3.064	24.868	0.8333	12	10	1.494	26.995	0.9565	23	22	3.052	29.265
0.6207	29	18	3.216	22.304	0.7333	15	11	1.770	24.924	0.8333	18	15	2.241	26.995	0.9583	24	23	3.187	29.296
0.6250	8	5	0.889	22.411	0.7333	30	22	3.540	24.924	0.8333	24	20	2.988	26.995	0.9600	25	24	3.323	29.325
0.6250	16	10	1.779	22.411	0.7368	19	14	2.246	25.001	0.8333	30	25	3.735	26.995	0.9615	26	25	3.459	29.351
0.6250	24	15	2.668	22.411	0.7391	23	17	2.723	25.050	0.8400	25	21	3.123	27.126	0.9630	27	26	3.594	29.376
0.6296	27	17	3.009	22.525	0.7391	23	17	2.723	25.050	0.8421	19	16	2.376	27.167	0.9643	28	27	3.730	29.399
0.6316	19	12	2.120	22.572	0.7407	27	20	3.199	25.085	0.8462	13	11	1.629	27.245	0.9655	29	28	3.866	29.420
0.6333	30	19	3.351	22.615	—	—	—	—	—	0.8462	26	22	3.259	27.245	0.9667	30	29	4.001	29.439
—	—	—	—	—	—	—	—	—	—	—	—	—	—	—	1.0000	u	u	—	30.000

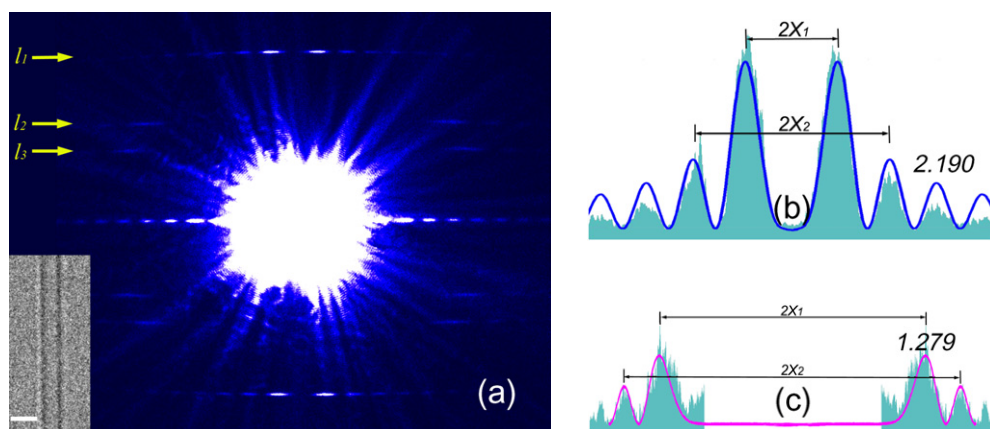


Figure 12. (a) Electron diffraction pattern of carbon nanotube (17,2). Inset is a high-resolution electron microscope image of the nanotube. The three principal layer lines, l_1 , l_2 and l_3 , are indicated in the figure. (b) Intensity profile of principal layer line l_1 . The ratio of the positions of the second peak (X_2) and the first peak (X_1) is 2.190, corresponding to $|J_2(X)|^2$ which is plotted as the solid line. (c) Intensity profile of principal layer line l_2 . The ratio of the positions of the second peak (X_2) and the first peak (X_1) is 1.279, corresponding to the Bessel function $|J_{17}(X)|^2$ which is plotted as the solid line. The chiral indices of the nanotube are therefore (17,2) [122].

current measurement, the errors of measuring D_1 and D_2 are 0.009 nm^{-1} . The errors in the deduction of the chiral indices are no larger than 0.2%.

4.5. Bundles of single-walled carbon nanotubes

Single-walled carbon nanotubes tend to form raft-like bundles when they are produced by laser evaporation or arc-discharge [11, 15, 16]. Though the diameter of the nanotubes can be measured in electron micrographs, their helicity distribution is yet to be well established. When they are packed in hexagonal closed packing, although their diameters are the same, it is not known if the helicity of all tubules are also the same, despite theoretical argument and geometry seeming to favour such a case [153].

For a bundle of single-walled carbon nanotubes of the same diameter, the total scattering amplitude is the coherent sum of all individual contributions:

$$F_T = \sum_m F_m(R, \Phi, l) \exp(2\pi i \delta_m), \quad (85)$$

where δ_m is the phase shift caused by relative rotation and translation. Given the weak bonding forces between the neighbouring nanotubes, it is reasonable to assume that the abovementioned two degrees of freedom will make the scattering to a large extent incoherent. In this case, the resultant diffraction intensity distribution will be approximately equal to the sum of individual scattering, in particular on layer lines $\ell \neq 0$.

Figure 14(a) shows a model structure of a raft-like bundle of single-walled carbon nanotubes. All nanotubes have similar diameter and they are in closed hexagonal packing. Figure 14(b) is an electron micrograph of such a raft-like bundle of single-walled carbon nanotubes produced by single-beam laser evaporation [16]. There are about 50 nanotubes, of about the same diameter, in this bundle. Figure 14(c) is an experimental electron diffraction pattern obtained from the bundle of nanotubes [112]. Letters A and Z designate the positions of the reflection peaks from armchair and zigzag nanotubes, respectively. The continuous distribution along the $(100)^*$ and $(110)^*$ arcs are symmetrical about the tubule axis, indicating

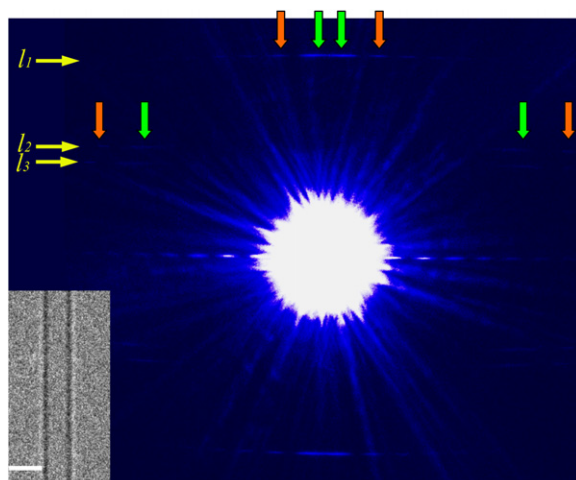


Figure 13. Electron diffraction pattern of nanotube (17,1). Inset is an electron microscope image of the nanotube. The arrows point to the peak positions on layer line l_1 and l_2 , respectively. The chiral indices of this nanotube were determined to be (17,1) [122].

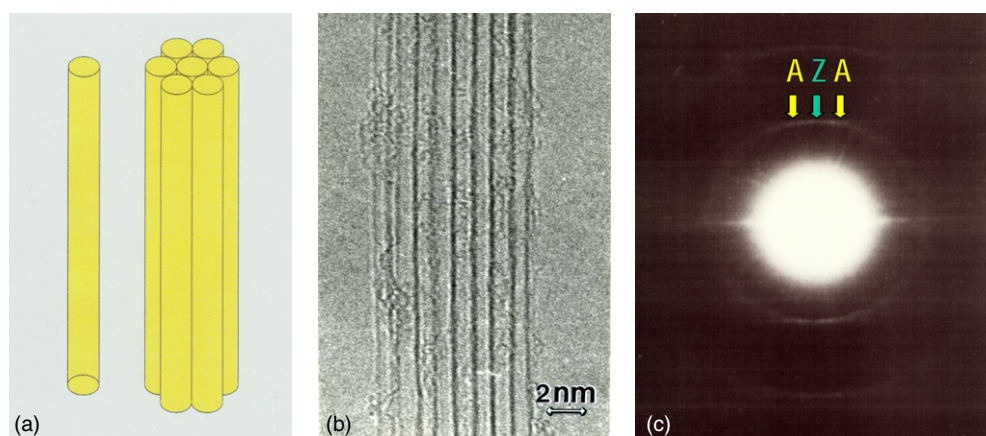


Figure 14. (a) Structural model of a bundle of single-walled carbon nanotubes in closed hexagonal packing. (b) Electron microscope image of a bundle of raft-like single-walled carbon nanotubes. (c) Electron diffraction pattern of the bundle where the reflection intensities form continuous arcs. Letters A and Z indicate positions of reflection maxima due to the armchair and zigzag structures, respectively [112].

that the scattering tubules possess a rather uniform distribution of helicity. The electron diffraction can be calculated using a simplified model as shown in figure 15(a). In this model, nine nanotubes of about the same diameter of 1.4 nm are arranged in closed hexagonal packing. The electron diffraction intensity distribution is displayed in figure 15(b). As expected, the intensities are distributed rather evenly between the positions corresponding to the zigzag and the armchair structures.

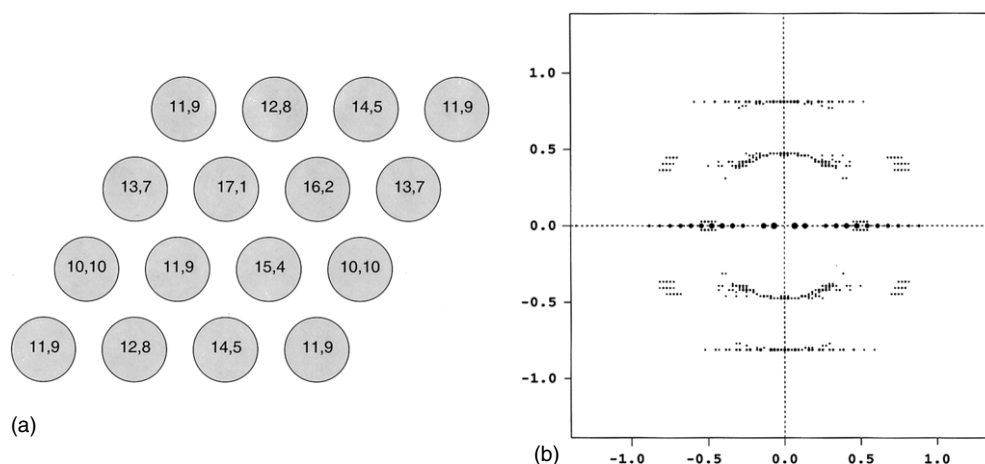


Figure 15. (a) A model structure composed of nine carbon nanotubes of about the same diameter. The chiral indices of each nanotube are also given in the figure. (b) Calculated electron diffraction pattern of the model structure. A continuous distribution of scattering intensities is formed due to the rather uniform distribution of helicity in the nanotubes.

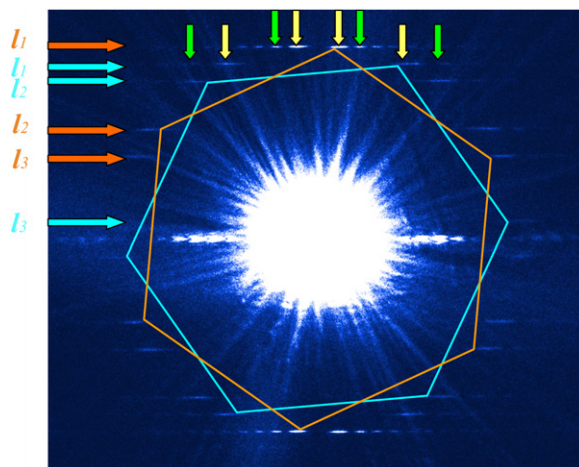


Figure 16. Electron diffraction pattern of a double-walled carbon nanotube. Two sets of diffraction patterns, indicated by arrows of different colours, are identified. The chiral indices of the two shells of this nanotube are (15,11) and (30,3), respectively. Their diameter and helicity are (1.770 nm, 24.92°) and (2.475 nm, 4.72°), respectively [152].

4.6. Multiwalled carbon nanotubes

For a multiwalled carbon nanotube, it is necessary to determine the chiral indices $[u_j, v_j]$ for each individual shell j . While the methods detailed in sections 4.1–4.4 are valid for multiwalled carbon nanotubes where the inter-layer interferences are not strong, due to the much larger diameter of multiwalled carbon nanotubes, complementary information such as equation (84) is often very helpful to eliminate ambiguities. When the layer lines are read from the digitized data, the uncertainties in measuring the ratio v/u can be reduced to less than 0.2%. Once all the chiral indices are determined, the inter-tubular distances between the neighbouring shells in the nanotube can also be obtained.

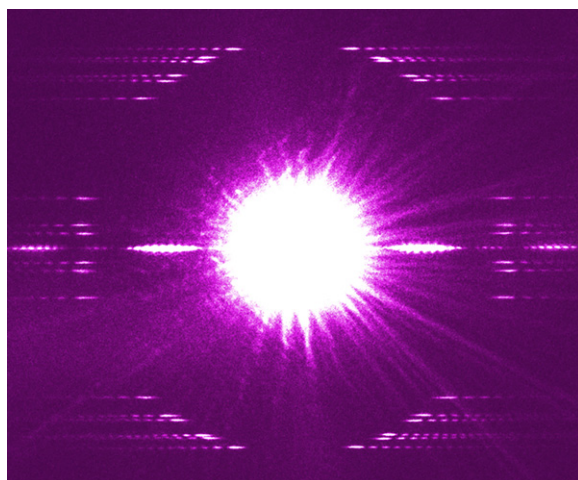


Figure 17. Electron diffraction pattern of a triple-walled carbon nanotube. The pattern consists of three sets of individual patterns due to the three shells of the nanotube. The chiral indices of the three shells are determined to be (35,14), (37,25) and (40,34), respectively. All shells are metallic [152].

Figure 16 shows an electron diffraction pattern of a double-walled carbon nanotube [152]. As can be seen from the pattern, there are now six pairs of principal layer lines across the equatorial layer line due to the two shells of the nanotube. The two sets of electron diffraction patterns are indicated by arrows coloured differently in the figure. The chiral indices of the two shells are determined to be (15,11) and (30,3), respectively. Their diameter and helicity are (1.770 nm, 24.92°) and (2.475 nm, 4.72°), respectively, with an inter-layer spacing of 0.355 nm.

Figure 17 shows an electron diffraction pattern of a triple-walled carbon nanotube where nine pairs of principal layer lines are present [154]. The chiral indices of the three shells are determined to be (35,14), (37,25) and (40,34), respectively. All the three shells are metallic.

Figure 18 shows the TEM image and the corresponding electron diffraction pattern of a quadruple-walled nanotube [124]. From the TEM image shown as the inset of figure 18(a), we can estimate that the nanotube has inner and outer diameters of 2.6 nm and 5.0 nm, respectively. The electron diffraction pattern of this nanotube, a magnified portion is shown in figure 18(b), was used to deduce the chiral indices of each and every shell of the nanotube accurately. It is also interesting to note that there are only three different helicities by examining the number of principal layer lines indicated by the arrows coloured in red, green and yellow in the electron diffraction pattern due to the fact that two of the four shells have the same helicity. By measuring the principal layer line spacings in the electron diffraction pattern in figure 18(b), the v/u ratios were obtained as 0.031, 0.642 and 0.927 and the helicities were 1.53°, 22.84° and 28.76°, respectively. Using the principal layer line l_1 and the positions of the intensity peaks on this layer line, the value of index v can be deduced: $v = 25$ for the helicity of 22.84° and $v = 24$ for the helicity of 28.76°. Combining with the v/u ratios determined above, the chiral indices for these two nanotubes are assigned to be (26,24) and (39,25), respectively, which are neighbouring shells in the nanotube.

Since there are four individual shells in the nanotube, two shells must have the same helicity. These two shells are identified by the modulations in the intensity distribution on the layer line marked with red arrows (helicity 1.53°), which indicate that two nanotubes have both contributed to these layer lines and their chiral indices were determined to be (32,1) and

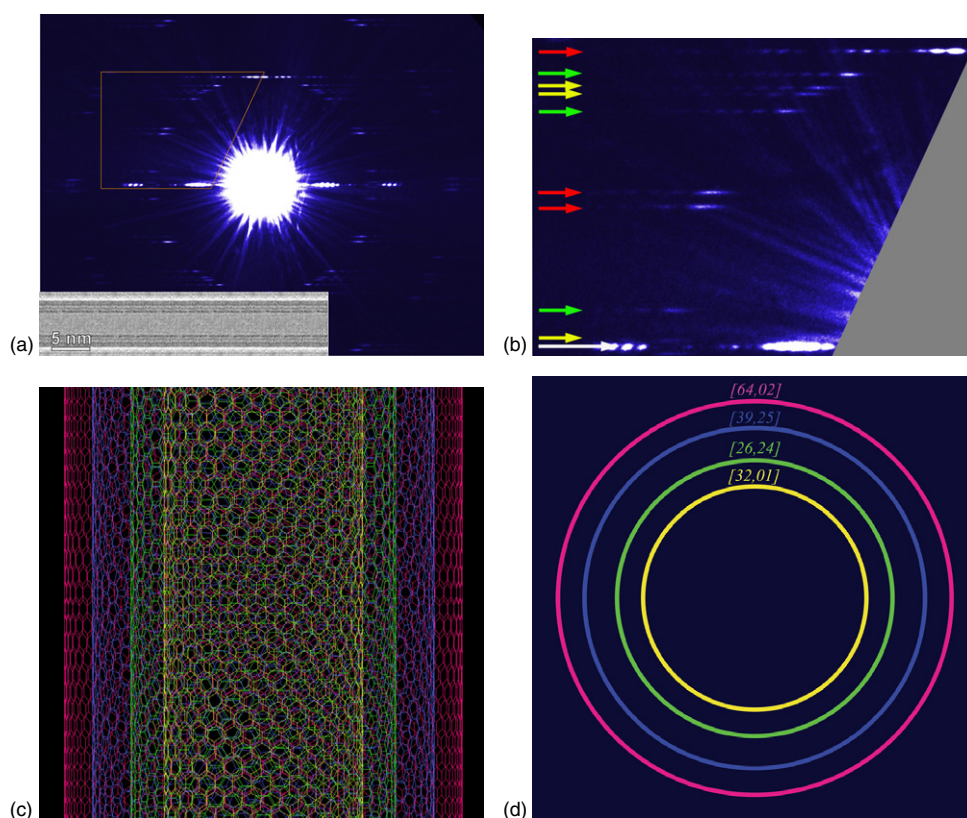


Figure 18. (a) Electron diffraction pattern of a quadruple-walled carbon nanotube (inset shows the electron microscope image). (b) Magnified portion of (a). Only three sets of individual electron diffraction patterns can be identified due to the overlapping of the diffraction patterns of two of them, indicating that these two shells have the same helicity. (c) Side view of the structure of the quadruple-walled carbon nanotube. (d) Cross-sectional view of the determined structure where the chiral indices of each shell are also indicated [124].

(64,2), respectively, by making use of the geometric constraints of the concentric shells in the multiwalled carbon nanotube. Figure 18(c) shows the determined structure in side view of the four shells of this nanotube with chiral indices (32,1), (26,24), (39,25) and (64,2), whose cross-sectional view is given in figure 18(d). All these shells are semiconducting. It is worth noting that the inter-tubular distances are not of the same value. They vary from 0.423 to 0.492 nm and to 0.358 nm from the outermost shell to the innermost shell in the nanotube.

The procedure presented here for determining the atomic structure of the quadruple-walled carbon nanotube can be extended to multiwalled carbon nanotubes with fewer or more shells. With the precision given in the present measurement, up to nine shells (outer diameter up to 10 nm) have been determined unambiguously [155]. Once the atomic structure of a multiwalled carbon nanotube is determined, we can predict their physical and chemical properties, including identifying which shell is metallic or semiconducting.

5. Symmetry of electron diffraction from carbon nanotubes

Observation and interpretation of the symmetry present in the electron diffraction pattern of a carbon nanotube have been carried out ever since the discovery of carbon nanotubes. For an

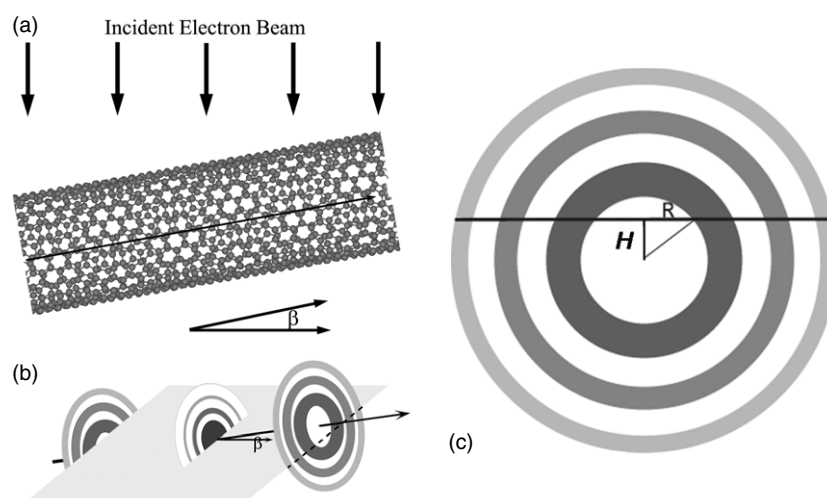


Figure 19. (a) Geometric relationship in electron diffraction from a carbon nanotube when it is tilted with respect to the tubule axis by an angle β . (b) Corresponding relationship in the reciprocal space, where the diffraction intensities due to the nanotube are represented by a set of concentric rings equally spaced in the axial direction. (c) Cross-sectional view of the intercept of the diffraction plane and the reciprocal space structure of the nanotube at an incline incident angle β . The observed separation R is smaller than the maximum value when the nanotube is perpendicular to the incident electron beam ($\beta = 0^\circ$). H is the vertical height of the intercept of the diffraction plane and the intensity rings relative to the centre of the intensity rings.

ideal (straight and cylindrical) single-walled carbon nanotube, it can have many symmetry elements, such as the inversion centre, rotational axes and reflection planes. Under the kinematical diffraction conditions, there is always an inversion centre in the diffraction intensity distribution, regardless of the symmetry possessed by the tubule structure due to the Friedel's law. The addition of the inversion centre will therefore make the symmetry of the diffraction patterns be no lower than the nanotube.

Due to the finite size of carbon nanotubes in the radial directions, the intensity distribution in the electron diffraction patterns from a carbon nanotube deviates noticeably from that of graphene which gives rise to regular hexagonal symmetry. The electron diffraction intensities elongate perpendicular to the tubule axis and form a set of layer lines normal to the tubule axis. The elongated intensity distribution stipulates that the electron diffraction pattern from carbon nanotubes loses hexagonal symmetry.

5.1. Single-walled carbon nanotubes

It has been observed experimentally that the electron diffraction pattern of a single-walled carbon nanotube showed 2mm symmetry [8]. This conclusion has recently been challenged in an analysis where the authors argue that the 2mm symmetry usually does not exist in the electron diffraction patterns of a single-walled carbon nanotube unless the atomic structure of the nanotube satisfies some special conditions, i.e. the crystallographic indices (u, v) are all even [109].

When the incident electron beam is perpendicular to the tubule axis, i.e. $\beta = 0^\circ$ as shown in figures 19(a) and (b), the tubule axis is in the diffraction plane that intersects the reciprocal space of the nanotube. Under normal incidence, the dark line in figure 19(c) (intersection

of the diffraction plane and the three-dimensional power spectrum of the carbon nanotube in the reciprocal space) should pass through the centre of the concentric corona representing the scattering intensities. Along the dark line, since the orders of all contributing Bessel functions n have the same evenness/oddity [151], the intensity distribution (cf, equation (48), for example) dependence on the azimuthal angle Φ observes the following relationship:

$$I(R, \Phi + \pi, l) = I(R, \Phi, l), \quad (86)$$

which is true for all the layer lines in the electron diffraction pattern. Equation (86) shows that the electron diffraction from a single-walled carbon nanotube has mirror symmetry about the nanotube axis. Combining with the inversion centre $\bar{1}$ due to the Friedel's law, the electron diffraction patterns of a single-walled carbon nanotube under normal incidence will therefore always have 2mm symmetry.

When the incident electron beam is not perpendicular to the tubule axis, i.e. $\beta \neq 0^\circ$, the diffraction plane does not coincide with the tubule axis in the reciprocal space of the carbon nanotube, although it still passes through the centre of the central diffraction coroneae. The points of intersection with the diffuse coroneae representing the scattering intensities, depend on the tilt angle β and the positions of the layer line planes in the reciprocal space, as shown schematically in figure 19(b). Figure 19(c) shows the side view of a layer line plane on the left of the origin and the dark line indicates the intersection of the diffraction plane and the power spectrum of the nanotube in the reciprocal space. In the electron diffraction pattern under inclined incidence, the diffraction intensities on layer line l are modulated by Bessel functions of the same orders as those under normal incidence as shown in figure 19(c). However, the scattering amplitude measured on the diffraction plane is

$$F_{uv}(R, \Phi, l) = \sum_{n,m} f \chi_{uv}(n, m) \gamma_{uv}(n, m) J_n \left(\pi d \sqrt{R^2 + \left(\frac{l \tan \beta}{c} \right)^2} \right) \exp \left[in \left(\Phi + \frac{\pi}{2} \right) \right]. \quad (87)$$

As discussed before, the evenness/oddity of n is the same for all allowed values. The electron diffraction intensities therefore also satisfy the following equation for all layer lines:

$$I(R, \Phi + \pi, l) = I(R, \Phi, l). \quad (88)$$

This means that the whole electron diffraction pattern of a single-walled carbon nanotube under inclined incidence also has 2mm symmetry.

Figure 20 shows the simulated electron diffraction patterns of the single-walled carbon nanotube (14,9) under several different incident directions. When the incident electron beam is perpendicular to the tubule axis ($\beta = 0^\circ$), the simulated electron diffraction intensities show 2mm symmetry, as shown in figure 20(a). When the tilting angle β is increased from 0° to 10° (figure 20(b)), the split diffraction intensities across the tubule axis on the layer lines move towards the tubule axis. At the same time, the layer line spacings increase by a factor of 1.015 ($=1/\cos 10^\circ$). As we continue to increase the tilting angle β to 20° , shown in figure 20(c), the split diffraction intensities on the layer lines move even closer to the tubule axis and they eventually merge into one single peak at the critical tilt angle $\beta_c = \theta = \tan^{-1}[(u_n/n) \tan(\alpha)] = 26.8^\circ$, where $n = 9$ and $u_n = 10.7$ is the value at which Bessel function $J_9(u)$ assumes its first peak. At $\beta = 30^\circ$, which is larger than the critical tilt angle β_c , the diffraction plane will not intersect with the first ring of the coroneae as illustrated in figure 20(c) and no significant intensity is observed at the position corresponding to the first major layer line as shown in figure 20(d). However, during the process of tilting, the 2mm symmetry of the whole electron diffraction patterns is retained.

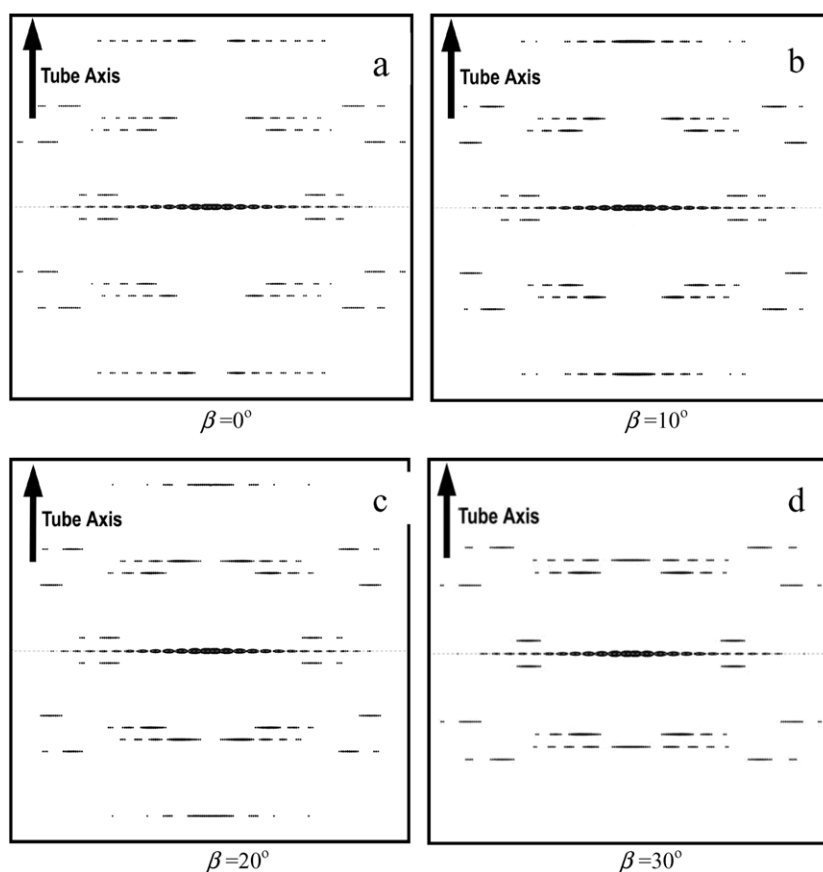


Figure 20. Simulated electron diffraction patterns of single-walled carbon nanotube (14,9) at various tilt angles. (a) $\beta = 0^\circ$; (b) $\beta = 10^\circ$; (c) $\beta = 20^\circ$ and (d) $\beta = 30^\circ$. 2mm symmetry is preserved at all tilt angles, though the geometry and intensity distribution of the diffraction pattern are different when the tilt angle β changes [151].

It should be pointed out that, in general, the atomic structure of a single-walled carbon nanotube does not have mirror symmetry perpendicular to the tubule axis when discrete atoms are located at continuous helices around the nanotube, even though the projection of continuous helices does have mirror symmetry about the tubule axis.

5.2. Multiwalled carbon nanotubes

While the 2mm symmetry had been often observed in the electron diffraction patterns of multiwalled carbon nanotubes, it is incorrect to assert that the electron diffraction patterns of multiwalled carbon nanotubes always have 2mm symmetry. When two or more shells of a multiwalled carbon nanotube have the same helicity, for instance, the inter-layer interferences may break the 2mm symmetry and leave only the inversion centre present in the electron diffraction pattern as stipulated by Friedel's law.

However, since the electron diffraction patterns of single-walled carbon nanotubes always possess 2mm symmetry [151], this symmetry will also be preserved in the electron diffraction patterns from a multiwalled carbon nanotube when there is no overlap of diffraction layer

lines from different shells. This is true if none of the axial periodicities is commensurate with another shell of the multiwalled carbon nanotube. On the other hand, when the ratio of the axial periodicities of two concentric shells is a rational number, some layer lines will coincide and interferences between the scattered electron waves from different shells can take place. The interferences between two shells produce the most profound effect when the two shells have the same helicity. Under this circumstance, the two shells satisfy exactly the same selection rule given in equation (36) and all the principal layer lines overlap. Since the electron diffraction intensity distribution on each layer line due to one shell is usually governed by a single Bessel function as discussed in section 4.4, the electron diffraction intensity on a common layer line l_0 due to both shells is [150]

$$I(R, \Phi, l_0) = \chi_0^2 f^2 \{|u_1 J_{n_1}(\pi d_1 R)|^2 + |u_2 J_{n_2}(\pi d_2 R)|^2 + 2u_1 u_2 J_{n_1}(\pi d_1 R) J_{n_2}(\pi d_2 R) \cos[(n_2 - n_1)(\Phi + \pi/2) + \Delta\phi]\}, \quad (89)$$

where χ_0 is a constant, n_1 and n_2 are the orders of the Bessel functions that dominate the intensity on layer line l_0 from the two shells (u_1, v_1) and (u_2, v_2) , respectively, and $\Delta\phi = \phi_2 - \phi_1$ is the relative phase shift between the two shells. From equation (89), we can obtain that, when n_1 and n_2 have opposite oddity/evenness, $I(R, \Phi + \pi, l_0) \neq I(R, \Phi, l_0)$, i.e. the electron diffraction pattern will no longer have 2mm symmetry. Therefore, the 2mm symmetry is broken under the condition that $n_1 - n_2$ is an odd number except that the observation is set at certain special azimuthal angles $\Phi = (L\pi - \Delta\phi)/(n_2 - n_1)$ (L is an integer) where $I(R, \Phi + \pi, l_0) = I(R, \Phi, l_0)$. Otherwise, when $n_1 - n_2$ is an even number, $I(R, \Phi + \pi, l_0) = I(R, \Phi, l_0)$ holds, i.e. the whole electron diffraction pattern will have 2mm symmetry.

These rules can be extended to include more than two shells of the same helicity to analyse the symmetry of the electron diffraction patterns of multiwalled carbon nanotubes.

Figure 21(a) shows an electron diffraction pattern of a quintuple-walled carbon nanotube. The inner and outer diameters of this nanotube are about 2.2 and 5.5 nm, respectively. Twelve pairs of principal layer lines can be observed, which indicate that four different helicities exist in the nanotube. Since there are five shells in the nanotube as indicated in the HREM image [150], there must be two shells that have the same helicity. The overlapped layer lines are indicated by the three arrows, from which the helicity is determined to be 21.6° . Using the methods described in section 4, the chiral indices of the five shells are (i) (22,9), (ii) (33,6), (iii) (34,20), (iv) (53,12) and (v) (51,30). The two shells, (34,20) and (51,30), have the same helicity of 21.48° which falls within the range of uncertainty of our measurement.

Examination of the intensity distribution on these layer lines indicates that the mirror symmetry about the equatorial plane or the axial direction is no longer present in the lower two layer lines l_2 , and l_3 , indicated by arrows and therefore the whole diffraction pattern does not have 2mm symmetry. The breakdown of the 2mm symmetry in the electron diffraction pattern in figure 21(a) can be understood from equation (89) and the rules developed above. For the three principal layer lines indicated by the arrows in figure 21(a), the indices of the three principal layer lines from top to bottom are $l_1 = (2u + v)/M = 44$, $l_2 = (u + 2v)/M = 37$, and $l_3 = (u - v)/M = 7$, respectively. For layer line $l_1 = 44$, n_1 and n_2 are $n_1 = v_1 = 20$ and $n_2 = v_2 = 30$, respectively, and $n_2 - n_1 = 10$ is an even number. Therefore, mirror symmetry is kept about the tubule axis for this layer line. However, for layer lines $l_2 = 37$ ($n_1 = -u_1 = -34$, $n_2 = -u_2 - 51$ and $n_2 - n_1 = -17$) and $l_3 = 7$ ($n_1 = u_1 + v_1 = 54$, $n_2 = u_2 + v_2 = 81$ and $n_2 - n_1 = 27$), both layer lines satisfy the condition under which the mirror symmetry breaks down, as shown in the electron diffraction pattern given in figure 21(a). Figure 21(b) shows the intensity profile of the enclosed region (layer line $l_2 = 37$) in figure 21(a) to illustrate the profound asymmetry about the tubule axis. The calculated intensity profile using

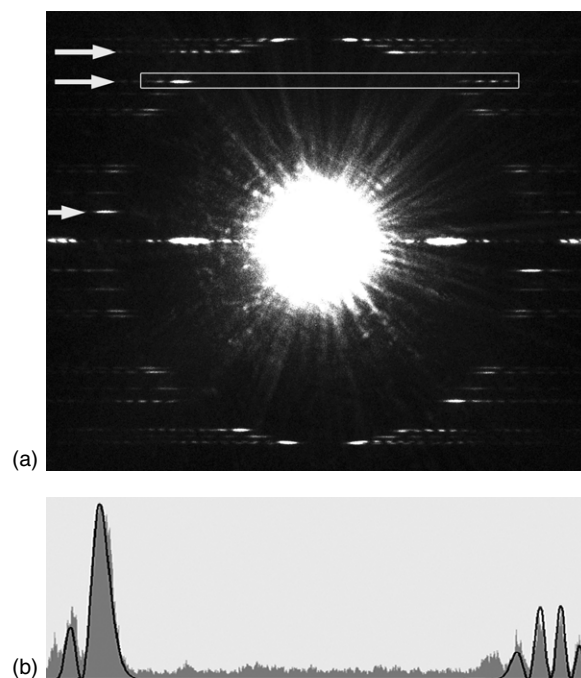


Figure 21. (a) Electron diffraction pattern from a quintuple-walled carbon nanotube showing breakdown of $2mm$ symmetry. The electron diffraction pattern does not possess $2mm$ symmetry, though the inversion centre is present due to Friedel's law. (b) Intensity profile of the principal layer line l_2 , where the asymmetry is apparent [150].

equation (89) is plotted as a solid line for comparison with the experimental data and they match extremely well.

By constructing a double-walled carbon nanotube composed of two concentric shells (34,20) and (51,30), respectively, depicted in figure 22(a), numerical simulations of the electron diffraction intensity distribution were also carried out to demonstrate the breakdown of the $2mm$ symmetry in this case [150]. Figure 22(b) displays a typical simulated electron diffraction pattern which matches the experimental observations very well, where layer line l_1 is symmetrical, while layer lines l_2 and l_3 are asymmetrical about the vertical axis and the equatorial plane.

When two shells have commensurate periodicities but different helicities in a multiwalled carbon nanotube, the overlapping layer lines may not necessarily be the three principal layer lines l_1 , l_2 , and l_3 as shown in figure 21(a). Though the rules discussed above are still valid, the experimentally observed intensities on these layer lines are usually much weaker than the principal layer lines, and therefore the loss of $2mm$ symmetry would not be as apparent as in the case discussed above.

Observation of $2mm$ symmetry breaking in the electron diffraction patterns of multiwalled carbon nanotubes is helpful to determine the chiral indices of carbon nanotubes. By applying the rules developed above, we can easily exclude some ambiguous choices and dramatically increase the efficiency in assigning the chiral indices for shells of the same helicity in a carbon nanotube.

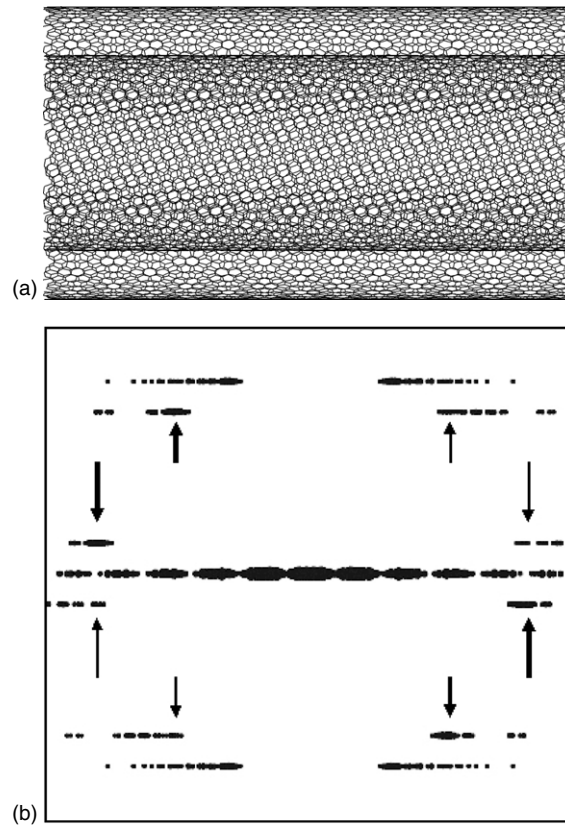


Figure 22. (a) Double-walled carbon nanotube composed of (34,20) and (51,30) of the same helicity $\alpha = 21.48^\circ$. (b) Simulated electron diffraction pattern of this nanotube. Arrows indicate that the intensities are no longer symmetrical about the equatorial plane and/or the vertical central axis, resulting in loss of the 2mm symmetry of the whole pattern [150].

5.3. Rotational extinctions

When an electron beam is incident on a nanotube positioned perpendicular to the electron beam, the electron scattering intensity as seen in an electron diffraction pattern, is not only dependent on the structure, but also on the relative orientation of the nanotube with respect to the incident electron beam, as can be recognized from the expressions for the scattering intensity. The orientational relationship becomes more interesting when the atomic structure of multiwalled carbon nanotubes is concerned as discussed in section 7.

For the nanotubes of zigzag structure, $(u, v) = (u, 0)$, the layer line selection rule becomes $l = (n/u) + 2m$ and the orientational dependence of the scattering amplitude can be further reduced to [156]

$$F_{u,0}(R, \Phi, l = \text{even}) = \sum_{s=0}^{+\infty} \left[1 + \exp\left(\frac{2\pi i}{3}l\right) \right] J_{2su}(\pi dR) \cos\left[2su\left(\Phi + \frac{\pi}{2}\right)\right], \quad (90)$$

and

$$F_{u,0}(R, \Phi, l = \text{odd}) = \sum_{s=0}^{+\infty} \left[1 + \exp\left(\frac{2\pi i}{3}l\right) \right] J_{(2s+1)u}(\pi dR) \cos\left[(2s+1)u\left(\Phi + \frac{\pi}{2}\right)\right]. \quad (91)$$

The summation over s is for all non-negative integers. Since only the Bessel functions of lowest orders contribute substantially to the total intensities, the significant terms are dominated by the Bessel functions of lowest orders, $s = 0$:

$$F_{u,0}(R, \Phi, l = \text{even}) \approx \left[1 + \exp\left(\frac{2\pi l i}{3}\right) \right] \left\{ J_0(\pi d R) + J_{2u}(\pi d R) \cos\left[2u\left(\Phi + \frac{\pi}{2}\right)\right] \right\}, \quad (92)$$

and

$$F_{u,0}(R, \Phi, l = \text{odd}) \approx \left[1 + \exp\left(\frac{2\pi l i}{3}\right) \right] J_u(\pi d R) \cos\left[u\left(\Phi + \frac{\pi}{2}\right)\right]. \quad (93)$$

The corresponding intensities are therefore

$$I_{u,0}(R, \Phi, l = \text{even}) = |F_{u,0}(R, \Phi, l = \text{even})|^2 \\ \approx 4J_0^2(\pi d R) \left\{ 1 + \frac{2J_{2u}(\pi d R)}{J_0(\pi d R)} \cos\left[2u\left(\Phi + \frac{\pi}{2}\right)\right] \right\} \cos^2\left(\frac{\pi l}{3}\right), \quad (94)$$

and

$$I_{u,0}(R, \Phi, l = \text{odd}) = |F_{u,0}(R, \Phi, l = \text{odd})|^2 \\ \approx 4J_u^2(\pi d R) \cos^2\left(\frac{\pi l}{3}\right) \cos^2\left[u\left(\Phi + \frac{\pi}{2}\right)\right]. \quad (95)$$

The intensity distribution is modulated by both the dominating Bessel functions and the orientational variable Φ . For the layer lines of even indices (equation (94)), the intensity dependence on the nanotube orientation is weak. However, for the layer lines of odd indices (equation (95)), the total layer line intensity distribution is modulated by $\cos^2[u(\Phi + (\pi/2))]$, which causes much stronger dependence on the orientational parameter Φ with a periodicity of π/u , though the angular structural periodicity is $2\pi/u$. Because of this angular modulation, extinction reflections occur at the following orientations:

$$\Phi_{\text{ext}} = \begin{cases} \frac{N\pi}{u}, & (u = \text{odd}), \\ \frac{(2N+1)\pi}{2u}, & (u = \text{even}), \end{cases} \quad N = 0, 1, 2, \dots, (2u-1). \quad (96)$$

There is a total of $2u$ orientations at which extinction takes place with an angular interval of π/u .

Figure 23(a) shows the TEM image of a single-walled carbon nanotube (16,0) (diameter $d = 1.253$ nm and helicity $\alpha = 0^\circ$) of zigzag structure and figure 23(b) is the corresponding nanobeam electron diffraction pattern in which the layer lines l_2 and l_3 overlap [156].

For the carbon nanotube (20,0), its angular structural periodicity is 18° , and the intensity distribution is periodic with a repetition of 9° . The total number of extinction orientations is 40 across the cylindrical circumference with an interval of $2\pi/40 = 9^\circ$. Figures 24(a)–(d) show the calculated electron scattering intensities from the (20,0) nanotube at angular orientations (projected structure of the model nanotube is also given in each figure) 0° , 1.5° , 3.0° and 4.5° . A total extinction of the odd layer lines occurs at $\Phi = 4.5^\circ$ (figure 24(d)). Figure 25(a) is an electron microscope image of zigzag carbon nanotube (20,0). Figure 25(b) shows an experimental electron diffraction pattern of nanotube (20,0) in which the odd layer lines ($l = \pm 1, \pm 3, \dots$) are in extinction. The inset shows the image of this nanotube, whose diameter is 1.566 nm. Excellent agreement has been obtained between the theoretical calculations and the experimental observations, indicated in figure 25(c) where the theoretical data (figure 24(d)) are plotted on the experimental electron diffraction data (figure 25(b)).

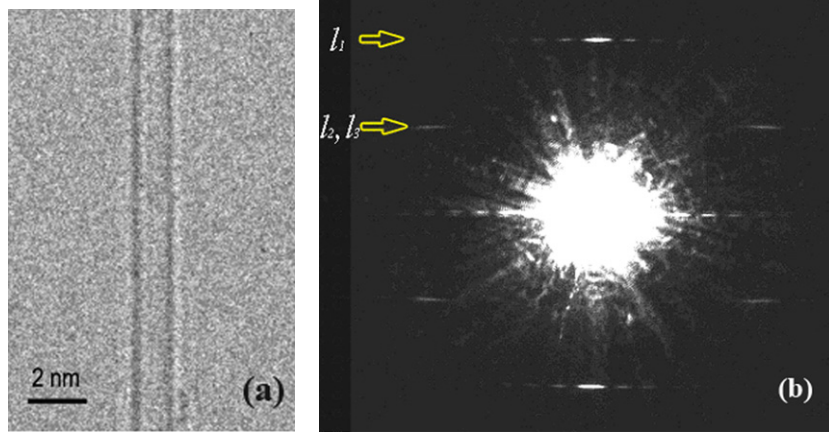


Figure 23. (a) Electron microscope image of single-walled carbon nanotube (16,0) of zigzag structure. (b) Electron diffraction pattern of the nanotube where the principal layer lines l_2 and l_3 overlap [156].

For nanotubes of armchair structure, i.e. $(u, v) = (u, u)$, the layer line selection rule is the same as for zigzag nanotubes, $l = (n/u) + 2m$, and the orientational dependence of the electron scattering intensities can be obtained similarly

$$I_{u,u}(R, \Phi, l = \text{even}) \approx 4J_0^2(\pi dR) \left\{ 1 + \frac{J_{2u}(\pi dR)}{J_0(\pi dR)} \cos \left[2u \left(\Phi + \frac{\pi}{2} \right) - \frac{\pi}{3} \right] \right\}, \quad (97)$$

and

$$I_{u,u}(R, \Phi, l = \text{odd}) \approx J_u^2(\pi dR) \cos^2 \left[u \left(\Phi + \frac{\pi}{2} \right) + \frac{\pi}{3} \right]. \quad (98)$$

Like the case for the zigzag nanotubes, the orientational dependence in the even layer lines are secondary (equation (97)) and a total extinction occurs in the odd layer lines when

$$\Phi_{\text{ext}} = \begin{cases} \frac{(3N+2)\pi}{3u}, & (u = \text{odd}), \\ \frac{(6N+1)\pi}{6u}, & (u = \text{even}), \end{cases} \quad N = 0, 1, 2, \dots, (2u-1). \quad (99)$$

There are also $2u$ orientations in which extinction occurs with an interval of π/u . Figure 26 shows the calculated electron diffraction patterns of an armchair nanotube (10,10) at orientations $\Phi = 0^\circ, 3^\circ, 9^\circ$ and 12° . For the (10,10) nanotube, the diffraction intensity distribution at $\Phi = 6^\circ$ is the same as $\Phi = 0^\circ$. The interval between neighbouring extinction orientations is 18° . Extinction on the odd layer lines occurs at $\Phi = 3^\circ$ (figure 26(b)).

The occurrence of extinction is due to the fact that at certain specific orientations, the periodicity of the projected structure of the achiral nanotube in the axial direction is halved. The projected structure with a halved periodicity at these specific orientations, as illustrated in figures 24(d) and 26(b), results in the doubling of the layer line spacing in the reciprocal space.

The orientational dependence of electron diffraction from carbon nanotubes is useful when the atomic structure of multiwalled carbon nanotubes is determined. It should be noted that the orientational dependence at other non-extinctive angular positions, even though rather weak, is also present as shown in the details of the calculated electron diffraction patterns [157]. When measurement of the electron diffraction intensities becomes more accurate, determination of

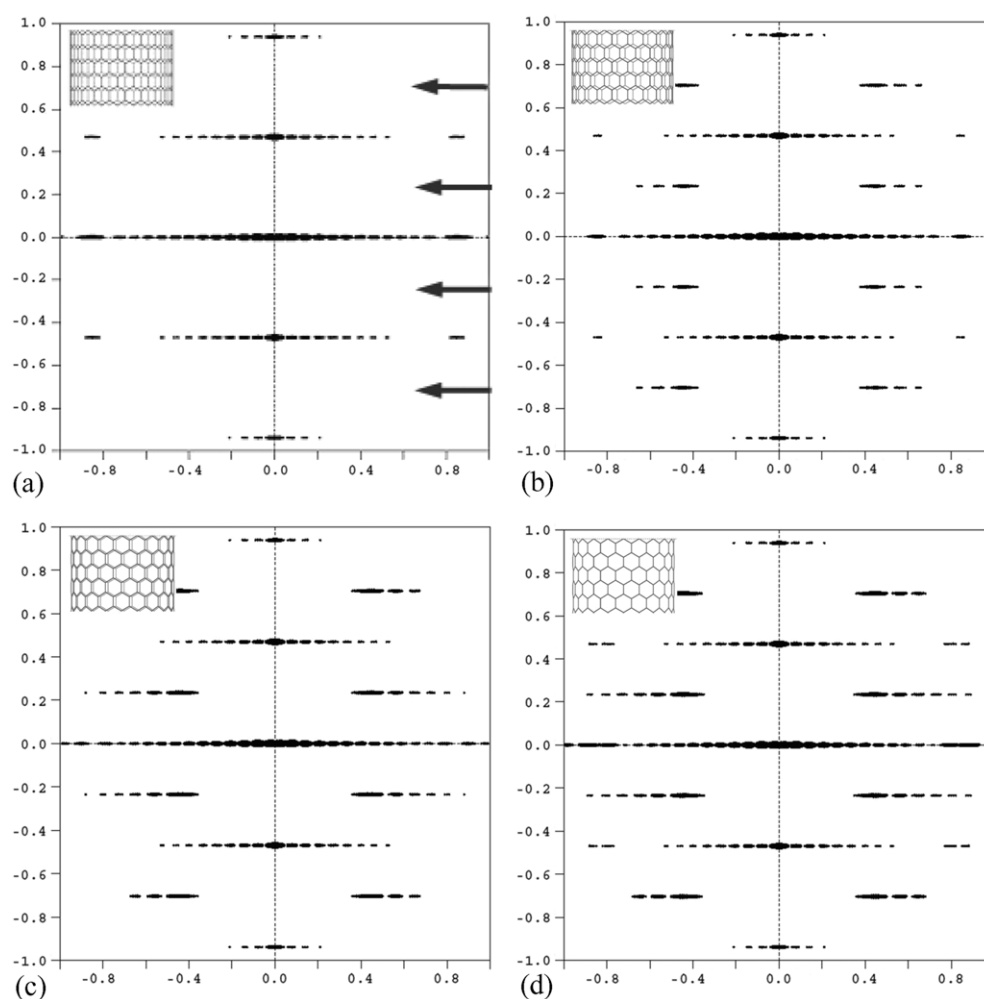


Figure 24. Calculated electron diffraction patterns of zigzag nanotube (20,0) when it is rotated about its axis at (a) 0° ; (b) 1.5° ; (c) 3.0° and (d) 4.5° . Extinction of the odd-indexed layer lines is observed as indicated by the arrows in (a) [156].

the absolute orientation will be possible. For example, for a double-walled carbon nanotube, when the diameter and helicity of each shell are determined, there are still three degrees of freedom that are undetermined. They are (a) the relative angular rotation between the two shells; (b) the relative translational displacement between the two shells in the axial direction; and (c) the respective enantiomorph of each shell. The present analysis will help resolve the first ambiguity in the determination of the atomic structure of multiwalled carbon nanotubes.

For multiwalled carbon nanotubes of more than two shells, the situation becomes more complex but the principles discussed here are valid for extensions.

6. Deformed carbon nanotubes

While carbon nanotubes have extremely high Young's modulus in the axial direction, it is rather soft in the radial direction as has been well demonstrated both theoretically and experimentally

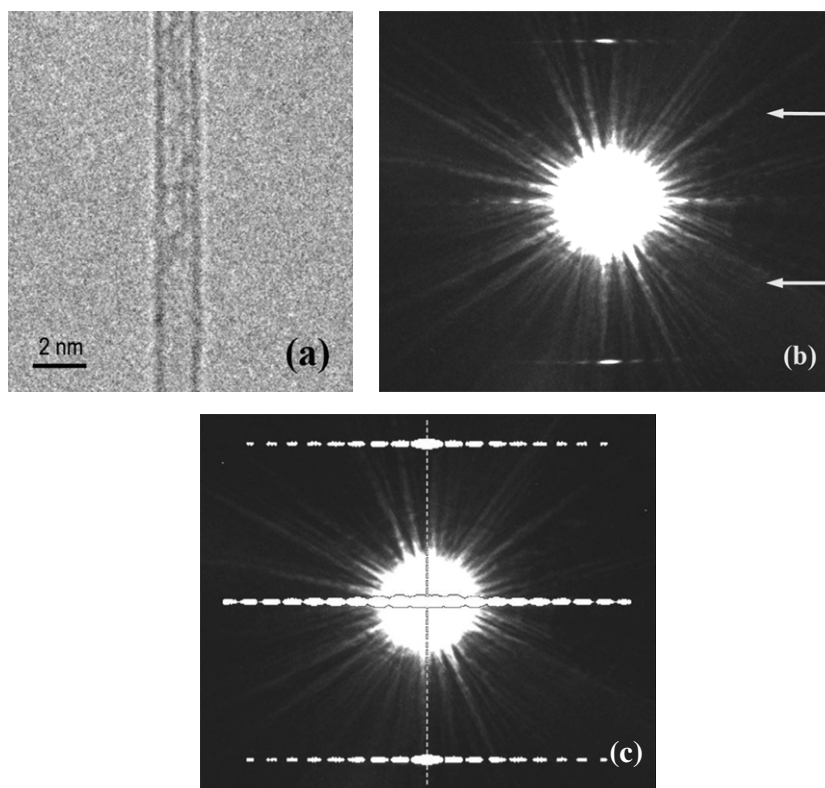


Figure 25. (a) Electron microscope image of zigzag carbon nanotube (20,0). (b) Electron diffraction pattern of the nanotube. The odd-indexed layer lines (indicated by arrows) are in extinction. (c) Overlap of the experimental diffraction pattern and the calculated pattern (figure 24(a)) [156].

[158–162]. Several forms of deformation can easily occur, and we consider the three simplest in the following: elliptical nanotube, axial twisting and nanotube ropes.

6.1. Elliptical nanotubes

When the case of nanotubes of elliptical cross-section with major axis a and minor axis b is considered, cylindrical nanotubes of circular cross-section can be treated as a special class of elliptical nanotubes. When $a = b$, it is the case for cylindrical nanotubes of radius $r_0 = a = b$.

In an elliptical carbon nanotube, each helix revolves on the surface of an elliptical cylinder which is characterized by its major axis a and minor axis b as shown in figure 27. Figure 27(a) shows schematically the side-view of a setting of electron diffraction where the elliptical carbon nanotube is tilted with respect to the horizontal plane by an angle β . Comparing with the kinematical theory of electron diffraction formulated for cylindrical carbon nanotubes, the analytic expression for the amplitude of electron scattering from an elliptical carbon nanotube has to take into account the ellipticity of the nanotube. The scattering amplitude for an elliptical carbon nanotube can be expressed as [163]

$$F(R, \Phi, l) = \sum_j \sum_{n,m} f \eta(n, l) J_n(2\pi r^* R) \exp \left[i n \left(\Phi^* + \frac{\pi}{2} \right) \right] \exp \left(-i n \varphi_j + \frac{2\pi i l z_j}{c} \right), \quad (100)$$

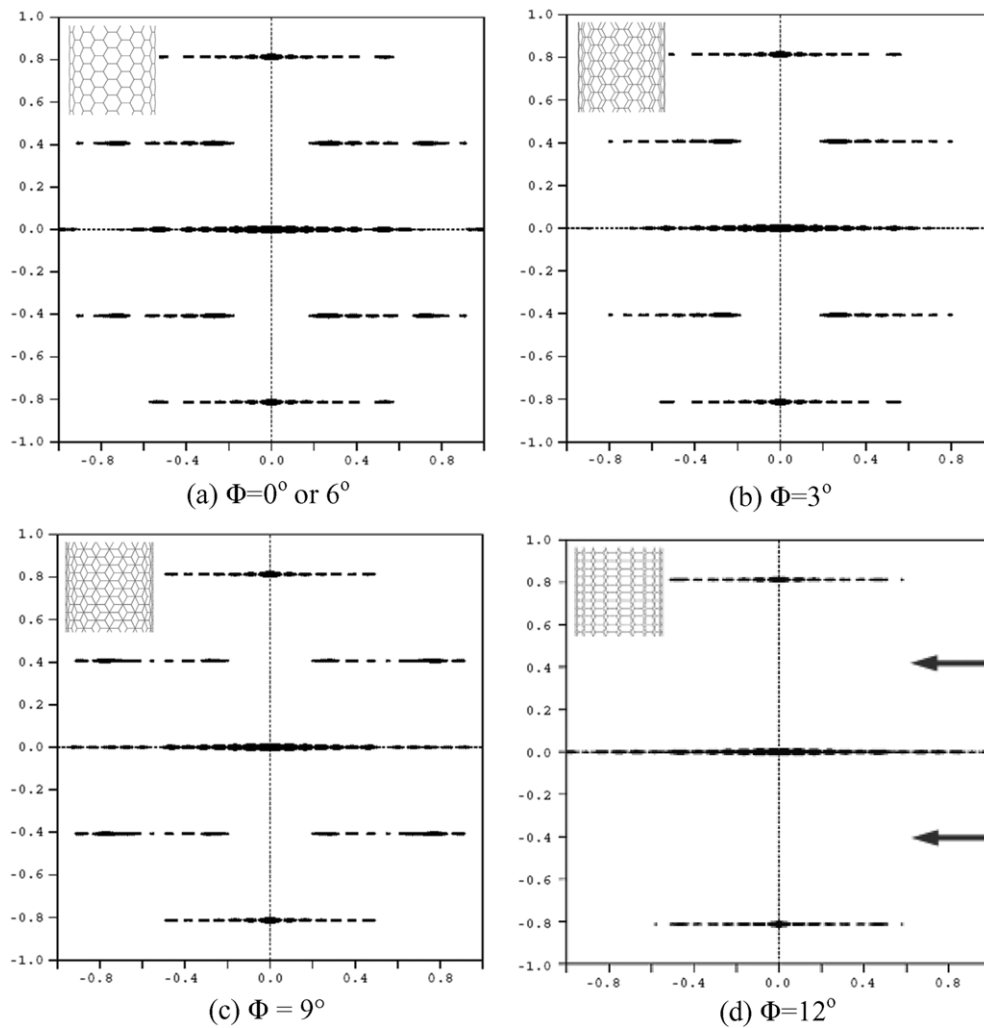


Figure 26. Calculated electron diffraction pattern of an armchair carbon nanotube (10,10) as a function of its azimuthal angle when the nanotube is rotated about its axis. Extinction of the odd-indexed layer lines is indicated by arrows in (d) [156].

where (R, Φ, l) denote the cylindrical coordinates in the reciprocal space, (φ_j, z_j) are the atomic coordinates of the j th atom in the asymmetrical unit cell of the carbon nanotube, $J_n(2\pi r^* R)$ is the Bessel function of order n , and n, l, m are all integers satisfying the same selection rule as for the cylindrical carbon nanotube

$$\frac{l}{c} = \frac{n}{C} + \frac{m}{\Delta}, \quad (101)$$

with C and Δ being the pitch length and axial distance between neighbouring atoms along the helix, respectively, and

$$r^* = \sqrt{a^2 \cos^2 \Phi + b^2 \sin^2 \Phi}, \quad (102)$$

$$\tan \Phi^* = \frac{b}{a} \tan \Phi, \quad (103)$$

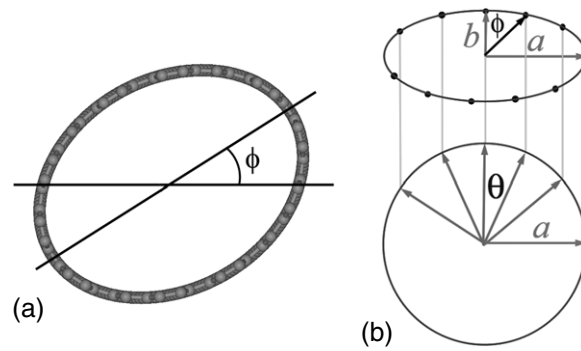


Figure 27. (a) Schematic illustrating the relative orientation of an elliptical carbon nanotube when it is also rotated relative to its major axis by angle ϕ . (b) Cross-sectional view defining the azimuthal angle ϕ in relation with the angle θ defined on a corresponding circle. The dots on the ellipse are evenly spaced on the perimeter representing the intercepts of atomic helices revolving on the surface of the elliptical nanotube [163].

and

$$\eta(n, l) = \int \frac{\exp[i(\frac{2\pi lz(\theta)}{c} - n\theta)]}{\sqrt{a^2 \cos^2 \theta + b^2 \sin^2 \theta}} d\theta \quad (104)$$

is a special function.

For a cylindrical carbon nanotube, $\Phi^* = \Phi$ and $r^* = r_0$ where r_0 is the radius of the carbon nanotube and $\eta(n, l)$ becomes a constant.

The selection rule for the elliptical carbon nanotube of chiral indices (u, v) remains the same as for the cylindrical carbon nanotube since the structural parameters in the axial direction are not changed by the elliptical deformation.

By taking one helix of the nanotube as a reference $(\varphi_0^{(0)}, z_0^{(0)})$, we have the following rotational and translational shifts for all the helices

$$\begin{aligned} \varphi_j^{(0)} &= A \left[\frac{2\pi j \cos \alpha}{\sqrt{u^2 + v^2 + uv}} (1 - e^2)^{1/4} |e| \right] \\ z_j^{(0)} &= -j a_0 \sin \alpha \end{aligned} \quad (105)$$

and

$$\begin{aligned} \varphi_j^{(1)} &= A \left[\frac{2\pi (j \cos \alpha + \frac{\sin \alpha}{\sqrt{3}})}{\sqrt{u^2 + v^2 + uv}} (1 - e^2)^{1/4} |e| \right] \\ z_j^{(1)} &= -j a_0 \sin \alpha + \frac{a_0 \cos \alpha}{\sqrt{3}} \end{aligned} \quad (106)$$

where the superscripts 0 and 1 stand for the two helices within the pair, and the subscript j ranges from 0 to $u - 1$ specifying all the u helices in the nanotube, e is the eccentricity of the elliptical nanotube $e = \sqrt{1 - b^2/a^2}$, and $A[x|e]$ is an elliptical function which is the inverse function of the elliptic integral of the second kind $E[x|e]$ [164].

There exist several major differences between the electron diffraction patterns of elliptical carbon nanotubes and circular carbon nanotubes including: (a) the elliptical nanotubes are much more anisotropic, i.e. the diffraction intensities vary more strongly with the change in orientation Φ , while the circular nanotubes have much weaker orientational dependence; (b) upon inclined incidence, the symmetry of the electron diffraction pattern from an elliptical nanotube may be lower than 2mm, while the latter always has 2mm symmetry [151].

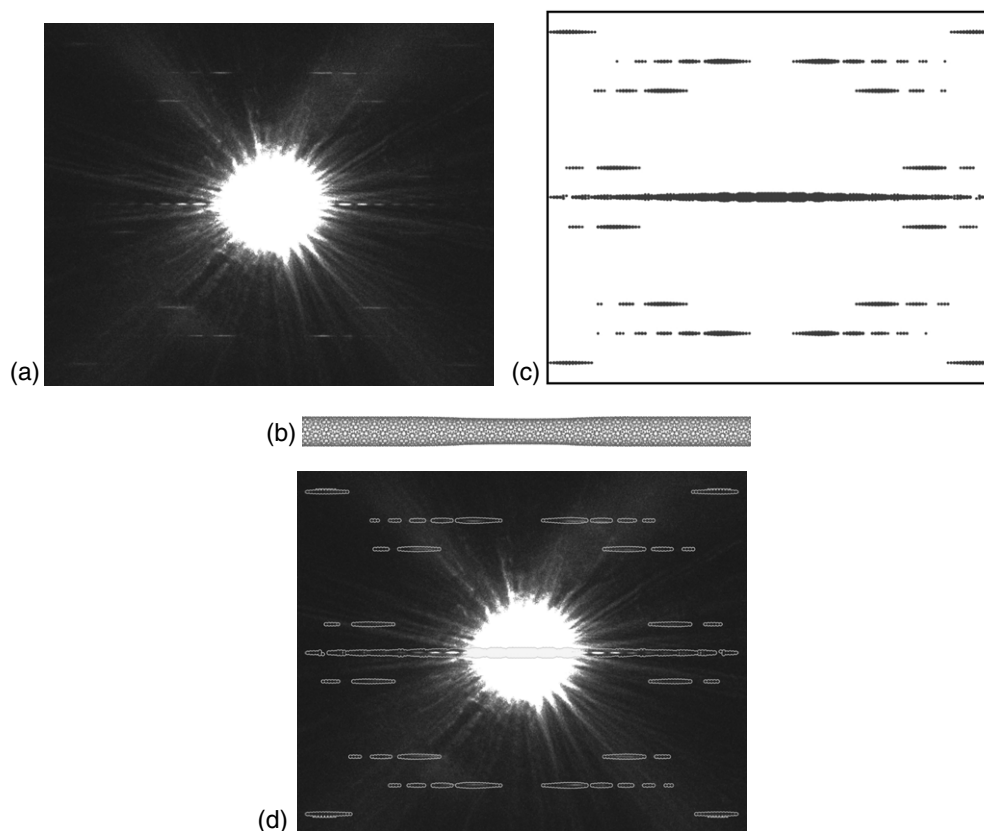


Figure 28. (a) Experimental electron diffraction pattern of an elliptical carbon nanotube of indices (15,7); (b) model structure of an elliptical carbon nanotube (15,7) with its central section deformed elliptically; (c) calculated electron diffraction pattern of the elliptical carbon nanotube; and (d) overlap of the calculated pattern (c) and the experimental pattern (a) showing excellent agreement [163].

The above theoretical analysis is very useful in analysing the electron diffraction patterns of deformed carbon nanotubes and accurately determining their atomic structure. Figure 28(a) is an experimental electron diffraction pattern of an elliptically deformed carbon nanotube. Nine reflection layer lines show up in the diffraction pattern. By measuring the electron scattering intensity distribution and the ratios of the spacings of the principal layer lines, we determined that the nanotube has chiral indices (15,7) with diameter 1.525 nm and helicity of 18.14° [163]. Figure 28(b) shows a model structure of single-walled carbon nanotube (15,7) that has been deformed elliptically. Figure 28(c) displays a simulated electron diffraction pattern from the model structure with a tilting angle of $\beta = 8^\circ$. As can be seen in the simulated pattern, the mirror symmetry across the tubule axis has indeed broken due to the orientation and tilting of the deformed carbon nanotube relative to the incident electron beam. In figure 28(d) the intensity profile of the calculated electron diffraction intensities are plotted on the experimental data. The intensity distribution matches very well for all the layer lines and suggests that the eccentricity of the nanotube is about 0.55 with a tilting angle of about 8° relative to the horizontal plane [163].

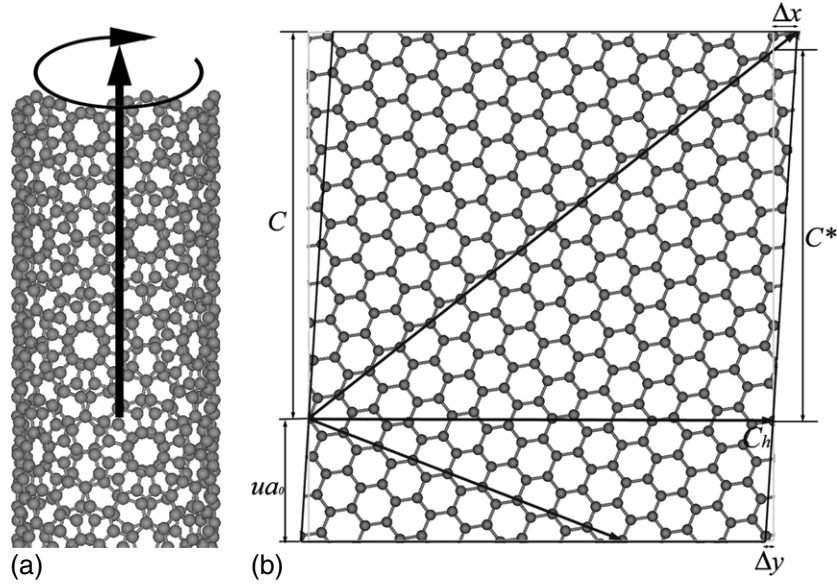


Figure 29. (a) Single-walled carbon nanotube (22,2) being twisted clockwise about its axis; (b) atomic positions of the twisted nanotube in radial projection. The light-lined rectangle and the dark-lined parallelepiped are the graphene cut before and after twisting. Δx and Δy are the atomic displacements caused by the twisting. C and C^* are the pitch lengths of the atomic helices before and after twisting, respectively [163].

6.2. Twisted nanotubes

Axial torsion is another interesting deformation of cylindrical nanotubes. Figure 29(a) shows the process of twisting a carbon nanotube axially: with one end fixed, the other end is twisted either in the clockwise direction or in the counterclockwise direction about the tubule axis. Although energetically this is equivalent to twisting an achiral (either armchair or zigzag) nanotube in either direction, twisting a helical carbon nanotube about its axis along the helical lines is energetically easier than twisting it against the helical lines [165]. Assuming that the cross-section of a twisted carbon nanotube is still circular as shown in figure 29(b), i.e. the twisting angle is not large enough to cause any buckling of the nanotube, we can consider the geometry of the twisted carbon nanotube in a sheared two-dimensional graphene lattice as shown in figure 29(b), where the hexagons have been uniformly deformed. By twisting a carbon nanotube (u, v) by an angle of $\Delta\vartheta(u + 2v)/(uM)$ for the periodicity length of c along the tubule axis with M being the maximum common divisor of $(2u + v)$ and $(u + 2v)$, the pitch length of the twisted helices becomes

$$C^* = C/(1 + \Delta\vartheta/2\pi), \quad (107)$$

although the distance between neighbouring atoms along a helix stays the same, i.e.

$$\Delta^* = a_0 \sin(60^\circ - \alpha), \quad (108)$$

where α is the helical angle of the untwisted nanotube and $a_0 = 0.246$ nm is the magnitude of the basis vectors of graphene. To make the twisted carbon nanotube still have a periodic structure along the tubule axis, C^* and Δ^* have to satisfy the following condition:

$$\frac{C^*}{\Delta^*} = \frac{2(u^2 + v^2 + uv)}{(u + 2v)(1 + (\Delta\vartheta/2\pi))} = \frac{p}{q}, \quad (109)$$

where p and q are integers, and we have converted the helicity angle α into the chiral indices (u, v) for this nanotube. Equation (109) requires that $\Delta\vartheta/2\pi = K_1/K_2$, where K_1 and K_2 are all integers. Thus the selection rule for the twisted carbon nanotube can be expressed as

$$l = (K_1 + K_2)(u + 2v)n + 2K_2(u^2 + v^2 + uv)m, \quad (110)$$

where the periodicity length of the twisted carbon nanotube has been assumed to be

$$c^* = uMK_2c, \quad (111)$$

which may not be the true primitive unit cell of the nanotube.

The scattering amplitude for the twisted carbon nanotube can be calculated by considering the geometric relationships of all the twisted helices in the nanotube as shown in figure 29(b). Although the carbon hexagons are deformed due to twisting, the total surface area of the nanotube in radial projection remains unchanged if no buckling occurred during the twisting process. Therefore a carbon nanotube of chiral indices (u, v) still consists of u pairs of properly-arranged helices as in the untwisted case. Choosing one pair of helices as a reference (cf figure 29(b)), the rotational and translational shifts of all the u pairs of helices can be expressed as

$$\begin{aligned} \varphi_j &= \frac{2\pi ja_0}{C_h} \left[\cos \alpha - \frac{\sin \alpha}{\tan(60^\circ - \alpha)} \frac{\Delta\vartheta}{2\pi} \right] \\ z_j &= -ja_0 \sin \alpha \end{aligned} \quad (112)$$

where the subscript j ranges from 0 to $u - 1$. The scattering amplitude for a twisted carbon nanotube (u, v) is therefore

$$F_{uv}(R, \Phi, l) = \sum_{n,m} f \chi_{uv}^*(n, m) \gamma_{uv}(n, m) \exp \left[i n \left(\Phi + \frac{\pi}{2} \right) \right] J_n(\pi d R), \quad (113)$$

where $\chi_{uv}^*(n, m)$ is a function depending on the nanotube helicity and the detailed bonding between neighbouring carbon atoms in the twisted hexagons, and

$$\gamma_{uv}(n, m) = \frac{1 - \exp[-2\pi i(n + mv)]}{1 - \exp[-2\pi i(n + mv)/u]} = \begin{cases} u, & \text{if } (n + mv)/u = \text{integer,} \\ 0, & \text{otherwise.} \end{cases} \quad (114)$$

Equation (113) is very similar to the scattering amplitude of untwisted carbon nanotubes with the exception of $\chi_{uv}^*(n, m)$, which only plays a minor role in determining the electron diffraction intensities.

The diffraction intensity distributions on the principal layer lines l_1, l_2 and l_3 are modulated by the same Bessel functions as those for untwisted carbon nanotubes, i.e. ignoring the Bessel functions of higher orders contributing to diffraction intensities on the principal layer lines, $n = v$ for l_1 , $n = -u$ for l_2 , and $n = u + v$ for l_3 . However, the axial periodicity of a twisted carbon nanotube (equation (111)) is different from that of the untwisted carbon nanotube, which results in changes of the ratios of layer line spacings between the principal layer lines. On the other hand, we can correlate the torsion angle $\Delta\vartheta$ with the measured layer line spacings D_1 and D_2 in the electron diffraction patterns from a twisted carbon nanotube by

$$\frac{\Delta\vartheta}{2\pi} = \frac{\zeta_0 - \zeta}{\zeta + v/u}, \quad (115)$$

where $\zeta_0 = (2u + v)/(u + 2v)$ and $\zeta = D_1/D_2$. Since the layer line spacings D_1 and D_2 can be measured very accurately, a very high accuracy ($0.1^\circ \text{ nm}^{-1}$) in the measurement of the torsion angle of a twisted carbon nanotube can be achieved by using the electron diffraction technique.

6.3. Carbon nanotube ropes

Another interesting morphology of carbon nanotube bundles is nanotube ropes, where single-walled carbon nanotubes form a twisted rope in contrast to the raft-like bundles described in section 4.6. In the configuration of a twisted nanotube rope, each single carbon nanotube is twisted without lowering the total formation energy substantially and the structural stability is greatly enhanced compared with the raft-like configuration. On the other hand, each single nanotube is not only twisted about its axis, it is also twisted about the rope axis. There is still no experimental data or in-depth discussion available in the literature on the electron diffraction from such nanotube ropes [166, 167].

7. Handedness of carbon nanotubes

As discussed in section 2, helical carbon nanotubes are enantiomorphic, though the definition of absolute handedness is rather arbitrary. Successful recognition of the handedness of a carbon nanotube may assist in exploring the handedness-related properties of carbon nanotubes [168–172]. When the carbon hexagonal rings are resolved in the scanning tunnelling microscopy images, the handedness can be revealed directly [90–92]. On the other hand, since electron diffraction measures the chiral indices accurately, it is of great interest to explore the possibilities for revealing the handedness of carbon nanotubes using electron diffraction.

7.1. Single-walled carbon nanotubes

The handedness of a nanotube can be assigned by observing the moving directions of the principal layer lines for a certain twisting direction in the electron diffraction pattern. The electron diffraction method for measuring the torsion angle presented in section 6.2 can be used to obtain the handedness of single-walled carbon nanotubes. For example, carbon nanotube (22,2) is a chiral nanotube and twisting it about the tubule axis in the clockwise direction is different from twisting it in the counterclockwise direction looking top-down against the tubule axis as shown in figure 29(a). Figure 30(a) shows an experimental electron diffraction pattern of an untwisted carbon nanotube (22,2). The simulated electron diffraction pattern of this nanotube is plotted on the experimental pattern and the compound pattern is given in figure 30(b), where the layer line spacings D_1 and D_2 are marked as references. Figures 30(c) and (d) show the simulated electron diffraction patterns of the nanotube (22,2) twisted in the counterclockwise and clockwise directions, respectively. It is noticeable that in comparison with the layer lines from the untwisted carbon nanotube, the principal layer spacing ratio D_1/D_2 in figure 30(c) increases due to the repulsive moving directions of the layer lines l_1 and l_2 , whereas D_1/D_2 in figure 30(d) decreases because of the attractive moving directions of the layer lines l_1 and l_2 . However, we can observe that the peak positions of diffraction intensities on all the layer lines remain the same in both figures 30(c) and (d). Thus by reference to equation (114), we can derive that the twisting angles of the twisted nanotube in figures 30(c) and (d) are $+1.95^\circ \text{ nm}^{-1}$ and $-1.95^\circ \text{ nm}^{-1}$ defining the plus sign for the counterclockwise direction, where we have divided the torsion angle by the length of the nanotube.

It is worth mentioning that if the nanotube has an opposite handedness, i.e. left-handedness for the nanotube (2,22), the diffraction layer lines would move in opposite directions compared with those for the right-handed nanotube (22,2) under the same twisting direction. This suggests that by twisting a chiral nanotube, we will be able to detect the handedness of the carbon nanotube. For example, we can assign the nanotube (22,2) presented above as right-handed, because the layer lines l_1 and l_2 in figure 30(c) move away from each other

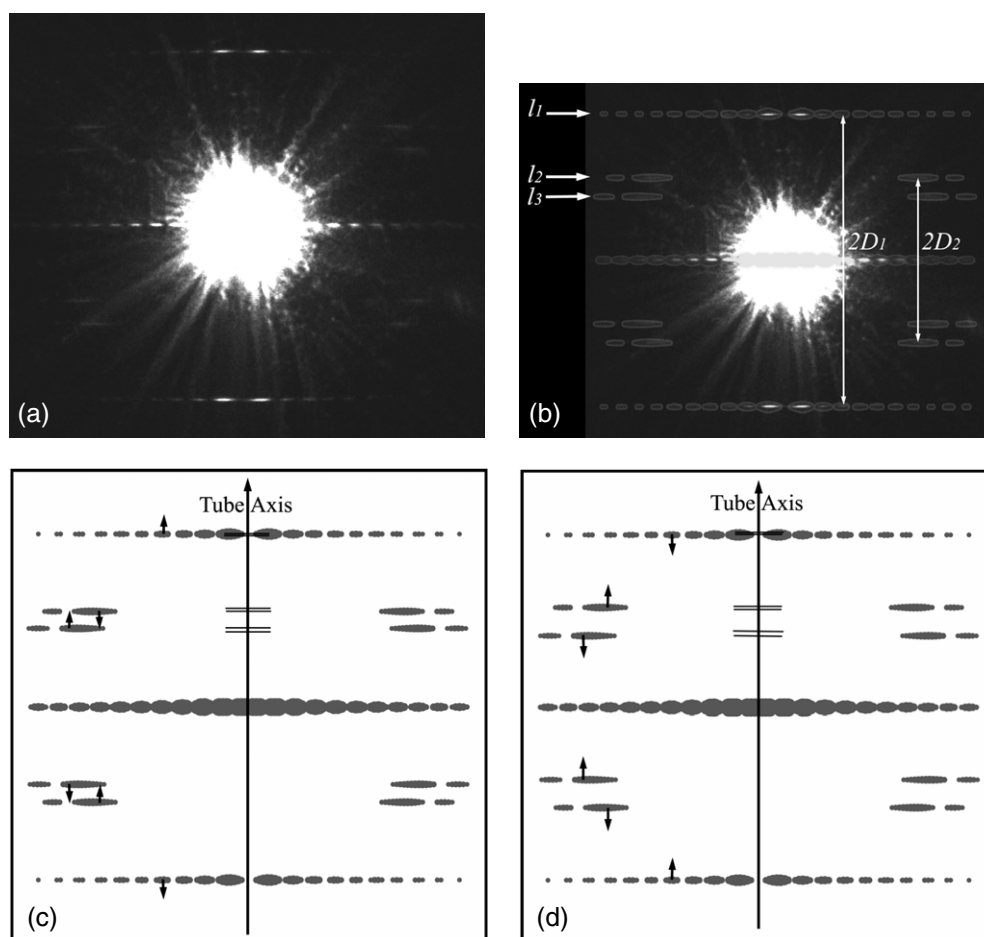


Figure 30. (a) Electron diffraction pattern of an untwisted carbon nanotube (2,2). (b) Simulated electron diffraction pattern of the untwisted carbon nanotube (2,2) plotted on the experimental pattern. (c) Calculated electron diffraction pattern of carbon nanotube (2,2) twisted counterclockwise by $\Delta\vartheta = -1.20^\circ \text{ nm}^{-1}$. (d) The same nanotube twisted clockwise $\Delta\vartheta = +1.20^\circ \text{ nm}^{-1}$. The arrows indicate the direction of shifts of the principal layer lines relative to the untwisted structure.

when we twist the nanotube in the counterclockwise direction. However, under the same counterclockwise twisting direction, if the layer lines l_1 and l_2 move towards each other as shown in figure 30(d), we can consider the nanotube as left-handed.

Experimental use of this method to obtain the handedness of carbon nanotubes can be found in [173].

7.2. Multiwalled carbon nanotubes

When there are two shells in a multiwalled carbon nanotube having the same helicity, electron diffraction can reveal the relative handedness of these two shells. To simplify the discussion but without loss of generality in principle, we can consider a double-walled carbon nanotube of two shells of chiral indices (u_1, v_1) and (u_2, v_2) , diameter d_1 and d_2 and the same helicity.

For this configuration, the layer lines will overlap completely. If the two shells also have the same handedness, the scattering intensities on the principal layer lines l_1 , l_2 and l_3 are [174]

$$I(R, \Phi, l_1) = \chi_0^2 f^2 \left\{ |u_1 J_{-v_1}(\pi d_1 R)|^2 + |u_2 J_{-v_2}(\pi d_2 R)|^2 \right. \\ \left. + 2u_1 u_2 J_{-v_1}(\pi d_1 R) J_{-v_2}(\pi d_2 R) \cos \left[(v_1 - v_2) \left(\Phi + \frac{\pi}{2} \right) + \Delta\varphi_1 \right] \right\}, \quad (116)$$

$$I(R, \Phi, l_2) = \chi_0^2 f^2 \left\{ |u_1 J_{u_1}(\pi d_1 R)|^2 + |u_2 J_{u_2}(\pi d_2 R)|^2 \right. \\ \left. + 2u_1 u_2 J_{u_1}(\pi d_1 R) J_{u_2}(\pi d_2 R) \cos \left[(u_2 - u_1) \left(\Phi + \frac{\pi}{2} \right) + \Delta\varphi_2 \right] \right\}, \quad (117)$$

and

$$I(R, \Phi, l_3) = \chi_0^2 f^2 \left\{ |u_1 J_{-(u_1+v_1)}(\pi d_1 R)|^2 + |u_2 J_{-(u_2+v_2)}(\pi d_2 R)|^2 \right. \\ \left. + 2u_1 u_2 J_{-(u_1+v_1)}(\pi d_1 R) J_{-(u_2+v_2)}(\pi d_2 R) \right. \\ \left. \times \cos \left[(u_1 - u_2 + v_1 - v_2) \left(\Phi + \frac{\pi}{2} \right) + \Delta\varphi_3 \right] \right\}, \quad (118)$$

where χ_0 is a constant.

$$\begin{cases} \Delta\varphi_1 = 152\varphi_0/7, \\ \Delta\varphi_2 = 0, \\ \Delta\varphi_3 = 152\varphi_0/7, \end{cases} \quad (119)$$

in which φ_0 is the rotational angle of the inner shell relative to the outer shell.

When the two shells have opposite handedness

$$I(R, \Phi, l_1) = \chi_0^2 f^2 \left\{ |u_1 J_{-v_1}(\pi d_1 R)|^2 + |u_2 J_{v_2}(\pi d_2 R)|^2 \right. \\ \left. + 2u_1 u_2 J_{-v_1}(\pi d_1 R) J_{v_2}(\pi d_2 R) \cos \left[(v_1 + v_2) \left(\Phi + \frac{\pi}{2} \right) + \Delta\varphi_1^* \right] \right\}, \quad (120)$$

$$I(R, \Phi, l_2) = \chi_0^2 f^2 \left\{ |u_1 J_{u_1}(\pi d_1 R)|^2 + |u_2 J_{-u_2}(\pi d_2 R)|^2 \right. \\ \left. + 2u_1 u_2 J_{u_1}(\pi d_1 R) J_{-u_2}(\pi d_2 R) \cos \left[(u_1 + u_2) \left(\Phi + \frac{\pi}{2} \right) + \Delta\varphi_2^* \right] \right\}, \quad (121)$$

and

$$I(R, \Phi, l_3) = \chi_0^2 f^2 \left\{ |u_1 J_{u_1+v_1}(\pi d_1 R)|^2 + |u_2 J_{u_2+v_2}(\pi d_2 R)|^2 \right. \\ \left. + 2u_1 u_2 J_{-(u_1+v_1)}(\pi d_1 R) J_{(u_2+v_2)}(\pi d_2 R) \right. \\ \left. \times \cos \left[(u_1 + u_2 + v_1 + v_2) \left(\Phi + \frac{\pi}{2} \right) + \Delta\varphi_3^* \right] \right\}, \quad (122)$$

where

$$\begin{cases} \Delta\varphi_1^* = 152\varphi_0/7, \\ \Delta\varphi_2^* = 0, \\ \Delta\varphi_3^* = -152\varphi_0/7. \end{cases} \quad (123)$$

As can be seen from equations (116)–(118) and equations (120)–(122), the dependence on the azimuthal angle Φ is different for the two shells having the same handedness (equations (116)–(118)) and opposite handedness (equations (120)–(122)). For example, the intensities on layer line l_2 have an angular periodicity of $2\pi/|u_2 - u_1|$ when the two shells have the same handedness. On the other hand, if the two shells have opposite handedness, the angular periodicity becomes $2\pi/|u_2 + u_1|$. The different dependence of the scattering intensities on the azimuthal angle can be used to obtain the relative handedness of the two shells.

Figure 31(a) shows a model structure of a double-walled carbon nanotube composed of two shells, (18,12) and (12,8) where the two shells have the same handedness. Figures 31(b)–(g) are the calculated electron diffraction patterns of this structure at various azimuthal angles where the arrow indicates the observed intensity on layer line l_2 . Figure 31(h) shows the dependence of the observed intensity of layer line l_2 where the data points corresponding to figures 31(b)–(g) are also indicated. For the particular structure, the angular periodicity on layer line l_2 is $\Delta\Phi = 2\pi/6 = \pi/3$.

On the other hand, if the two shells have opposite handedness as shown schematically in figure 32(a), the angular periodicity would become $\Delta\Phi^* = 2\pi/30 = \pi/15$. Figures 32(b)–(e) depict a series of simulated electron diffraction patterns for this configuration at azimuthal angles $\Phi = 0$ (figure 32(b)), $\Phi = 3^\circ$ (figure 32(c)), $\Phi = 6^\circ$ (figure 32(d)) and $\Phi = 9^\circ$ (figure 32(e)). A plot of the intensity peak on the principal layer line l_2 as a function of the azimuthal angle Φ is displayed in figure 32(f) where the data points corresponding to the four simulated electron diffraction patterns are also indicated in the figure.

An *in situ* experiment to determine the relative handedness of the shells of the same helicity using the abovementioned method has been recently carried out successfully by rotating a triple-walled carbon nanotube [175].

Appendix

In a polar coordinate system, the coordinates (r, ϕ, z) are related to the Cartesian coordinates (x, y, z) by the following transformation

$$\begin{cases} lx = r \cos(\phi), \\ ly = r \sin(\phi), \\ lz = z. \end{cases} \quad (\text{A1})$$

For the coordinates in reciprocal space, the corresponding equations are

$$\begin{cases} lX = R \cos(\Phi), \\ lY = R \sin(\Phi), \\ lZ = Z. \end{cases} \quad (\text{A2})$$

The structure factor in the polar coordinate system is

$$\begin{aligned} F(R, \Phi, Z) &= \int V(\vec{r}) \exp(2\pi i \vec{q} \cdot \vec{r}) d\vec{r} \\ &= \int_{-\infty}^{+\infty} \int_0^{2\pi} \int_0^{\infty} V(r, \phi, z) \exp\{2\pi i[rR \cos(\phi - \Phi) + zZ]\} r dr d\phi dz, \\ &= \int_{-\infty}^{+\infty} \int_0^{2\pi} \int_0^{\infty} V(r, \phi, z) \exp[2\pi i r R \cos(\phi - \Phi)] \exp(2\pi i z Z) r dr d\phi dz, \end{aligned} \quad (\text{A3})$$

and this is a general expression for any object in a polar coordinate system.

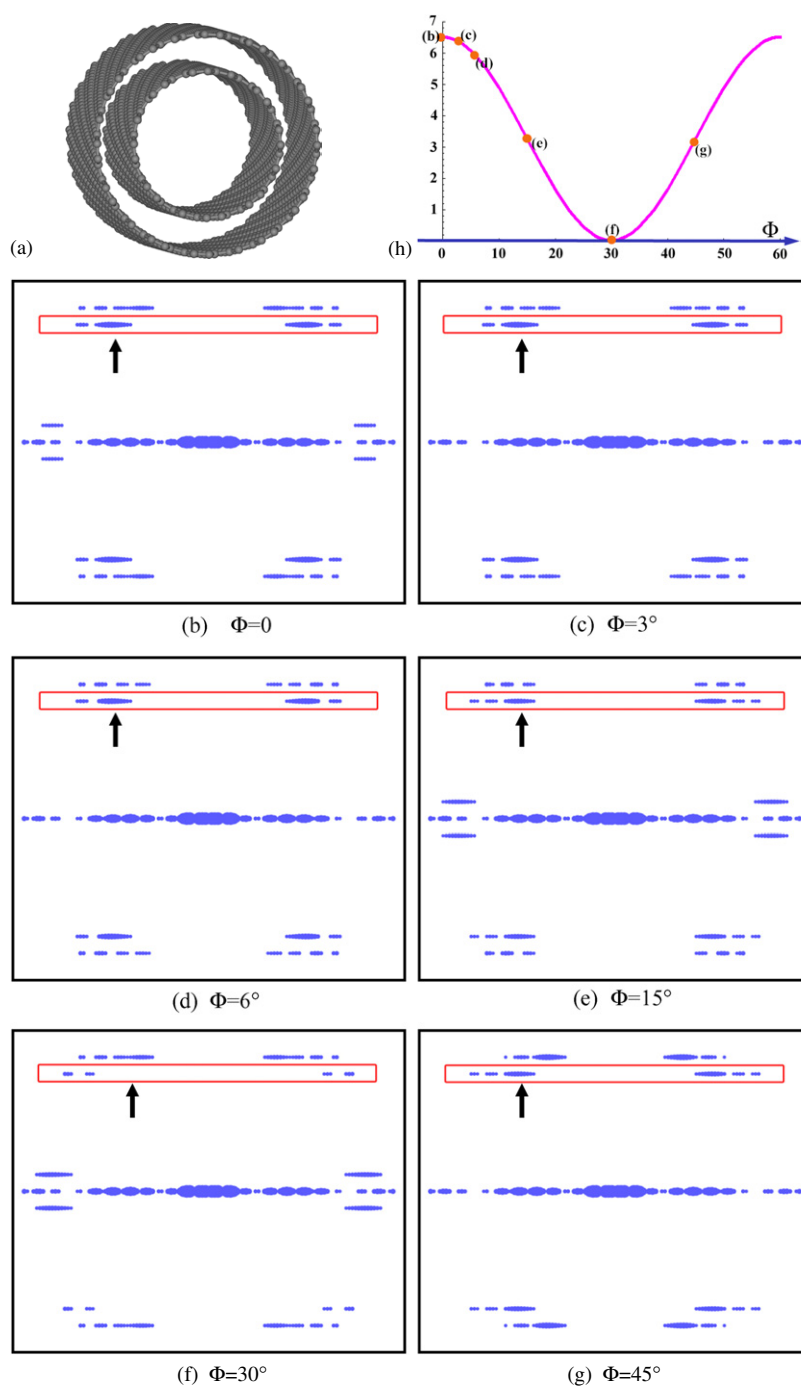


Figure 31. (a) Atomic structure of a double-walled carbon nanotube where the two shells (18,12) and (12,8) have the same handedness and same helicity. (b)–(g) Simulated electron diffraction patterns of the structure at azimuthal angles (b) $\Phi = 0$, (c) $\Phi = 3^\circ$, (d) $\Phi = 6^\circ$, (e) $\Phi = 15^\circ$, (f) $\Phi = 30^\circ$ and (g) $\Phi = 45^\circ$. (h) Maximum intensity on principal layer line l_2 as a function of the azimuthal angle Φ . The rotational periodicity of scattering intensities on this layer line (l_2 , enclosed in rectangle) is $\Delta\Phi = 60^\circ$.

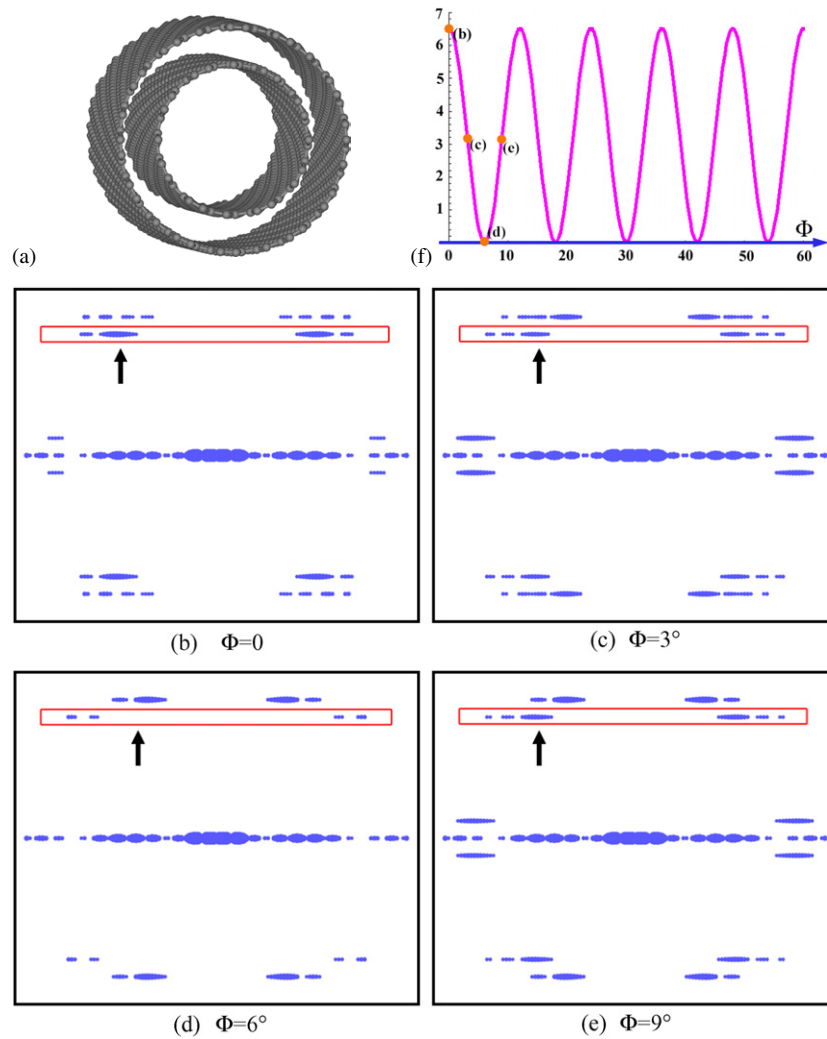


Figure 32. (a) Atomic structure of a double-walled carbon nanotube where the two shells (18,12) and (8,12) have the same helicity but opposite handedness. (b)–(e) Simulated electron diffraction patterns of the structure at azimuthal angles (b) $\Phi = 0^\circ$, (c) $\Phi = 3^\circ$, (d) $\Phi = 6^\circ$ and (e) $\Phi = 9^\circ$. (f) Maximum intensity on principal layer line l_2 as a function of azimuthal angle Φ . The rotational periodicity of the scattering intensities on this layer line (l_2 , enclosed in rectangle) is $\Delta\Phi^* = 12^\circ$.

Introducing the Bessel function J_n of order n defined by

$$2\pi i^n J_n(u) = \int_0^{2\pi} \exp(iu \cos \phi + in\phi) d\phi \quad (\text{A4})$$

and the following relationships

$$\exp(iu \cos \phi) = \sum_{n=-\infty}^{+\infty} J_n(u) \exp\left[in\left(\phi + \frac{\pi}{2}\right)\right] \quad (\text{A5})$$

$$J_{-n}(u) = (-1)^n J_n(u), \quad (\text{A6})$$

we can obtain

$$\begin{aligned}
 F(R, \Phi, Z) &= \sum_n \int_{-\infty}^{+\infty} \int_0^{\infty} V(r, \phi, z) \exp(in\Phi) \\
 &\times \left\{ \int_0^{2\pi} \sum_{n=-\infty}^{+\infty} J_n(2\pi r R) \exp \left[in \left(\Phi - \phi + \frac{\pi}{2} \right) \right] d\phi \right\} \exp(2\pi iz Z) r dr d\phi dz \\
 &= \sum_n \exp \left[in \left(\Phi + \frac{\pi}{2} \right) \right] \int_{-\infty}^{+\infty} \int_0^{2\pi} \int_0^{\infty} V(r, \phi, z) J_n(2\pi r R) \\
 &\times \exp(-in\phi + 2\pi iz Z) r dr d\phi dz. \tag{A7}
 \end{aligned}$$

When the potential $V(r, \phi, z)$ has an N -fold rotation axis along the z -direction, i.e.

$$V(r, \phi, z) = V \left(r, \phi + \frac{2\pi}{N}, z \right), \tag{A8}$$

the Fourier expansion (A4) can be written in the following form

$$V(r, \phi, z) = \sum_n V_{nN}(r, z) \exp(inN\phi), \tag{A9}$$

where

$$V_{nN}(r, z) = \frac{N}{2\pi} \int_0^{2\pi/n} V(r, \phi, z) \exp(-inN\phi) d\phi, \tag{A10}$$

and the structure factor becomes

$$\begin{aligned}
 F(R, \Phi, Z) &= N \sum_{n=-\infty}^{+\infty} \exp \left[inN \left(\Phi + \frac{\pi}{2} \right) \right] \int_{-\infty}^{+\infty} \int_0^{2\pi} \int_0^{\infty} V(r, \phi, z) J_{nN}(2\pi r R) \\
 &\times \exp(2\pi iz Z) \exp(-inN\phi) r dr d\phi dz. \tag{A11}
 \end{aligned}$$

If the object is periodic along the z -direction with periodicity c , the Fourier expansion (A4) can be written as

$$V(r, \phi, z) = \sum_{n=-\infty}^{+\infty} \sum_{l=-\infty}^{+\infty} V_{nl}(r) \exp \left(-in\phi + \frac{2\pi ilz}{c} \right), \tag{A12}$$

and we can similarly incorporate the z -components into the relevant equations to obtain the following expression of the structure factor:

$$\begin{aligned}
 F(R, \Phi, l) &= \frac{1}{c} \sum_{n=-\infty}^{+\infty} \exp \left[in \left(\Phi + \frac{\pi}{2} \right) \right] \int_0^c \int_0^{2\pi} \int_0^{\infty} V(r, \phi, z) J_l(2\pi r R) \\
 &\times \exp \left[i \left(-n\phi + \frac{2\pi lz}{c} \right) \right] r dr d\phi dz. \tag{A13}
 \end{aligned}$$

Acknowledgments

The author would like to thank his former graduate student, Dr Zejian Liu, for his contributions including preparation of many of the figures presented in this paper, and Dr Qi Zhang for her assistance. Financial support from the W M Keck Foundation, the University of North Carolina at Chapel Hill (UNC) and the UNC Research Council is gratefully acknowledged.

References

- [1] Bragg W H and Bragg W L 1913 The structure of the diamond *Nature* **91** 557
- [2] Bragg W H and Bragg W L 1913 The structure of the diamond *Proc. R. Soc. (Lond.) A* **89** 277
- [3] Bernal J D 1924 The structure of graphite *Proc. R. Soc. (Lond.) A* **106** 749
- [4] Iijima S 1991 Helical microtubules of graphitic carbon *Nature* **354** 56
- [5] Ando Y and Ohkochi M 1982 Ultrafine power of β -SiC by arc discharge *J. Cryst. Growth* **60** 147
- [6] Kroto H W, Heath J R, O'Brien S C, Curl R F and Smalley R E 1985 C₆₀: Buckminsterfullerene *Nature* **318** 162
- [7] Krätschmer W, Lamb L D, Fostiropoulos K and Huffman D R 1990 Solid C₆₀: a new form of carbon *Nature* **347** 354
- [8] Iijima S and Ichihashi T 1993 Single-shell carbon nanotubes of 1 nm diameter *Nature* **363** 603
- [9] Bethune D S, Kiang C -H, de Vries M S, Gorman G, Savoy R, Vazquez J and Beyers R 1993 Cobalt-catalysed growth of carbon nanotubes with single-atomic-walls *Nature* **363** 605
- [10] Ebbesen T W and Ajayan P M 1992 Large-scale synthesis of carbon nanotubes *Nature* **358** 220
- [11] Journet C, Maser W K, Bernier P, Loiseau A, Lamy de la Chapelle M, Lefrant S, Deniards P, Lee R and Fischer J E 1997 Large-scale production of single-walled carbon nanotubes by the electric-arc technique *Nature* **388** 756
- [12] Wang X K, Lin X W, Dravid V P, Ketterson J B and Chang R P H 1995 Carbon nanotubes synthesized in a hydrogen arc-discharge in hydrogen *Appl. Phys. Lett.* **66** 2430
- [13] Zhao X, Ando Y, Ohkohchi M, Wang M, Iijima S and Ichihashi T 1997 Preparation of high-grade carbon nanotubes by hydrogen arc-discharge *Carbon* **35** 775
- [14] Guo T, Nikolaev P, Thess A, Colbert D T and Smalley R E 1995 Catalytic growth of single-shell nanotubes by laser evaporation *Chem. Phys. Lett.* **243** 49
- [15] Thess A, Lee R, Nikolaev P, Dai H J, Petit P, Robert J, Xu C H, Lee Y H, Kim S G, Rinzlev A G, Colbert D T, Scuseria G E, Tomanek D, Fischer J E and Smalley R E 1996 Crystalline ropes of metallic carbon nanotubes *Science* **273** 483
- [16] Qin L -C and Iijima S 1997 Structure and formation of raft-like bundles of single-walled helical carbon nanotubes produced by laser evaporation *Chem. Phys. Lett.* **269** 65
- [17] Gibson J A E 1992 Early nanotubes? *Nature* **359** 369
- [18] Bacon R 1960 Growth, structure and properties of graphite whiskers *J. Appl. Phys.* **31** 283
- [19] Oberlin A, Endo M and Koyama T 1976 Filamentous growth of carbon through benzene decomposition *J. Cryst. Growth* **32** 335
- [20] Baker R T K and Harris P S 1978 The formation of filamentous carbon *Chem. Phys. Carbon* **14** 83
- [21] Endo M 1988 Grow carbon-fibers in the vapor phase *Chemtechnology* **18** 568
- [22] Endo M, Takeuchi K, Igarashi S, Kobori K, Shirashi M and Kroto H W 1993 The production and structure of pyrolytic carbon nanotubes (PCNTs) *J. Phys. Chem. Solids* **54** 1841
- [23] Amelinckx S, Zhang X B, Bernaerts D, Zhang X F, Ivanov V and Nagy J B A formation-mechanism for catalytically grown helix shaped graphite nanotubes 1994 *Science* **265** 635
- [24] Dai H, Rinzler A G, Nikolaev P, Thess A, Colbert D T and Smalley R E 1996 *Chem. Phys. Lett.* **260** 471
- [25] Li W Z, Xie S S, Qian L X, Chang B H, Zou B S, Zhou W Y, Zhao R A and Wang G 1996 Large-scale synthesis of aligned carbon nanotubes *Science* **274** 1701
- [26] Qin L-C 1997 CVD synthesis of carbon nanotubes *J. Mater. Sci. Lett.* **16** 457
- [27] Qin L-C and Iijima S 1997 Fibrilliform growth of carbon nanotubes *Mater. Lett.* **30** 311
- [28] Ren Z F, Huang Z P, Wu J W, Wang J H, Bush P, Siegal M P and Provencio P N 1998 Synthesis of large arrays of well-aligned carbon nanotubes on glass *Science* **282** 1105
- [29] Kong J, Soh H, Cassell A, Quate C F and Dai H 1998 Synthesis of individual single-walled carbon nanotubes on patterned silicon wafers *Nature* **295** 878
- [30] Huang S, Cai X, Du C and Liu J 2003 Oriented long single walled carbon nanotubes on substrates from floating catalysts *J. Phys. Chem. B* **107** 13251
- [31] Fu Q, Huang S and Liu J 2004 Chemical vapor depositions of single-walled carbon nanotubes catalyzed by uniform Fe₂O₃ nanoclusters synthesized using diblock copolymer micelles *J. Phys. Chem. B* **108** 6124
- [32] Hata K, Futaba D N, Mizuno K, Namai T, Yumura M and Iijima S 2004 Water-assisted highly efficient synthesis of impurity-free single-walled carbon nanotubes *Science* **306** 1362
- [33] Calderon-Moreno J M and Yoshimura M 2001 Hydrothermal processing of high-quality multiwall nanotubes from amorphous carbon *J. Am. Chem. Soc.* **123** 741
- [34] Jiang Y, Wu Y, Zhang S Y, Xu C Y, Yu W C, Xie Y and Qian Y T 2000 A catalytic-assembly solvothermal route to multiwall carbon nanotubes at a moderate temperature *J. Am. Chem. Soc.* **122** 12383

- [35] Vohs J K, Brege J J, Raymond J E, Brown A E, Williams G L and Fahlman B D 2004 Low-temperature growth of carbon nanotubes from the catalytic decomposition of carbon tetrachloride *J. Am. Chem. Soc.* **126** 9936
- [36] Lu J Q, Kopley T E, Moll N, Roitman D, Chamberlin D, Fu Q, Liu J, Russell T P, Rider D A, Manner I and Winnik M A 2005 High-quality single-walled carbon nanotubes with small diameter, controlled density, and ordered locations using a polyferrocenylsilane block copolymer catalyst precursor *Chem. Mater.* **17** 2227
- [37] Wang W, Poudel B, Wang D Z and Ren Z F 2005 Synthesis of multiwalled carbon nanotubes through a modified Wolff-Kishner reduction process *J. Am. Chem. Soc.* **127** 18018
- [38] Qin L -C, Zhou D, Krauss A R and Gruen D M 1998 Growing carbon nanotubes by microwave plasma-enhanced chemical vapor deposition *Appl. Phys. Lett.* **72** 3437
- [39] Bower C, Zhou O, Zhu W, Werder D J and Jin S 2000 Nucleation and growth of carbon nanotubes by microwave plasma chemical vapor deposition *Appl. Phys. Lett.* **77** 2767
- [40] Wang Y Y, Gupta S and Nemanich R J 2004 Role of thin Fe catalyst in the synthesis of double- and single-walled carbon nanotubes via microwave chemical vapor deposition *Appl. Phys. Lett.* **85** 2601
- [41] Hamada N, Sawada S and Oshiyama A 1992 New one-dimensional conductors: graphite microtubules *Phys. Rev. Lett.* **68** 1579
- [42] Saito R, Fujita M, Dresselhaus G and Dresselhaus M S 1992 Electronic structure of chiral graphene tubules *Appl. Phys. Lett.* **60** 2204
- [43] Mintmire J W, Dunlap B I and White C T 1992 Are fullerene tubules metallic? *Phys. Rev. Lett.* **68** 631
- [44] Olk C H and Heremans J P 1994 Scanning tunneling spectroscopy of carbon nanotubes *J. Mater. Res.* **9** 259
- [45] Yorikawa H and Muramatsu S 1995 Energy gaps of semiconducting nanotubes *Phys. Rev. B* **52** 2723
- [46] Kleiner A and Eggert S 2001 Band gaps of primary metallic carbon nanotubes *Phys. Rev. B* **63** 073408
- [47] Collins P G, Zettl A, Bando H, Thess A and Smalley R E 1997 Nanotube nanodevice *Science* **278** 100
- [48] Yao Z, Postma, H W Ch, Balents L and Dekker C 1999 Carbon nanotube intramolecular junctions *Nature* **402** 273
- [49] Kong J, Franklin N R, Zhou C, Chapline M G, Peng S, Cho K and Dai H 2000 Nanotube molecular wires as chemical sensors *Science* **287** 622
- [50] Avouris P 2002 Molecular electronics with carbon nanotubes *Acc. Chem. Res.* **35** 1026
- [51] Yoo S, Jung Y M, Lee D S, Han W T, Oh K, Murakami Y, Edamura T and Maruyama S 2005 Optical anisotropy in single-walled carbon nanotubes *Opt. Lett.* **30** 3201
- [52] Kazaoui S, Minami N, Nalini B, Kim Y, Takada N and Hara K 2005 Near-infrared electroluminescent devices using single-wall carbon nanotubes thin films *Appl. Phys. Lett.* **87** 211914
- [53] Chen J, Perebeinos V, Freitag M, Tsang J, Fu Q, Liu J and Avouris P 2005 Bright infrared emission from electrically induced excitons in carbon nanotubes *Science* **310** 1171
- [54] Robertson D H, Brenner D W and Mintmire J W 1992 Energetics of nanoscale graphitic tubules *Phys. Rev. B* **45** 12592
- [55] Calvert P 1992 Strength in disunity *Nature* **357** 365
- [56] Overney G, Zhong W and Tomanek D 1993 Structural rigidity and low-frequency vibrational modes of long carbon tubules *Z. Phys. D* **27** 93
- [57] Tracy M M J, Ebbesen T W and Gibson J M 1996 Exceptionally high Young's modulus observed for individual carbon nanotubes *Nature* **381** 678
- [58] Yao N and Lordi V 1998 Young's modulus of single-walled carbon nanotubes *J. Appl. Phys.* **84** 1939
- [59] Lu J-P 1997 Elastic properties of carbon nanotubes and nanoropes *Phys. Rev. Lett.* **79** 1297
- [60] Gao R P, Wang Z L, Bai Z G, de Heer W A, Dai L M and Gao M 2000 Nanomechanics of individual carbon nanotubes from pyrolytically grown arrays *Phys. Rev. Lett.* **85** 622
- [61] Dohn S, Kjelstrup-Hansen J, Madsen D N, Molhave K and Boggild P 2005 Multi-walled carbon nanotubes integrated in microcantilevers for application of tensile strain *Ultramicroscopy* **105** 209
- [62] Mori H, Hirai Y, Ogata S, Akita S and Nakayama Y 2005 Chirality dependence of mechanical properties of single-walled carbon nanotubes under axial tensile strain *Japan. J. Appl. Phys.* **44** L1307
- [63] Barber A H *et al* 2005 On the tensile strength distribution of multiwalled carbon nanotubes *Appl. Phys. Lett.* **87** 203106
- [64] Rinzler, A G, Hafner J H, Nikolaev P, Lou L, Kim S G, Tomanek D, Nordlander P, Colbert D T and Smalley R E 1995 Unraveling nanotubes—field-emission from an atomic wire *Science* **269** 1550
- [65] de Heer W A, Châtelain A and Ugarte D 1995 A carbon nanotube field-emission electron source *Science* **270** 1179
- [66] Collins P G and Zettl A 1996 A simple and robust electron beam source from carbon nanotubes *Appl. Phys. Lett.* **69** 1969

- [67] Wang Q H, Corrigan T D, Dai J Y, Chang R P H and Krauss A R 1997 Field emission from nanotube bundle emitters at low fields *Appl. Phys. Lett.* **70** 3308
- [68] Bonard J M, Salvétat J P, Stockli T, de Heer W A, Forro L and Chatelain A 1998 Field emission from single-wall carbon nanotube films *Appl. Phys. Lett.* **73** 918
- [69] Zhu W, Bower C, Zhou O, Kochanski G and Jin S 1999 Large current density from carbon nanotube field emitters *Appl. Phys. Lett.* **75** 873
- [70] Bonard J M, Klinke C, Dean K A and Coll B F 2003 Degradation and failure of carbon nanotube field emitters *Phys. Rev. B* **67** 115406
- [71] Yue G Z, Qiu Q, Gao B, Cheng Y, Zhang J, Shimoda H, Chang S, Lu J P and Zhou O 2002 *Appl. Phys. Lett.* **81** 355
- [72] Cheng Y, Zhang J, Lee Y Z, Gao B, Dike S, Lin W, Lu J P and Zhou O 2004 Dynamic radiography using a carbon-nanotube-based field-emission x-ray source *Rev. Sci. Instrum.* **75** 3264
- [73] Choi W B, Chung D S, Kang J H, Kim H Y, Jin Y W, Han I T, Lee Y H, Jung J E, Lee N S, Park G S and Kim J M 1999 Fully sealed, high-brightness carbon-nanotube field-emission display *Appl. Phys. Lett.* **75** 3129
- [74] Fransen M J, Van Rooy T L and Kruit P 1999 Field emission energy distribution from individual multiwalled carbon nanotubes *Appl. Surf. Sci.* **164** 312
- [75] Bonard J M, Salvétat J P, Stöckli T, Forró L and Châtelain A 1999 Field emission from carbon nanotubes: perspectives for applications and clues to the emission mechanism *Appl. Phys. A* **69** 245
- [76] Bonard J M, Dean K A, Coll B F and Klinke C 2002 Field emission of individual carbon nanotubes in the scanning electron microscope *Phys. Rev. Lett.* **89** 197602
- [77] de Jonge N, Lamy Y, Schoots K and Oosterkamp T H 2002 High brightness electron beam from a multi-walled carbon nanotube *Nature* **420** 393
- [78] de Jonge N, Lamy Y and Kaiser M 2003 Controlled mounting of individual multiwalled carbon nanotubes on support tips *Nano Lett.* **3** 1621
- [79] Zhang J, Tang J, Yang G, Qiu Q, Qin L-C and Zhou O 2004 Efficient fabrication of carbon nanotube point electron sources by dielectrophoresis *Adv. Mater.* **16** 1219
- [80] Dai H, Hafner J H, Rinzler A G, Colbert D T and Smalley R E 1996 Nanotubes as nanoprobe tips in scanning probe microscopy *Nature* **384** 147
- [81] Hafner J H, Cheung C-L and Lieber C M 1999 Growth of nanotube for probe microscopy tip *Nature* **398** 761
- [82] Hafner J H, Cheung C-L, Woolley A T and Lieber C M 2001 Structural and functional imaging with carbon nanotube AFM probes *Prog. Biophys. Mol. Biol.* **77** 73
- [83] Tang J, Yang G, Zhang Q, Parhat A, Maynor B, Liu J, Qin L-C and Zhou O 2005 Rapid and reproducible fabrication of carbon nanotube AFM probes by dielectrophoresis *Nano Lett.* **5** 11
- [84] Rao A M *et al* 1997 Diameter-selective Raman scattering from vibrational modes in carbon nanotubes *Science* **275** 187
- [85] Jorio A, Pimenta M A, Souza A G, Saito R, Dresselhaus G and Dresselhaus M S 2003 Characterizing carbon nanotube samples with resonance Raman scattering *New J. Phys.* **5** 139
- [86] Bachilo S M, Strano M S, Kittrell C, Hauge R H, Smalley R E and Weisman R B 2002 Structure assisted optical spectra of single-walled carbon nanotubes *Science* **298** 2361
- [87] Strano M S, Doorn S K, Haroz E H, Kittrell C, Hauge R H and Smalley R E 2003 Assignment of (n, m) Raman and optical features of metallic single-walled carbon nanotubes *Nano Lett.* **3** 1091
- [88] Ge M and Sattler K 1993 Vapor-condensation generation of and STM analysis of fullerene tubes *Science* **260** 515
- [89] Ge M and Sattler K 1994 STM of single-shell nanotubes of carbon *Appl. Phys. Lett.* **65** 2284
- [90] Lin N, Ding J, Yang S and Cue N 1996 Scanning tunneling microscopy and spectroscopy of a carbon nanotube *Carbon* **34** 1295
- [91] Wildoer J W G, Venema L C, Rinzler A G, Smalley R E and Dekker C 1998 Electronic structure of atomically resolved carbon nanotubes *Nature* **391** 59
- [92] Odom T W, Huang J-L, Kim P and Lieber C M 1998 Atomic structure and electronic properties of single-walled carbon nanotubes *Nature* **391** 62
- [93] Cochran W, Crick F C H and Vand V 1952 The structure of synthetic polypeptides. I. The transform of atoms on a helix *Acta Cryst.* **5** 581
- [94] Watson J D and Crick F H C 1953 A structure of deoxy-ribose nucleic acid *Nature* **171** 737
- [95] Wilkins M H F, Stokes A R and Wilson H R 1953 Molecular structure of deoxypentose nucleic acids *Nature* **171** 738
- [96] Franklin R and Gosling 1953 Molecular configuration in sodium thymonucleate *Nature* **171** 739
- [97] Klug A, Crick F H C and Wyckoff H W 1958 Diffraction by helical structures *Acta Cryst.* **11** 199

- [98] Vainshtein B K 1966 *Diffraction of X-Rays by Chain Molecules* (Amsterdam: Elsevier)
- [99] Sherwood D 1976 *Crystals X-Rays and Proteins* (London: Longman)
- [100] Lucas A A and Lambin P 2005 Diffraction by DNA, carbon nanotubes and other helical nanostructures *Rep. Prog. Phys.* **68** 1181
- [101] Qin L -C 1994 Electron diffraction from cylindrical nanotubes *J. Mater. Res.* **9** 2450
- [102] Lucas A A, Bruyninckx V and Lambin Ph 1996 Calculating the diffraction of electrons or x-rays by carbon nanotubes *Europhys. Lett.* **35** 355
- [103] Lambin P and Lucas A A 1997 Quantitative theory of diffraction by carbon nanotubes *Phys. Rev. B* **56** 3571
- [104] Zhang X F, Zhang X B, Van Tendeloo G, Amelinckx S, Op de Beeck M and Van Landuyt J 1993 Carbon nanotubes; their formation process and observation by electron microscopy *J. Cryst. Growth* **130** 368
- [105] Zhang X B, Zhang X F, Amelinckx S, Van Tendeloo G and Van Landuyt J 1994 The reciprocal space of carbon-tubes: a detailed interpretation of the electron diffraction effects *Ultramicroscopy* **54** 237
- [106] Zhang X B and Amelinckx S 1994 On the determination of the chiral angle in carbon nanotubes *Carbon* **32** 1537
- [107] Amelinckx S, Devouard B and Baronnet A 1996 Geometric aspects of the diffraction space of serpentine rolled microstructures: their study by means of electron diffraction and microscopy *Acta Cryst. A* **52** 850
- [108] Bernaerts D, Amelinckx S, Lambin P and Lucas A A 1998 The diffraction space of circular and polygonized multishell nanotubes *Appl. Phys. A* **67** 53
- [109] Amelinckx S, Lucas A and Lambin P 1999 Electron diffraction and microscopy of nanotubes *Rep. Prog. Phys.* **62** 1471
- [110] Qin L -C, Ichihashi T and Iijima S 1997 On the measurement of helicity of carbon nanotubes *Ultramicroscopy* **67** 181
- [111] Cowley J M, Nikolaev P, Thess A and Samlley R E 1997 Electron nano-diffraction study of carbon single-walled nanotube ropes *Chem. Phys. Lett.* **265** 379
- [112] Qin L -C, Iijima S, Kataura H, Maniwa Y, Suzuki S and Achiba Y 1997 Helicity and packing of single-walled carbon nanotubes studied by electron nanodiffraction *Chem. Phys. Lett.* **268** 101
- [113] Qin L -C 1998 Measuring the true helicity of carbon nanotubes *Chem. Phys. Lett.* **297** 23
- [114] Qin L -C 2000 Helical diffraction from tubular structures *Mater. Charact.* **44** 407
- [115] He R R, Jin H Z, Zhu J, Yan Y J and Chen X H 1998 Physical and electronic structure in carbon nanotubes *Chem. Phys. Lett.* **298** 170
- [116] Kociak M, Suenaga K, Hirahara K, Saito Y, Nagahara T and Iijima S 2002 Linking chiral indices and transport properties of double-walled carbon nanotubes *Phys. Rev. Lett.* **89** 155501
- [117] Colomer J-F, Henrard L, Lambin P and Van Tendeloo G 2001 Electron diffraction study of small bundles of single-walled carbon nanotubes with unique helicity *Phys. Rev. B* **64** 125425
- [118] Colomer J-F, Henrard L, Lambin P and Van Tendeloo G 2002 Electron diffraction and microscopy of single-walled carbon nanotube bundles produced by different methods *Euro. Phys. J. B* **27** 111
- [119] Colomer J-F, Henrard L, Launois P, Van Tendeloo G, Lucas A A and Lambin P 2004 Interpretation of electron diffraction from carbon nanotube bundles presenting exact helicity *Phys. Rev. B* **70** 075408
- [120] Gao M, Zuo J M, Twesten R D, Petrov I, Nagahara L A and Zhang R 2003 Structure determination of individual single-wall carbon nanotubes by nanoarea electron diffraction *Appl. Phys. Lett.* **82** 2703
- [121] Zuo J M, Vartanyants I, Gao M, Zhang R and Nagahara L A 2003 Atomic resolution imaging of a carbon nanotube from diffraction intensities *Science* **300** 1419
- [122] Liu Z and Qin L-C 2005 A direct method to determine the chiral indices of carbon nanotubes *Chem. Phys. Lett.* **408** 75
- [123] Liu Z, Zhang Q and Qin L -C 2005 Determination and mapping of diameter and helicity for single-walled carbon nanotubes using nanobeam electron diffraction *Phys. Rev. B* **71** 245413
- [124] Liu Z, Zhang Q and Qin L-C 2005 Accurate determination of atomic structure of multiwalled carbon nanotubes by nondestructive nanobeam electron diffraction *Appl. Phys. Lett.* **86** 191903
- [125] Liu M and Cowley J M 1994 Structures of the helical carbon nanotubes *Carbon* **32** 393
- [126] Liu M and Cowley J M 1994 Structures of carbon nanotubes studied by HRTEM and nanodiffraction *Ultramicroscopy* **53** 333
- [127] Fan X D and Bursil L A 1995 Principles for structure analysis of carbon nanotubes by high-resolution transmission electron microscopy *Phil. Mag. A* **72** 139
- [128] Bernaerts D, Zettl A, Chopra N G, Thess A and Smalley R E 1998 Electron diffraction study of single-wall carbon nanotubes *Solid State Commun.* **105** 145

- [129] Hirahara K, Bandow S, Suenaga K, Kato H, Okazaki T, Shinohara H and Iijima S 2000 One-dimensional metallofullerenes crystal generated inside single-walled nanotubes *Phys. Rev. Lett.* **85** 5384
- [130] Lambin P, Meunier V, Henrard L and Lucas A A 2000 Measuring the helicity of carbon nanotubes *Carbon* **38** 1713
- [131] Henrard L, Loiseau A, Journet C and Bernier P 2000 Study of the symmetry of single wall nanotubes by electron diffraction *Eur. Phys. J. B* **13** 661
- [132] Lucas A A, Moreau F and Lambin P 2002 Optical simulations of electron diffraction by carbon nanotubes *Rev. Mod. Phys.* **74** 1
- [133] Schlittler R R, Seo J W, Gimzewski J K, Durkan C, Saifullah M S M and Welland M E 2001 Single crystals of single-walled carbon nanotubes formed by self-assembly *Science* **292** 1136
- [134] Chisholm M F, Wang Y H, Lupini A R, Eres G, Puzos A A, Brinson B, Melechko A V, Geohegan D B, Cui H T, Johnson M P, Pennycook S J, Lowndes D H, Arepalli S, Kittrell C, Sivaram S, Kim M, Lavin G, Kono J, Hauge R and Smalley R E 2003 Comment on 'Single crystals of single-walled carbon nanotubes formed by self-assembly' *Science* **300** 1236
- [135] Kociak M, Suenaga K, Hirahara K, Saito Y, Nakahira T and Iijima S 2002 Linking chiral indices and transport properties of double-walled carbon nanotubes *Phys. Rev. Lett.* **89** 155501
- [136] Kociak M, Hirahara K, Suenaga K and Iijima S 2003 How accurate can the determination of chiral indices of carbon nanotubes be? An experimental investigation of chiral indices determination of DWNT by electron diffraction *Eur. Phys. J. B* **32** 457
- [137] Ruland W, Schaper A K, Hou H and Greiner A 2003 Multi-wall carbon nanotubes with uniform chirality: evidence for scroll structures *Carbon* **41** 423
- [138] Colomer J-F, Henrard L, Van Tendeloo G, Lucas A A and Lambin P 2004 Study of the packing of double-wall carbon nanotubes into bundles by transmission electron microscopy and electron diffraction *J. Mater. Chem.* **14** 603
- [139] Zhang G Y, Jiang X and Wang E G 2003 Tubular graphite cones *Science* **300** 472
- [140] Luo J, Zhu J and Ye H Q 2004 Comment on 'Tubular graphite cones' *Science* **303** 766c
- Zhang G Y, Bai X D, Jiang X and Wang E G 2004 Response to Comment on 'Tubular graphite cones' *Science* **303** 766c
- [141] Hirahara K, Bandow S, Kataura H, Kociak M and Iijima S 2004 *Phys. Rev. B* **70** 205422
- [142] Meyer J C, Paillet M, Duesberg G S and Roth S 2005 Electron diffraction analysis of individual single-walled carbon nanotubes *Ultramicroscopy* **106** 176
- [143] Saito R, Dresselhaus G and Dresselhaus M S 1998 *Physical Properties of Carbon Nanotubes* (London: Imperial College Press)
- [144] Mott N F 1930 The scattering of electrons by atoms *Proc. R. Soc. Lond.* **127** 658
- [145] Humphreys C J 1979 The scattering of fast electrons by crystals *Rep. Prog. Phys.* **42** 1825
- [146] Hoerni J A and Ibers J A 1953 Complex amplitudes for electron scattering by atoms *Phys. Rev.* **91** 1182
- [147] Doyle P A and Turner P S 1968 Relativistic Hartree-Fock x-ray and electron scattering factors *Acta Cryst.* **24** 390
- [148] Peng L-M and Cowley J M 1988 Errors arising from numerical use of the Mott formula in electron image simulation *Acta Cryst.* **44** 1
- [149] Fox A G, O'Keefe M A and Tabbenrnr 1989 Relativistic Hartree-Fock x-ray and electron scattering factors at high angles *Acta Cryst. A* **45** 786
- [150] Liu Z and Qin L-C 2005 Breakdown of 2mm symmetry in electron diffraction from multiwalled carbon nanotubes *Chem. Phys. Lett.* **402** 202
- [151] Liu Z and Qin L-C 2004 Symmetry of electron diffraction from single-walled carbon nanotubes *Chem. Phys. Lett.* **400** 430
- [152] Liu Z 2006 *PhD Thesis* University of North Carolina at Chapel Hill
- [153] Ball P 1996 The perfect nanotube *Nature* **382** 207
- [154] Liu Z and Qin L-C in preparation
- [155] Zhang Q, Liu Z and Qin L-C in preparation
- [156] Liu Z and Qin L-C 2005 Extinction and orientational dependence of electron diffraction from single-walled carbon nanotubes *Chem. Phys. Lett.* **412** 399
- [157] Zhang J and Zhu J 2006 Orientation dependence of diffraction intensities from helical structures *Chem. Phys. Lett.* **420** 171
- [158] Iijima S, Brabec C, Maiti A and Bernholc J 1996 Structural flexibility of carbon nanotubes *J. Chem. Phys.* **104** 2089
- [159] Lordi V and Yao N 1998 Radial compression and controlled cutting of carbon nanotubes *J. Chem. Phys.* **109** 2509

- [160] Tang J, Qin L-C, Matsushita A, Kikegawa T, Yudasaka M, Bandow S and Iijima S 2000 Study of carbon nanotubes under high pressure *Mater. Res. Soc. Symp. Proc.* **593** 179
- [161] Tang J, Qin L-C, Sasaki T, Yudasaka M, Matsushita A and Iijima S 2000 Compressibility and polygonization of single-walled carbon nanotubes under hydrostatic pressure *Phys. Rev. Lett.* **85** 1887
- [162] Lopez M J, Rubio A, Alonso J A, Qin L-C and Iijima S 2001 New polygonized phase of single wall carbon nanotube bundles *Phys. Rev. Lett.* **86** 3056
- [163] Liu Z and Qin L-C 2005 Electron diffraction from elliptical nanotubes *Chem. Phys. Lett.* **406** 106
- [164] Abramovitz M and Stegun I A 1972 *Handbook of Mathematical Functions* (Washington DC: National Bureau of Standards)
- [165] Liu Z and Qin L-C 2005 A practical approach to determine the handedness of chiral carbon nanotubes by electron diffraction *Chem. Phys. Lett.* **405** 265
- [166] Qin L-C and Iijima S 2000 Twisting of single-walled carbon nanotube bundles *Mater. Res. Soc. Symp. Proc.* **593** 33
- [167] Liu Z and Qin L-C 2005 Structure and energetics of carbon nanotube ropes *Carbon* **43** 2146
- [168] Krstic V, Roth S, Burghard M, Kern K and Rikken G L J A 2002 Magneto-chiral anisotropy in charge transport through single-walled carbon nanotubes *J. Chem. Phys.* **117** 11315
- [169] Miyamoto Y, Louie S G and Cohen M L 1996 Chiral conductivities of nanotubes *Phys. Rev. Lett.* **76** 2121
- [170] Kibis O V 2001 Features of electron-phonon interaction in nanotubes with chiral symmetry placed in a magnetic field *Phys. Solid State* **43** 2336
- [171] Ivchenko E L and Spivak B 2002 Chirality effects in carbon nanotubes *Phys. Rev. B* **66** 155404
- [172] Margulis L, Dluzewski P, Feldman Y and Tenne R 1996 TEM study of chirality in MoS₂ nanotubes *J. Microsc.* **181** 68
- [173] Meyer J C, Paillet M and Roth S 2005 Single-molecule torsional pendulum *Science* **309** 1539
- [174] Liu Z and Qin L-C 2005 Measurement of handedness in multiwalled carbon nanotubes by electron diffraction *Chem. Phys. Lett.* **411** 291
- [175] Liu Z and Qin L-C in preparation